

**Dissertation zur Erlangung des Doktorgrades
der Fakultät für Chemie und Pharmazie
der Ludwig-Maximilians-Universität München**



**Functional Characterization of Transient Receptor Potential
Mucolipin-1 Channels – Potential Target for Cancer Therapy**

Siow, Wei Xiong
aus Johor, Malaysia
2022

Erklärung

Diese Dissertation wurde im Sinne von § 7 der Promotionsordnung vom 28. November 2011 von Frau Prof. Dr. Angelika M. Vollmar betreut.

Eidesstattliche Versicherung

Diese Dissertation wurde eigenständig und ohne unerlaubte Hilfe erarbeitet.

München, den 10.02.2022

.....
(Siow, Wei Xiong)

Dissertation eingereicht am: 10.02.2022

1. Gutachterin: Prof. Dr. Angelika M.Vollmar

2. Gutachter: Prof. Dr. Stefan Zahler

Mündliche Prüfung am: 21.03.2022

Contents

1	Abstract	7
2	Introduction.....	11
2.1	Pathogenesis and druggable target of hepatocellular carcinoma.....	11
2.2	Endolysosomal system - Transient Receptor Potential Mucolipin-1 (TRPML1) as a novel target for cancer therapy	12
2.3	Modulators of calcium: From TRPML1 to mitochondria	14
2.4	Regulation of TRPML1 in cancer cell metastasis – collective or individual migration?	15
2.5	Aim of Study.....	19
3	Materials and Methods	21
3.1	Materials	21
3.1.1	Compounds	21
3.1.2	Reagents.....	21
3.1.3	Technical equipment	24
3.2	Cell culture	26
3.2.1	Solution and Reagents	26
3.2.2	Cell line.....	26
3.2.3	Passaging.....	27
3.2.4	Freezing and Thawing	27
3.3	Genomic Editing – CRISPR/Cas9 System.....	27
3.3.1	Establish of RIL175 TRPML1 knockout (KO) cell line.....	27
3.3.2	Cloning and Transformation of <i>E.coli</i>	28
3.3.3	Transfection and Evaluation of Targeting Efficiency	30
3.3.4	Clonal selection and Knockout Verification	30
3.3.5	Off-target screening.....	31
3.4	Quantitative Real-Time PCR (qPCR) Analysis.....	31
3.5	Endolysosome patch-clamp.....	31

3.6	Proliferation assays	32
3.6.1	Cell viability test	32
3.6.2	Impedance measurement	33
3.7	Proteomic Analysis	33
3.7.1	Stimulation	33
3.7.2	Sample processing and Liquid-Chromatography Mass Spectrometry	33
3.7.3	Proteomic Data Processing	34
3.8	Flow cytometry	34
3.8.1	Apoptosis and Necrosis assay	34
3.8.2	Mitochondrial Membrane Potential ($\Delta\Psi_m$)	35
3.8.3	Intracellular calcium	35
3.8.4	Mitochondrial calcium	36
3.8.5	Mitochondrial ROS	36
3.9	Immunofluorescence Analysis	36
3.9.1	Mitochondrial morphology	36
3.9.2	Lysosomal morphology	36
3.9.3	Actin morphology	37
3.9.4	E-cadherin morphology	37
3.10	Transmission electron microscopy (TEM)	37
3.11	Western blot	38
3.11.1	Cell lysis and total protein isolation	38
3.11.2	Sodium Dodecyl Sulfate Polyacrylamide Gel Electrophoresis (SDS-PAGE) and Immunoblotting	38
3.12	Seahorse measurement	40
3.13	High-resolution respirometry	41
3.13.1	Mitochondria isolation	41
3.14	Migration assays	41
3.14.1	Boyden chamber	41
3.14.2	Microcontact printing live-cell imaging	41

3.15	Statistical analysis	42
4	Results.....	44
4.1	Part 1: Lysosomal ion channel TRPML1, a novel regulator of mitochondrial function in hepatocellular carcinoma cells	44
4.1.1	Generation of a cellular model with CRISPR/Cas9 system to study TRPML1 function	44
4.1.2	Functional characterisation of cellular activation and knockout models.....	45
4.1.3	TRPML1 plays a critical role in the regulation of mitochondrial morphology.	47
4.1.4	Modulation of TRPML1 activity interferes with mitochondrial function	50
4.1.5	TRPML1 activation induces mitochondrial stress via calcium overloading.....	53
4.2	Loss of TRPML1 function disturbs mitochondrial function by deregulation of mitophagy	55
4.3	Part 1: Summary	61
5	Part 2: TRPML1 as a novel modulator of cancer cell movement	62
5.1	Functional characterization of TRPML1 in cancer cell migration	62
5.2	TRPML1 plays a critical role in cancer cell movement and cell-cell contact	63
5.3	Loss of TRPML1 alters cytoskeleton morphology and adjunctive cellular protein .	64
5.4	TRPML1 regulates the cell-cell contact via Notch1	67
5.5	Part 2: Summary	69
6	Discussion.....	71
6.1	Part 1: Lysosomal ion channel TRPML1, a novel regulator of mitochondrial function in hepatocellular carcinoma cells	71
6.1.1	Modulating mitochondria by transient receptor potential mucolipin 1 channel as a therapeutic target for hepatocarcinoma cancer	71
6.1.2	Multiple functions of TRPML1 – Overloading mitochondria calcium.....	71
6.1.3	Multiple functions of TRPML1 – Deficit mitochondrial renewal	73
6.2	Part 2: TRPML1 as a novel modulator of cancer cell movement	76
7	References.....	80

8	Appendix	90
8.1	Abbreviations.....	96
8.2	Index of figures	99
8.3	Index of tables.....	101
8.4	List of Publications	102
9	Acknowledgements.....	103

To my family

ABSTRACT



1 Abstract

Hepatocellular carcinoma (HCC) is the most common form of liver cancer and remains the fourth most lethal cancer worldwide. A novel druggable target is urgently needed to establish therapeutic strategies. The role of cation channel TRPML1 residing on endolysosomal membranes has been discussed in cancer research representing a potential target. Here, we discovered an isoform-selective TRPML1 activator ML1-SA1 and used the CRISPR/Cas9 system to generate genetically TRPML1 knockout (KO) cells for over-activation and loss-of-function studies upon TRPML1 in HCC. ML1-SA1 represents potent cytotoxicity toward cancer cells in the micromolar range using proliferation and apoptosis assays. We unravelled that over-activation and loss of TRPML1 alter mitochondrial proteins using proteomic analysis. Furthermore, in-depth studies of mitochondria were conducted using confocal and transmission electron microscopy, combined with SeahorseTM and Oroboros[®] functional analysis. We have uncovered that ML1-SA1 over-activates TRPML1, leading to calcium overloading and thus impairment of mitochondrial function. Additionally, TRPML1 loss-of-function interferes with mitochondrial renewal, leading to aberrant cancer proliferation. The results of this study clearly reveal a dual-facet role of TRPML1 as a regulator in mitochondrial function and its activators as a promising molecule for anticancer options in HCC therapy.

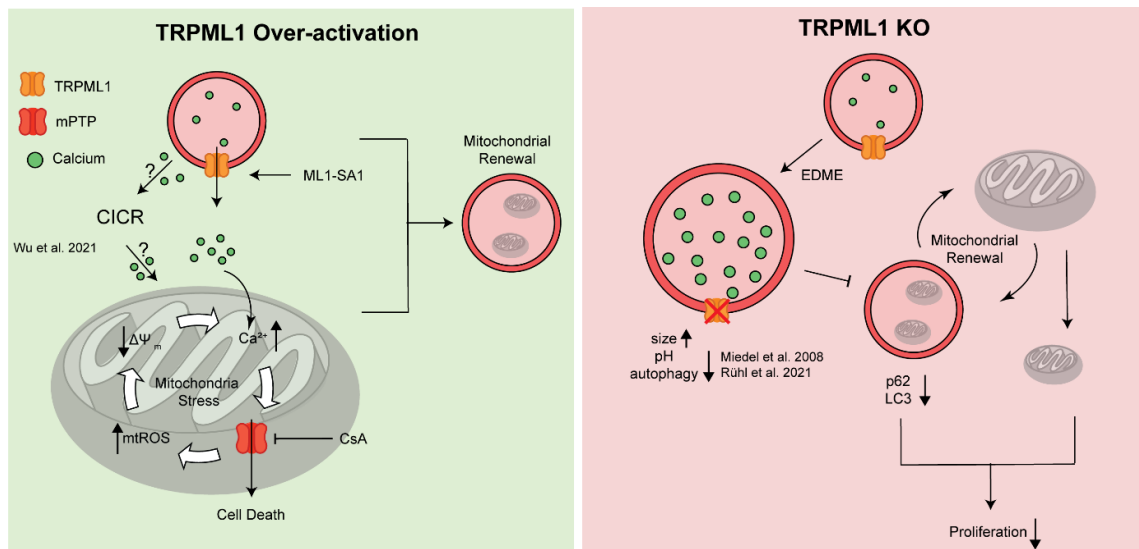


Figure 1. Model of TRPML1 as a mitochondrial balancer function in HCC – the project at a glance.

(Left panel) ML1-SA1 over-activates TRPML1 and leads to lysosomal Ca^{2+} release into the cytosol. This calcium can further induce calcium-induced calcium release from other organelles or calcium influx in mitochondria. Upregulation of mitochondrial calcium causes depolarization of mitochondrial membrane and generation of ROS, leading to an opening of the mitochondrial transition pore (mPTP) and cell death, which can be rescued by CsA. (right panel) Loss of TRPML1 alters the lysosomal size, pH and lysosomal function, leading to disrupted mitophagy and, therefore, mitochondrial renewal. Taken together, the impairment of mitochondrial and lysosomal function causes impairment of cellular proliferation rate.

Besides the anti-proliferative effect of TRPML1, we investigated the role of TRPML1 in cancer cell migration. We analysed collective and individual migration using a microcontact patterning technique and the underlying mechanisms in detail, facilitating confocal and western blot analysis. We unravelled that loss of TRPML1 decreases the migration capacity of various cancer cell lines by reprogramming cancer movement from collective to individual migration E-cadherin dependently. Mechanistically, TRPML1 might regulate E-cadherin by modulating cell-cell communication Notch1 signalling pathway. However, the underlying mechanism remains unknown and needs to be further investigated. In short, our study discovered a novel interaction of lysosomal TRPML1 and cell-cell contact in collective cancer migration, which sets a basis for targeting TRPML1 as an anti-metastatic option.

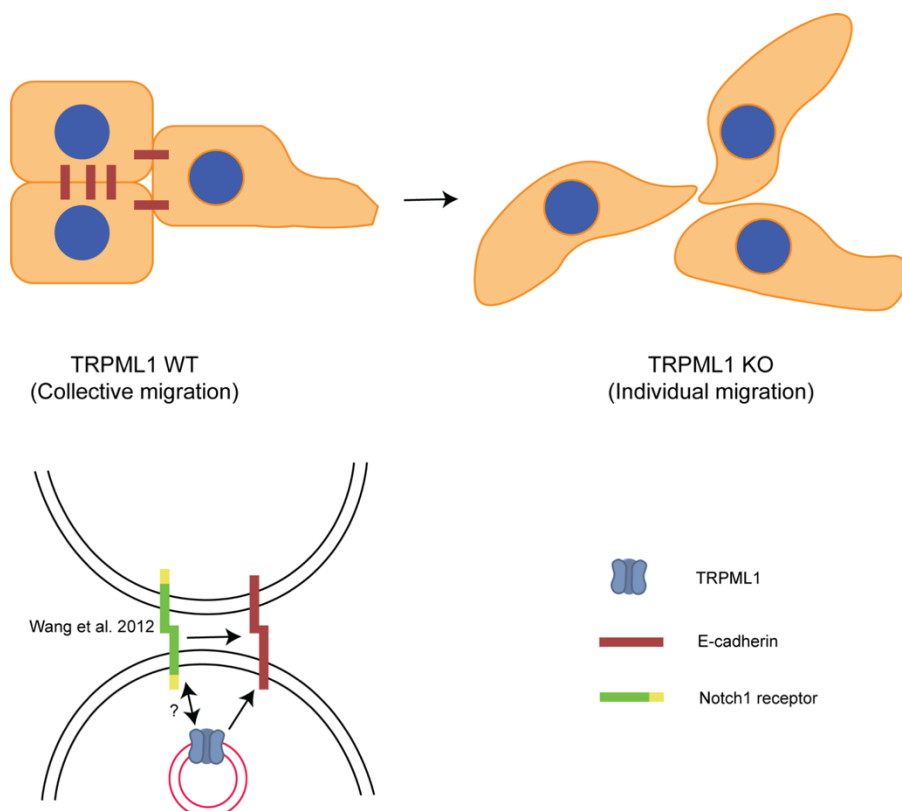


Figure 2. Characterization of TRPML1 in cancer collective migration – the project at a glance.

Loss of TRPML1 alters the expression of the tight junction protein, E-cadherin. It further leads to disruption of cell-cell contacts and reprogramming of cellular movement, causing a switch from collective to individual migration. Furthermore, this could indicate that the E-cadherin level is modulated by Notch1, a cell-cell communication protein, which in turn could be regulated by TRPML1.

INTRODUCTION



2 Introduction

2.1 Pathogenesis and druggable target of hepatocellular carcinoma

Hepatocellular carcinoma (HCC) represents the majority of primary liver malignancies, and is the fourth most common cause of cancer deaths worldwide [1, 2]. The high fatality rate is primarily due to high chemoresistance and poor prognosis [2]. In general, chronic hepatitis B or C virus (HBV or HCV) infection or alcohol abuse is suspected as a primary underlying cause of HCC [1, 2]. The molecular mechanism of HCC development is complex and heterogeneous. Several oncogenes and tumour suppressor protein mutations lead to the deregulation of normal cellular pathways. For instance, Wnt/ β -catenin, TP53/cell cycle, oxidative stress response, PI3K/AKT/mTOR, and Ras/Raf/MAPK [2]. Alteration of various molecular signalling pathways endows cancer development and the progression of HCC [3]. The diversity of molecular alteration complicates the discovery of effective chemotherapy. In clinical practice, HCC patients are commonly classified according to the Barcelona Clinic Liver Cancer (BCLC) staging system (**Figure 3**) [4, 5], and treatment options are strongly dependent on HCC stages. Current treatment options have been classified into clinical non-drug therapies and systematic pharmacological treatments [3, 5]. Clinical non-drug therapies such as hepatic resection or a liver transplant can cure patients in the early stages but are not suitable for advanced-stage patients [3]. Hence, systematic pharmacological treatments are often used for non-surgical patients, such as multi tyrosine kinase inhibitor Sorafenib, considered first-line treatment in pharmacological strategy [5]. The existing treatment can only offer survival benefits for 30 % of HCC patients [3]. Herein, the need for novel druggable targets in HCC or cancer provided the rationale and idea for this study.

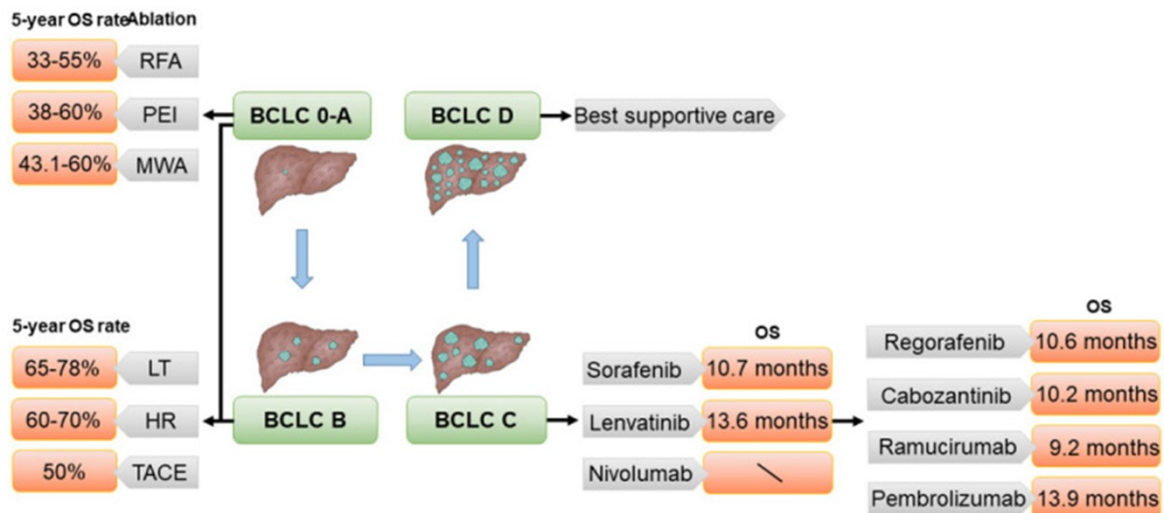


Figure 3. Classification of HCC patients and treatment options.

HCC stage is classified according to the Barcelona Clinic Liver Cancer (BCLC) staging system. The red box indicates the overall survival of patients after specific treatments. Possible treatments consist of RFA (radiofrequency ablation), PEI (percutaneous ethanol injection), MWA (microwave ablation), LT (liver transplantation), HR (hepatic resection), and TACE (transarterial chemoembolization). The figure is adapted from Chen. et al. [5].

2.2 Endolysosomal system - Transient Receptor Potential Mucolipin-1 (TRPML1) as a novel target for cancer therapy

Researchers have shown an increasing interest in the role of the endolysosomal system (ES). It consists of lysosomes, early, late, recycling endosomes, and autophagosomes. In general, the ES has emerged as critical in regulating macromolecules degradation and recycling, homeostasis, and energy metabolism. In addition, more and more evidence shows that the ES plays a critical role in cancer, in particular revealing that the autophagy-lysosome pathway helps cancer to escape from cell death or apoptosis pathways [6, 7]. Hence, targeting the endolysosomes has become an attractive strategy in cancer research. The function of the endolysosomes is intimately associated with membrane proteins such as ion channels. Transient receptor potential channels (TRP channels) are groups of ion channels on the plasma membrane and membranes of acidic vesicles of the ES [8, 9]. Transient Receptor Potential Mucolipin channels (TRPMLs) are subfamilies of TRP channels. The mucolipins consist of 3 channel subtypes, TRPML1, -2, and -3, encoded by MCOLN1, -2, and -3 genes, respectively [8]. They are non-selective permeable to cations, for instance, calcium, sodium, and magnesium. TRPML1 and TRPML2 are primarily localised to the late endosome and lysosome. In contrast, TRPML3 is present at the plasma membrane and early endosome [8].

The structure of TRPML1 [10, 11] and TRPML3 [12] were revealed by electron cryo-microscopy. TRPML1 channel consists of four subunits, and each subunit contains six transmembrane helices S1- S6, two-pore helices (PH1 and PH2), and a luminal domain [10, 11] (**Figure 4**). The transmembrane domains, S5 and S6, play a critical role in channel opening as they can form a binding pocket for activators [10, 11]. The binding of TRPML1 endogenous activator (PtdIns (3,5) P2) or synthetic molecules (MLSA-1) results in conformation changes, which in turn cause conformational changes that open the gate and allow ions to pass through the channel [11, 13]. TRPML3 has a similar general architecture with TRPML1 but reacts differently to pH changes [12]. Among three TRPML channels, TRPML1 was reported as a genetic determinant of a human lysosomal disorder (LSD), namely, mucopolipidosis type IV (ML-IV) [14, 15]. ML-IV patients are often characterised by abnormal neurodevelopment and ophthalmologic diseases [16]. No evidence yet shows TRPML2 or TRPML3 to have any link with disease in humans.

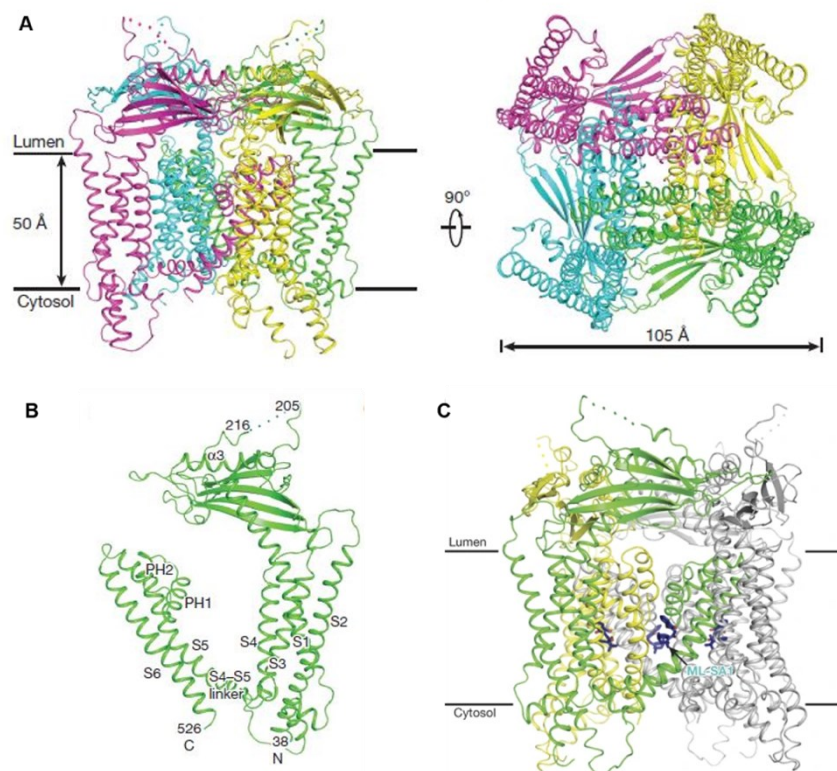


Figure 4. Structure of human TRPML1.

(A) TRPML1 consists of four subunits. (B) Each subunit has six transmembrane helices (S1- S6), two-pore helices (PH1 and PH2), and a luminal domain. (C) The binding of ML-SA1 facilitates activation of the channel to the binding pocket, which is formed by the S5, S6, and PH1 domains. The figure was adapted from Schmiede et al [11].

TRPML1 has recently come into focus for researchers as accumulating evidence has supported the view that TRPML1 is highly correlated with cancer cell progression [17-21]. Furthermore, aberrant expression of TRPML1 was correlated with poor survival outcomes of pancreatic cancer [21] and glioblastoma [18]. In particular, silencing of TRPML1 reduced proliferation [17, 18, 20] and migration of cancer cells [19]. The dysfunction of TRPML1 alters lysosomal trafficking via mTORC1 related autophagy, which further attenuates cancer cell proliferation [20] as well as migration [19]. By contrast, hyperactivation of TRPML1 was reported as a beneficial factor for glioblastoma cells in order to decrease cancer progression [18]. Since TRPML1 is a cation channel, unsurprisingly, it was proposed that TRPML1 controls Ca^{2+} levels, leading to an imbalance of autophagy via the mTOR pathway [22]. Recently, it has been reported that activation of TRPML1 disrupts autophagy, leading to cell cycle arrest [23]. In contrast, inhibition of the TRPML1 function was also reported to impair autophagy pathways and decrease cancer cell invasion. Consequently, the role of TRPML1 remains largely unclear in cancer and needs to be further investigated.

2.3 Modulators of calcium: From TRPML1 to mitochondria

TRPML1 has been recently reported as a regulator of mitochondrial Ca^{2+} and Zn^{2+} ion levels [24, 25]. In general, calcium is a critical ion that takes part in tremendous cellular functions in physiological states, for instance, signal transduction pathway for neurotransmission, muscle contraction, cell cycle progression and cell death [26]. Nearly all organelles need calcium to maintain their biological function, for instance, Golgi apparatus and mitochondria [27]. Mitochondria generate adenosine triphosphate (ATP) by the sequential passage of electrons in the mitochondrial electron transport chain, which is susceptible to cellular Ca^{2+} [28]. Calcium can be transported into mitochondria via voltage-dependent anion channels (VDACs), mitochondrial calcium uniporter (MCU)[29] or $\text{Na}^+/\text{Ca}^{2+}/\text{Li}^+$ exchanger (NCLX) [28]. The calcium level in mitochondria is delicately regulated to sustain the proper mitochondrial function and dynamic; for instance, Ca^{2+} is required in ATP production or mitophagy, a specialised process for renewal dysfunctional mitochondria [30, 31]. Therefore, an imbalance of the mitochondrial calcium will cause severe cellular malfunction, eventually leading to cell death [32]. For instance, the overloading of Ca^{2+} can transiently open the mitochondrial permeability transition pore (mPTP), a protein residing in the inner membranes of mitochondria. Induction of mPTP is often accompanied by a burst of reactive oxygen species

(ROS), the release of cytochrome c, and mitochondrial fragmentation, which lead to apoptotic cell death [32]. Interestingly, it is reported that dysfunction of TRPML1 is linked with defective Ca^{2+} uptake of the mitochondria [25], while TRPML1 induces mitochondrial-related cell death by releasing lysosomal Zn^{2+} [24]. Since the TRPML1 is likely to be a key balancer in mitochondrial function, we further investigated the role of the TRPML1 channel in hepatocellular carcinoma.

2.4 Regulation of TRPML1 in cancer cell metastasis – collective or individual migration?

Cancer progression can be briefly divided into cancer proliferation and metastasis. The strategy to inhibit cancer proliferation was introduced in the previous chapter 2.3, but metastasis of cancer cells equally leads to several difficulties during cancer therapy. Metastasis is termed as the development of secondary tumours in the part of the body that migrate from original primary cancers [33]. Primary cancer cells must increase motility to achieve metastasis. Hence, a better understanding of cancer migration is mandatory for establishing a therapeutical strategy. Recently, TRPML1 has been reported in the regulation of regular cell migration [34, 35] as well as in cancer cells [19, 36, 37]. Mechanistically, it is hypothesized that inhibition of autophagy suppresses the tumour protein 53 activity, which leads to inhibition of migration. A complex and dynamic process, epithelial-mesenchymal transition (EMT) (**Figure 5**), is initiated during the cancer metastasis, transforming epithelial cells into mesenchymal cells [38-40]. During EMT, epithelial cells disassociate cell-cell junctions and gain migratory properties to become mesenchymal cells. Various molecules such as E-cadherin and N-cadherin regulate cell-cell junctions [41]. In cancer, E-cadherin is downregulated while N-cadherin is upregulated during the EMT and this “cadherin switch” endows invasive traits, leading to an inferior patient survival rate [42, 43]. E-cadherin-mediated cell junction is associated with the actin cytoskeleton via binding to adapter proteins such as α -, β -, and γ -catenins [44]. The actin cytoskeleton rearrangement is regulated by the Rho family of GTPases, including Rac1 and RhoA [45]. Activation of Rac1 triggers cell edges protrusion by promoting actin assembly and focal adhesion turnover during EMT in cancer cells [46].

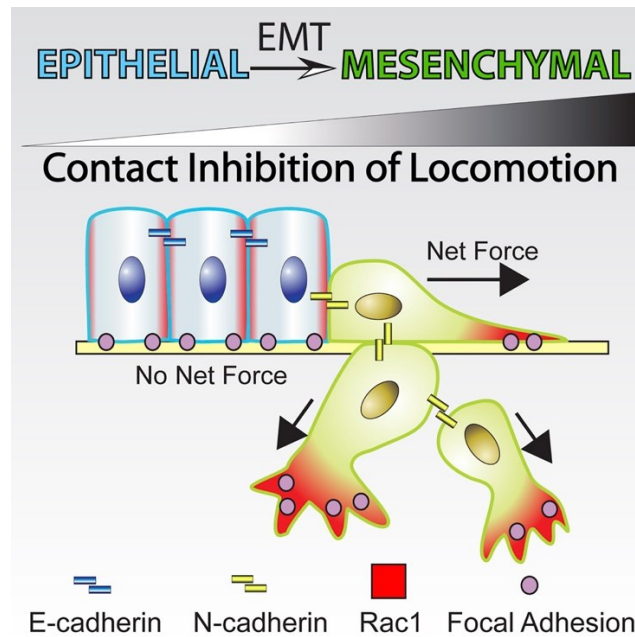


Figure 5. Regulation of cadherin switch and Rac1 in epithelial-mesenchymal transition.

E-cadherin maintains cell-cell adhesions in epithelial cells. During the EMT, E- to N-Cadherin switch remodels the cell and redistributes the Rac1 and focal adhesion, resulting in cell protrusions. The figure was adapted from Scarpa et al. [40].

Cancer cells primarily relocate using collective migration as efficiency is higher than individual migration [47]. Collective cell migration mainly relies on cell-cell interactions to control migratory dynamics [48, 49]; thus, E-cadherin plays an essential role in consolidating cell-cell connection [41]. High expression of E-cadherin facilitates collective migration by maintaining a solid adherent junction (**Figure 6**) [50-52]. In contrast, loss of E-cadherin promotes cells to detach from each other after cell-cell contact, and this process is termed contact inhibition of locomotion [40]. Until now, the mechanism behind collective migration has not been fully clarified. However, several EMT proteins were proposed as candidate markers during the transition of collective migration; for instance, E-cadherin, N-cadherin and Rac1 are the initiative proteins for mesenchymal migration and podoplanin acts as surface mucin, which remodels actin cytoskeleton and RhoA in order to increase the cell invasion [53].

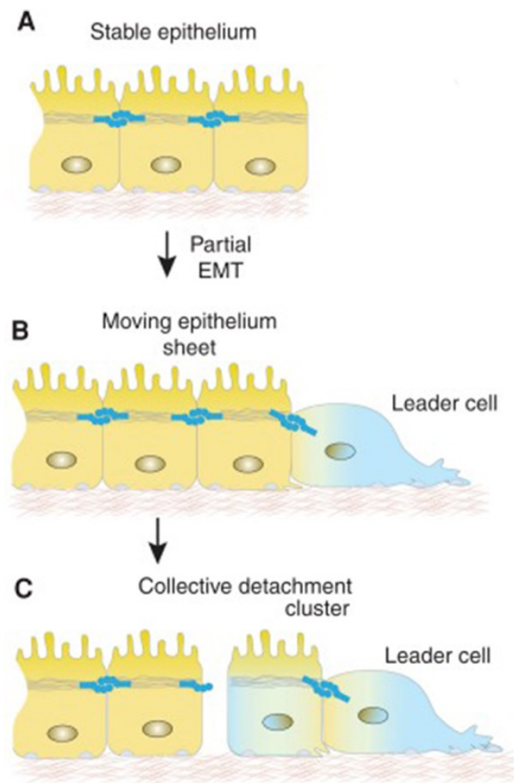


Figure 6. Modes of collective and individual migration

(A) Stable epithelial cells initiate the partial epithelial-mesenchymal transition, (B) leading cells can retain tight junction and promote collective migration. (C) Migration clusters maintain the stable cell adhesion by regulating E-cadherin or undergo mesenchymal plasticity. The figure was adapted from Friedl et al. 2017 [52].

Considering that collective migration is intensely associated with cell-cell interaction, Notch1, a surface receptor [54], has been reported in E-cadherin regulation during cancer metastasis [55, 56]. Notch1 is a member of Notch family receptors and shares similar structural characteristics with other Notch receptors. Notch1 consists of extracellular, transmembrane and intracellular domains. When the extracellular domain binds to a specific ligand such as Dll4, it initiates γ -secretase to cleave Notch1 and further releases the Notch intracellular domain (NICD), which in turn is translocated to the nucleus via endocytosis for facilitating gene transcription (**Figure 7**) [57]. Notch1 signalling pathway is essential in maintaining cell-cell interactions and EMT during cancer development [58]. Moreover, direct evidence points out that the binding of Notch1 and Dll4 is facilitated by calcium [59] and required by collective migration in cancer cells [60, 61]. In short, cell-cell contact plays a decisive role in cancer cell migration, though, it remains unknown whether loss of TRPML1 affects collective migration hence the reason for its investigation in this study.

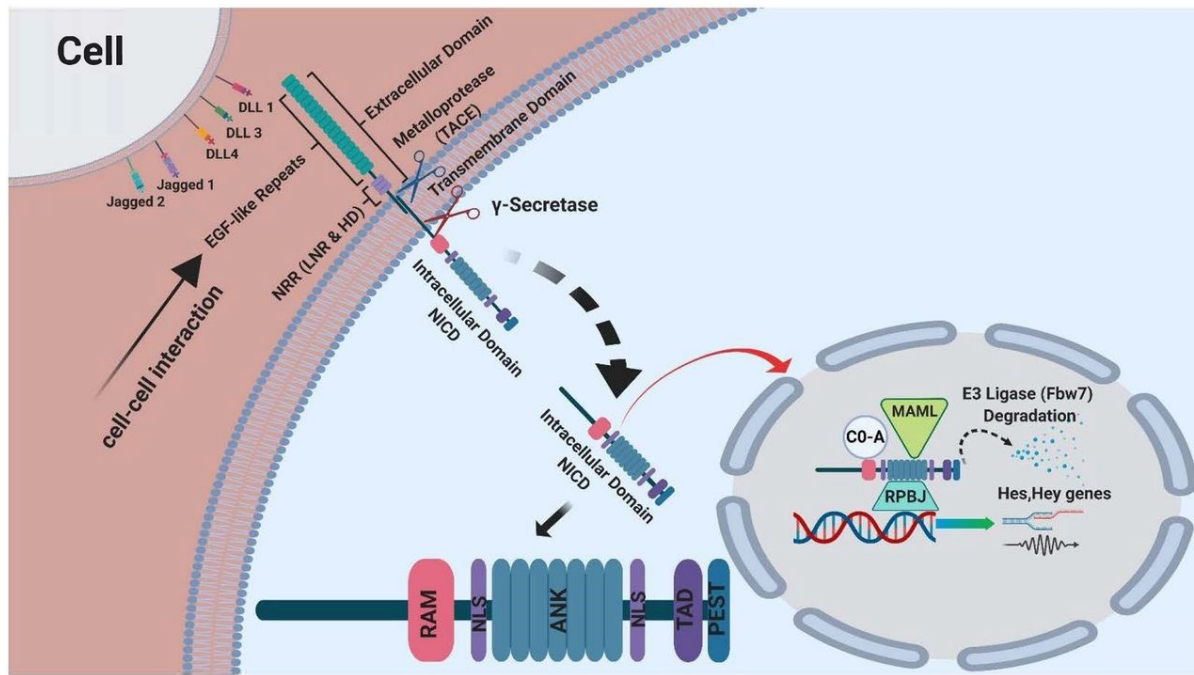


Figure 7. Notch1 signalling pathway

The extracellular domain comprises EGF-like repeats, heterodimerization and Lin-12 and Notch repeats. While the extracellular domain binds to any ligands (Jagged1, Jagged2, DLL1, -3 or -4), it triggers the cleavage of Notch1 by metalloprotease (TACE: tumour necrosis factor- α -converting enzyme) or α -secretase. Notch intracellular domain (NICD; ANK, ankyrin repeats; NLS, nuclear localization signal; RAM, RBP-j-associated molecule; PEST, proline, glutamic acid, serine, and threonine domain) can be further released into the cytosol, followed by translocation into the nucleus. NICD binds to the transcription complex (MAML, a coactivator of the Mastermind-like family; CO-A, coactivator; RBPJ, DNA binding factor—recombination signal binding protein for immunoglobulin κ J region) for Notch target transcription. The figure was adapted from Gharaibeh et al. 2020 [57].

2.5 Aim of Study

The main objectives of this study are to evaluate if TRPML1 can be utilised as a therapeutical target for cancer treatment, and, concurrently, to discover a novel TRPML1 compound. In addition, to identify and investigate the role of TRPML1 in cancer metastasis.

Part 1: Lysosomal ion channel TRPML1, a novel regulator of mitochondrial function in hepatocellular carcinoma cell line

1. Functional characterization of lysosomal ion channel TRPML 1 as a target for tumour therapy in hepatocellular carcinoma
2. Studies of the potential antitumour effects of a synthetic TRPML1 activator
3. Studies on the loss of TRPML1 function in cancer cells
4. Mechanistic studies of drug and target interaction

Part 2: TRPML1 as a novel modulator of cancer cell movement

1. Functional studies in tumour cells concerning migration and movement
2. Studies on a migratory pattern in genetic TRPML1 knockout cells
3. Mechanistic studies of TRPML1-mediated cell contact

MATERIALS AND METHODS



3 Materials and Methods

3.1 Materials

3.1.1 Compounds

Reagent	Producer
ML1-SA1	Dr. Eva Plesch (Prof. Bracher, Ludwig Maximilian University of Munich, Germany)
MLSA-1	Sigma-Aldrich, Taufkirchen, Germany
MLSA-5	Prof. Christian Grimm, Ludwig Maximilian University of Munich, Germany
MK683	Dr. Marco Keller (Prof. Bracher, Ludwig Maximilian University of Munich, Germany)
EDME	Philip Rühl (Prof. Bracher, Ludwig Maximilian University of Munich, Germany)

Table 1. Compounds

3.1.2 Reagents

Reagent	Producer
Ampicillin	ThermoFisher, Waltham, Massachusetts, USA
Anti-Mouse Igκ/Negative Control (FBS)	BD Bioscience, San Jose, USA
Compensation Particles Set	
Agarose	VMR, Radnor, Pennsylvania, USA
BCN-cRGDfk	Synaffix, Amsterdam, The Netherlands
Bovine serum albumin (BSA)	Sigma-Aldrich, Taufkirchen, Germany
Boyden chamber, 8 µm pore size	Sigma-Aldrich, Taufkirchen, Germany
BD PE Mouse IgG1, κ/ Isotype Control	BD Bioscience, San Jose, USA
BD Alexa Fluor Mouse IgG1, κ/ Isotype Control	BD Bioscience, San Jose, USA
Bradford reagent Roti® Quant	Bio-Rad, Munich, Germany

Reagent	Producer
Cal-520 [®] AM	Biomol, Hamburg, Germany
cDNA reverse transcription kit	Applied Biosystems, Waltham, USA
CellTiter-Blue [®] reagent	Promega, Mannheim, Germany
CellTiter-Glo [®] reagent	Promega, Mannheim, Germany
Collagen G	Biochrom AG, Berlin, Germany
Complete [®]	Roche Diagnostics, Penzberg, Germany
Competent DH5 α -E. coli	New England BioLabs, Frankfurt a.M., Germany
Cyclosporin A	Sigma-Aldrich, Taufkirchen, Germany
Dimethylsulfoxide (DMSO)	Sigma-Aldrich, Taufkirchen, Germany
Dithiothreitol (DTT)	Sigma-Aldrich, Taufkirchen, Germany
Dulbecco's Modified Eagle Medium (DMEM)	Pan Biotech, Aidenbach, Germany
eBioscience [™] Annexin V-FITC Apoptosis Detection Kit	Invitrogen, Carlsbad, California, USA
ECL Plus WB Detection reagent	GE Healthcare, München, Germany
Ethylenediaminetetraacetic acid (EDTA)	Sigma Aldrich, Taufkirchen, Germany
Eagle's Minimum Essential Medium (EMEM)	Pan Biotech, Aidenbach, Germany
Fetal calf serum (FCS)	Pan Biotech, Aidenbach, Germany
Fibronectin	R&D Systems, Minneapolis, USA
FluorSave [®] reagent mounting medium	Merck, Darmstadt, Germany
Fura2-AM	Invitrogen, Carlsbad, California, USA
High-Capacity cDNA Reverse Transcription Kit	Applied Biosystems, Waltham, USA
Hoechst 33342	Sigma-Aldrich, Taufkirchen, Germany
ibidiTreat μ -slides	ibidi GmbH, Munich, Germany
JC-1 dye	ThermoFisher, Waltham, Massachusetts, USA
Lipofectamine 3000	ThermoFisher, Waltham, Massachusetts, USA

Reagent	Producer
Lysotracker™ Red DND-99	ThermoFisher, Waltham, Massachusetts, USA
MitoTracker™ Red	ThermoFisher, Waltham, Massachusetts, USA
MitoSox	ThermoFisher, Waltham, Massachusetts, USA
Nitrocellulose membrane (0.2 µM)	Hybond-ECLTM, Amersham Bioscience, Freiburg, Germany
Page Ruler™ Prestained Protein Ladder	Fermentas, St. Leon-Rot, Germany
16% Formaldehyde Solution, Methanol-free	ThermoFisher, Waltham, Massachusetts, USA
Penicillin/Streptomycin 100x	Pan Biotech, Aidenbach, Germany
Phenylmethylsulfonyl fluoride (PMSF)	Sigma-Aldrich, Taufkirchen, Germany
Phusion Hot Start II DNA Polymerase	ThermoFisher, Waltham, Massachusetts, USA
PLL(20)-g[3.5]- PEG-N3(3) (APP)	Susos AG, Dubendorf, Switzerland
Polyacrylamide	Carl Roth, Karlsruhe, Germany
Poly-D-lysine hydrobromide (mol wt 70,000-150,000)	Sigma-Aldrich, Taufkirchen, Germany
Polyvinylidene difluoride (PVDF) membrane (0.2 µM)	Hybond-ECLTM, Amersham Bioscience, Freiburg, Germany
PowerUp™ SYBR® Green Master Mix	Applied Biosystems, Waltham, USA
Porcine trypsin	Promega, Madison, WI, USA
Primers	Metabion, Planegg, Germany
Propidium Iodide	BD Bioscience, San Jose, USA
Probenecid	Sigma-Aldrich, Taufkirchen, Germany
Puromycin	Sigma-Aldrich, Taufkirchen, Germany
Pluronic®F-127	Sigma-Aldrich, Taufkirchen, Germany
Rhod-2	ThermoFisher, Waltham, Massachusetts, USA

Reagent	Producer
RNeasy® Mini Kit (250)	QIAGEN, Hilden, Germany
Seahorse XFe96 FluxPaks (inc. mini)	Agilent Technologies, Santa Clara, USA
Sodium chloride	Carl Roth, Karlsruhe, Germany
Sodium orthovanadate (Na ₃ VO ₄)	ICN, Biomedicals, Aurora, OH, USA
Sodiumdodecylsulfate (SDS)	Carl Roth, Karlsruhe, Germany
T4 DNA ligase	New England BioLabs, Frankfurt a.M., Germany
Transwell Permeable Supports (8 µm pore polycarbonate inserts)	Corning Incorporated, New York, NY, USA
Tris Base	Sigma-Aldrich, Taufkirchen, Germany
Trypsin	PAN Biotech, Aidenbach, Germany
QIAprep Spin Miniprep Kit	QIAGEN, Hilden, Germany
QIAGEN plasmid Maxiprep Kit	QIAGEN, Hilden, Germany
QuickExtract DNA extraction solution	Biozyme, Oldendorf, Germany
QIAquick gel extraction kit	QIAGEN, Hilden, Germany
TurboFect transfection reagent	ThermoFisher, Waltham, Massachusetts, USA
Vacuolin	Sigma-Aldrich, Taufkirchen, Germany

Table 2. Reagents**3.1.3 Technical equipment**

Name	Producer
Canon 450D camera	Canon, Krefeld, Germany
Canon DS 126181 camera	Canon, Krefeld, Germany
ChemiDoc™ Touch Imaging System	Bio-Rad Laboratories GmbH
BD FACS Canto II	Becton Dickinson, Heidelberg, Germany
EPC-10 patch-clamp amplifier	HEKA, Lambrecht, Germany
Easy-Spray column	ThermoFisher, Waltham, Massachusetts, USA

Name	Producer
Eclipse Ti inverted microscope	Nikon, Dusseldorf, Germany
1200EX Electron microscope	JEOL, Japan
ICP-OES	CirosVision, SPECTRO Analytical Instruments, Kleve, Germany
KeenView II digital camera	Olympus, Germany
Leica SP8 Inverted Scanning Confocal Microscope	Leica Microsystems, Wetzlar, Germany
Mikro 22R centrifuge	Hettich, Tuttlingen, Germany
Monochromator-based imaging system	Polychrome IV monochromator, TILL Photonics,
Nanodrop® Spectrophotometer	PEQLAB Biotechnologie GmbH
Olympus DP25 camera	Olympus, Hamburg, Germany
Olympus BX41 microscope	Olympus, Hamburg, Germany
Oxygraph-2k	Oroboros Instruments Corp, Innsbruck, Austria
Plasma cleaner type “ZEPTO”	Diener electronic, Ebhausen, Germany
QuantStudio™ 3 Real-Time PCR System	Applied Biosystems, Waltham, USA
Q Exactive HF X mass spectrometer	ThermoFisher, Waltham, Massachusetts, USA
Seahorse XFe96 Analyzer	Agilent Technologies, Santa Clara, USA
SpectraFluor Plus™	Tecan, Crailsheim, Germany
Ultrasonic homogeniser	Sonopuls GM3200, BR30, Bandelin, Berlin, Germany
Ultimate 3000 nano-chromatography system	ThermoFisher, Waltham, Massachusetts, USA
Vi-Cell™ XR	Beckman Coulter, Fullerton, CA, USA
xCELLigence System	Roche Diagnostics, Mannheim, Germany
Zeis LSM 510 Meta confocal laser scanning microscope	Zeis, Jena, Germany

3.2 Cell culture

3.2.1 Solution and Reagents

PBS(pH 7.4)		PBS+Ca ²⁺ /Mg ²⁺ (pH 7.4)	
NaCl	132.2 mM	NaCl	137 mM
Na ₂ HPO ₄	10.4 mM	KCl	2.68 mM
KH ₂ PO ₄	3.2 mM	Na ₂ HPO ₄	8.10 mM
H ₂ O		KH ₂ PO ₄	1.47 mM
		MgCl ₂	0.25 mM
		H ₂ O	
Growth medium		Freezing medium	
DMEM/EMEM	500 mL	FCS	90 %
FCS	50 mL	DMSO	10 %
Penicillin/Streptomycin	5 mL		
Trypsin/EDTA (T/E)		Collagen G	
Trypsin	0.05%	Collagen G	0.001%
EDTA	0.20%	PBS	
PBS			

Table 3. Cell culture buffers and solutions

3.2.2 Cell line

HUH7, Hep3B, MDA-MB-231 and SKMEL5 cells were obtained from the Japanese Collection of Research Bioresources (JCRB) or American Type Culture Collection (ATCC). RIL175 cells were kindly provided by Simon Rothenfußer (Center of Integrated Protein Science Munich (CIPS-M) and Division of Clinical Pharmacology, Department of Internal Medicine IV, Klinikum der Universität München). MDA-MB-231 TRPML1 KO and SKMEL5 KO were kindly provided by Prof. Dr. Dr. Christian Grimm.

Cancer cell lines were cultured in DMEM (RIL175 WT and TRPML1 KO, HUH7, HepG2, MDA-MB-231 WT and TRPML1KO, SKMEL5 WT and TRPML1KO) or EMEM (Hep3B), supplemented by 10% FCS or inactivated FCS (SKMEL5) and 1% of penicillin/streptomycin. The cells were incubated at 37 °C in a humidified atmosphere of 5% CO₂.

3.2.3 Passaging

When cells reached confluency, they were subcultured in 75 cm² culture flasks or seeded in multiwell-plates or dishes for further experimentation. Cells were firstly detached by incubating with trypsin/EDTA for 1-3 min in a 37 °C incubator. Trypsin/EDTA was removed by centrifugation with 200 x g, 5 min, room temperature (RT) to prepare the cells for plating. Tryptic digestion was terminated by adding a complete growth medium and counting the required cells with Vi-Cell™ XR.

3.2.4 Freezing and Thawing

Cells were detached as described previously and resuspended in an ice-cold freezing medium for long-term storage. Aliquots of 1 ml (equal to 3x10⁶ cells) were transferred into cryovials. After initial storage at -80°C for 24h, cryovials were moved to liquid nitrogen for long-term storage. For the thawing process, cryovials were warmed to 37°C, and the cell suspension was immediately cultured in a prewarmed growth medium for 24 h and replaced by a fresh growth medium until confluent.

3.3 Genomic Editing – CRISPR/Cas9 System

3.3.1 Establish of RIL175 TRPML1 knockout (KO) cell line

For the knockout of TRPML1 in murine RIL175 cells, the CRISPR/cas9 system was used as described previously [62]. The InDel-mutation methods into exon2 of TRPML1 were decided, and the strategy was sketched in **Figure 28**. Genomic DNA was isolated from wildtype RIL175 cells using QuickExtract DNA extraction solution according to the manufacturer's protocol. The genomic region of interest was amplified with appropriate sequencing primers via PCR using the Phusion® high fidelity DNA polymerase kit described by the manufacturer. Correct amplification was checked by agarose gel electrophoresis (1% agarose in Tris/Borate/EDTA buffer, 150 V, 45 min). Sequencing services were provided by Eurofins Genomics GmbH (Ebersberg, Germany).

	Forward primer (5'-3')	Reverse primer (5'-3')
MCOLN1 exon 2	ACAGAATCCTAGACTGGCCT	AAGGTGGGTACAGGAGTGGT

Table 4. Sequencing primers for exon 2

The single guide RNA (sgRNA) was designed by CRISPR online tool (<http://crispor.tefor.net/>) based on the MCOLN1 sequence from ENSEMBL (<https://www.ensembl.org/>). sgRNA sequences/cloning oligomers (underline indicates protospacer sequences for sgRNA)

	Sequences (5'-3')
Upstream sgRNA_top	<u>CACCGTATACCCAAAATGTCCCG</u>
Upstream sgRNA_bottom	<u>AAACCGGGGACATTTTGGGTATAC</u>
Downstream sgRNA_top	<u>CACCGGGAAGGACGTAGGTAGATC</u>
Downstream sgRNA_bottom	<u>AAACGATCTACCTACGTCCTTCCC</u>

Table 5. sgRNA sequences

3.3.2 Cloning and Transformation of *E.coli*

Target sgRNA upstream (5') and downstream (3') of exon 2 was cloned into eCas9(1.1)-2A-Puro backbone and eSpCas9_2A_Blasti plasmid via BbsI restriction site by using T4 DNA ligase, respectively. Hence, cloning oligomers were firstly annealed using a PCR cyclor (5 min at 95°C, ramp down to 25°C) and diluted (1:200 in H₂O).

Reagents	Volume [μL]
sgRNA_top (100 μM)	1
sgRNA_bottom (100 μM)	1
T4 ligation buffer	1
H ₂ O	7

Table 6. Oligo-annealing master mix

eSpCas9 (1.1)-2A-Puro was cloned by introducing T2A puromycin resistance cassette from PX459 into eSpCas9(1.1) via FseI and NotI restriction site; both plasmids were a gift from Feng Zhang, addgene plasmids #62988 and #71814, respectively). The downstream sgRNA was applied with similar strategy and cloned into eSpCas9_2A_Blasti plasmid (provided by Lars König, Klinikum der Universität München, Munich, Germany). For insertion of annealed

sgRNA into the desired plasmid, the restriction enzyme mix was prepared and incubated at 37 °C for 30 min.

Reagents	Volume [μ L]
Cas9 plasmid (150 ng)	x
FD Buffer colorless 10 X	6
FD Bpil	4
H ₂ O	48.7

Table 7. Digestion of Cas9 plasmid

The insertion of annealed sgRNA and cleaved plasmid was assembled using a ligation mix containing T4 DNA ligase and subsequently incubated at RT for 30 min. PlasmidSafe ATP-dependent DNase was used according to the manufacturer's protocol to remove residues ligated plasmid.

Reagents	Volume [μ L]
Restricted plasmid	10
Annealed oligomers (diluted)	2
T4 ligation buffer (10X)	2
T4 DNA ligase	1
H ₂ O	5

Table 8. Ligation of annealed oligos and Cas9 plasmid

Reagents	Volume [μ L]
Ligation product	11
PlasmidSafe buffer (10x)	1.5
ATP (25 mM)	0.6
PlasmidSafe Exonuclease	1
H ₂ O	Ad 15

Table 9. Digestion of non-ligated plasmid

Completed plasmid-DNAs were transformed into competent DH5 α -E.coli. The E.coli and plasmid DNA mixture was first kept on ice for 10 minutes, then heat-shocked at 42°C for 45 s and returned to the ice for 2 minutes. Subsequently, bacterial suspension was plated on an agar plate containing 100 μ g/mL ampicillin and incubated at 37°C for 24 h. 3-5 colonies were picked per plasmid and amplified in 5 ml LB (+) medium containing 100 μ g/mL ampicillin. Plasmids were then isolated by mini-prep using the QIAprep Spin Miniprep kit according to the manufacturer's protocol. Correct insertion and amplification were confirmed by restriction analysis (restriction enzyme: Ehel) and sequencing (U6-F-primer: 5'-GAGGGCCTATTTCCCATGATTCC-3') before selected plasmids were amplified and isolated using the QIAGEN plasmid Maxiprep Kit according to the manufacturer's protocol.

3.3.3 Transfection and Evaluation of Targeting Efficiency

Construct with sgRNA was subsequently transfected by using lipofectamine 3000 according to the manufacturer's protocol. RIL175 cells were cultured in a 6-well plate to a 70 % confluency, then added a mixture of lipofectamine 3000 and constructed for 24 h. The medium was replaced with a selection medium containing 2 μ g/mL puromycin and 7.5 μ g/mL blasticidin for 48 h. After the selection, cells were recovered in a complete medium until confluent for analysis by agarose gel electrophoresis.

3.3.4 Clonal selection and Knockout Verification

Single-cell dilution was used to isolate clonal cell lines. Therefore, cells were diluted to 0.6 cells/well before being seeded into 96-wells plates for two weeks. Single-cell colonies were transferred to a 24-well plate until confluency. Genomic DNA from potential cell colonies was isolated by using QuickExtract DNA extraction solution according to the manufacturer's instructions. The extracted genomic DNA was further amplified by standard PCR using MCOLN1 exon2 and MCOLN1 exon2 spanning primers with Phusion Hot Start II DNA Polymerase. PCR products were applied to 0.7 % agarose gel. Certain bands were cut off from gel before extracting gDNA using the QIAquick gel extraction kit according to the manufacturer manual. Knockout verification is conducted by using standard qPCR with MCOLN1 NMD primers.

	Forward primer (5'-3')	Reverse primer (5'-3')
MCOLN1 exon 2	ACAGAATCCTAGACTGGCCT	AAGGTGGGTACAGGAGTGGT
MCOLN1 exon2 spanning	CCCACAGAAGAGGAAGACCT	GCACAGTGACCACCAAGAT
MCOLN1 NMD	CGCCGCCTCAAGTACTTCTT	CTGCACAGTGACCACCAAGA

Table 10. Primers used for PCR analysis of exon 2 deletion**3.3.5 Off-target screening**

Ten predicted off-target sequences in exons or introns with the highest cutting frequency determination (CFD) scores were amplified using PCR reaction. The PCR product was subsequently analysed by Sanger sequencing and compared with WT cells. The investigated off-targets and the used primer pairs are listed in **Table 16** and **Table 17**.

3.4 Quantitative Real-Time PCR (qPCR) Analysis

The RNA was isolated by RNeasy Mini Kit according to manufacturer protocol and was reversely transcribed by cDNA reverse transcription kit. The qPCR was carried out using SYBR Master Mix and performed qPCR measurement using QuantStudio™ 3 Real-Time PCR system. Actin was used as a housekeeping gene. The changes in mRNA levels were evaluated by the $\Delta\Delta CT$ method described in the previous study [63]. The primers for qPCR were as follows:

Target genes	Forward primer (5'-3')	Reverse primer (5'-3')
MCOLN1 <i>Homo sapiens</i>	TCTTCCAGCACGGAGACAAC	GCCACATGAACCCCAACAAC
MCOLN1 <i>Mus musculus</i>	GCCTTGGGCCAATGGATCA	CCCTTGGATCAATGTCAAAGGTA
Actin <i>Homo sapiens</i>	CCAACCGCGAGAAGATGA	CCAGAGGCGTACAGGGATAG
Actin <i>Mus musculus</i>	CCACCATGTACCCAGGCATT	AGGGTGTAACGCAGCTCA

Table 11. Primers used for PCR analysis**3.5 Endolysosome patch-clamp**

Whole-endolysosome recordings were conducted by Dr Yu-Kai Chao and Rachel Tang (Prof. Grimm, Ludwig Maximilian University of Munich, Germany). The protocol has been described

previously in detail [64]. In brief, cells were treated with Vacuolin (1 μ M overnight. Compounds were washed out entirely before the patch-clamp performance. Capillary glass micropipettes were applied to cut the edge of the plasma membrane and push the enlarged vesicle of interest out of the cell. Afterwards, electrode micropipettes were used to establish whole-intracellular organelle configurations. Currents were recorded using an EPC-10 patch-clamp amplifier and PatchMaster acquisition software (HEKA). Data were digitised at 40 kHz and filtered at 2.8 kHz. Fast and slow capacitive transients were cancelled by the compensation circuit of the EPC-10 amplifier. Recording glass pipettes were polished and had a 4–8 MW resistance. Salt-agar bridges were used to connect the reference Ag-AgCl wire for all experiments. Liquid junction potential was corrected accordingly. Unless otherwise stated, cytoplasmic solution (bath) contained (mM) 140 K-MSA, 5 KOH, 4 NaCl, 0.39 CaCl₂, 1 EGTA, and 10 HEPES (pH was adjusted with KOH to 7.2). The luminal solution contained (mM) 140 Na-MSA, 5 K-MSA, 2 Ca-MSA, 1 CaCl₂, 10HEPES, and 10 MES (pH was adjusted with NaOH to 7.2). For optimal conditions of TRPML1, luminal pH was adjusted to 4.6, and Na-MSA was used in the luminal solution. For optimal conditions of TRPML2, luminal pH was adjusted to 7.2, and Na-MSA was used in the luminal solution [65]. For optimal conditions of TRPML3, luminal pH was adjusted to 7.2, and K-MSA was applied to replace Na-MSA in the luminal solution [66]. In all experiments, 500 ms voltage ramps from -100 to +100 mV were applied every 5 s, holding potential at 0 mV. The current amplitudes at -100 mV were extracted from individual ramp current recordings. Origin8 software was used for all statistical analyses.

3.6 Proliferation assays

3.6.1 Cell viability test

Cells were seeded and treated with ML1-SA1 accordingly for 70 h. The CellTiter-Blue® was loaded to the cells according to the manufacturer's manual. The CTB solution was added with 16.6 % (V/V) final concentration at 0 h as a background control. After indicated incubation time, cells were loaded with CTB solution for 2 h. The absorbance was measured at 590 nm using a microplate reader. The results were calculated by the following formula:

$$\text{cell viability (\%)} = \frac{(72 \text{ h treated abs.} - \text{background abs.})}{72 \text{ h DMSO control abs.}} * 100$$

3.6.2 Impedance measurement

The proliferation rates of RIL175 WT and TRPML1 KO were measured by the xCELLigence RTCA device. The cells were seeded at a density of 2×10^3 cells per well into a collagen G precoated and equilibrated 16-well E-plates. In principle, E-plates provide an electron flow from a negative terminal to a positive terminal. Since cells are added or grown, the electron flow will further be impeded and generate a parameter as cell index. The cell index is proportional to the cell number. Slopes were calculated using the xCELLigence RTCA software for each cell line until reaching plateau phase using the following equation:

$$\text{Slope (1/h)} = \frac{\text{cell index} - \text{intercept}}{\text{time (h)}}$$

3.7 Proteomic Analysis

3.7.1 Stimulation

Cells were seeded at a density of 4×10^5 cells per well into 6-well plates before stimulation with 30 μ M of ML1-SA1 for 24 h. Cells were washed five times with PBS to eliminate the medium and detached with trypsin/EDTA. Cells with a density of 1×10^6 were taken out from the detached cells and were centrifuged (200 x g, 5 min, RT). Cell pellets were resuspended in 100 μ L of PBS and stored at -80°C until further processing.

3.7.2 Sample processing and Liquid-Chromatography Mass Spectrometry

Protein mass spectrometry was conducted by Dr. Florian Flenkenthaler (Dr. Thomas Fröhlich, Ludwig Maximilian University of Munich, Germany). Cells were lysed in 8 M Urea / 400 mM NH_4HCO_3 using an ultrasonic homogeniser with a cup resonator. Protein concentration was determined using a Bradford assay. 10 μ g of total protein was reduced with dithioerythritol (5mM final concentration) for 30 min at 37 °C and alkylated for 30 min using iodoacetamide at a final concentration of 15 mM. The sample was diluted with water to give a final concentration of 1M Urea and digested overnight at 37 °C with modified porcine trypsin at an enzyme/protein ratio of 1/50. The Ultimate 3000 nano-chromatography system coupled to Q Exactive HF X mass spectrometer was used for mass spectrometry analysis. One μ g of peptides was injected and separated at 250 nl/min using 0.1% formic acid in water as solvent A and 0.1% formic acid in acetonitrile as solvent B. As separation column, an Easy-Spray column (PepMap RSLC C18 2 μ m 100 Å 75 μ m x 50 cm) was used. The separation method

consisted of a 160 min gradient from 3% to 25% solvent B and a 10 min gradient from 25% to 40% solvent B. MS and MS/MS spectra were acquired with a top 15 data-dependent method.

3.7.3 Proteomic Data Processing

MaxQuant (v.1.6.1.0) and the murine subset of the UniProtKB/Swiss-Prot database were used for protein identification [67]. Gene ontology and Functional Enrichment Analysis were performed with STRING.

3.8 Flow cytometry

3.8.1 Apoptosis and Necrosis assay

Cells were seeded at a density of 1×10^5 cells per well in a 24-well plate and incubated for 24 h. Treatment was performed with indicated concentration and time. Apoptosis and necrosis were determined by eBioscience™ Annexin V-FITC Apoptosis Detection Kit according to the manufacturer's protocol. In brief, cells were harvested and centrifuged (600 xg, 10 min, 4°C) before resuspending in 1x binding buffer containing (2.5 % v/v) Annexin V-FITC for 10 min at RT. Next, cells were washed with 1x binding buffer by centrifugation (600 xg, 10 min, 4°C), followed by incubation with (5 % v/v) PI solution in 1x binding buffer for 5 min at 4°C. Ten thousand events of cells were collected by flow cytometry for each measurement.

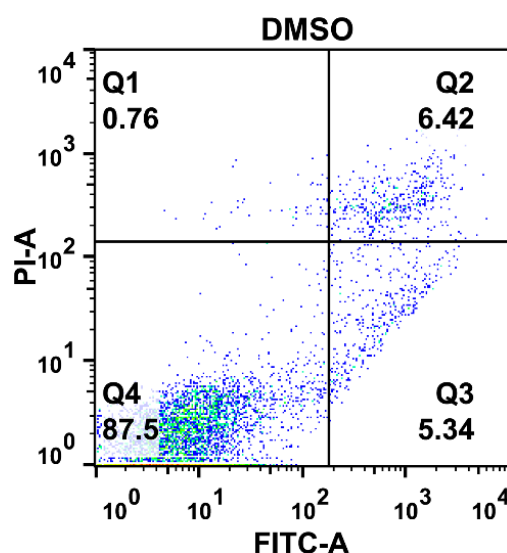


Figure 8. Gating strategy for Annexin V-FITC Apoptosis assay.

The gating strategy for identifying necrosis, early apoptotic, late apoptotic, or living cells in apoptosis and necrosis assay. Q1: necrosis; Q2: late apoptosis; Q3: early apoptosis; Q4: living cells

3.8.2 Mitochondrial Membrane Potential ($\Delta\Psi_m$)

Mitochondrial membrane potential was detected by JC-1 dye, which indicates the intactness of mitochondria. In healthy mitochondria, JC-1 molecules accumulate in mitochondria and form a complex called J aggregates which elicits red fluorescence. By contrast, unhealthy mitochondria do not reach a sufficient JC-1; therefore, it fails to trigger the formation of J aggregates, thus retaining green fluorescence. In brief, cells were seeded with a density of 1×10^5 cells per well in a 24-well plate, followed by 24 h incubation before stimulation. Cells were introduced to 1 $\mu\text{g}/\text{mL}$ of JC-1 and incubated at 37 °C for 1 h. The JC-1 was eliminated by centrifugation (400 xg, 5 min, RT) with PBS before resuspending in PBS. For Cyclosporin A (CsA) rescued experiment, 10 μM of CsA was pre-treated for 2 h prior to indicated stimulation. Meanwhile, compensation samples were prepared using Anti-Mouse Ig, κ /Negative Control (FBS) Compensation Particles Set and a BD PE Mouse IgG1, κ / Isotype Control and a BD Alexa Fluor® 488 Mouse IgG1 κ Isotype Control as described by the manufacturer. Compensation setup was performed on BD FACS Canto II. Ten thousand events of cells were collected by flow cytometry for each measurement.

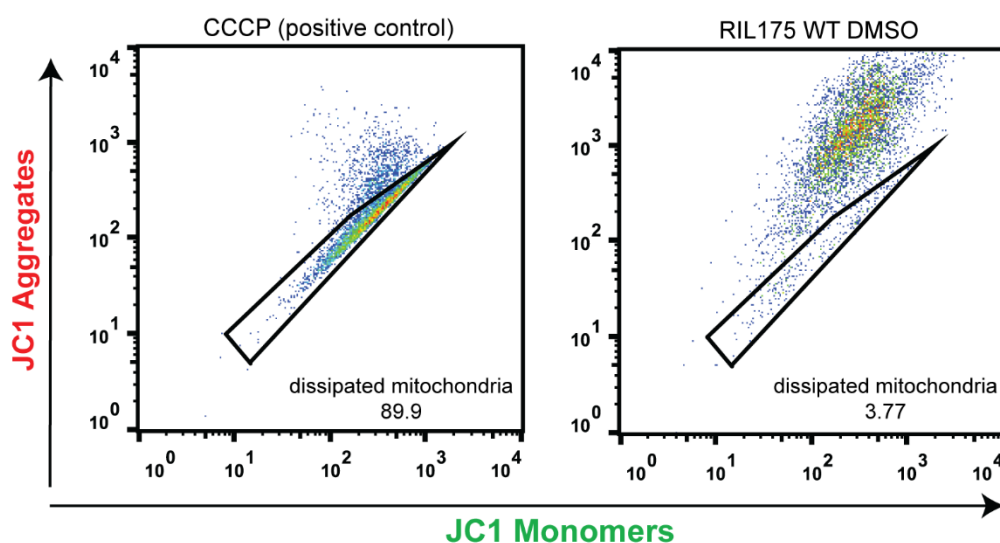


Figure 9. Gating strategy for identifying dissipated mitochondria.

The selected population is regarding positive control 100 μM of CCCP.

3.8.3 Intracellular calcium

Intracellular calcium was stained by Cal-520®AM, a dye that binds to calcium, and its lipophilic blocking groups can be cleaved by intracellular esterase, resulting in negatively charged fluorescence that stays inside cells. In brief, cells were seeded at a density of 1×10^5 cells per

well in a 24-well plate, subsequently incubated for 24 h prior to stimulation. 1 μ M Cal-520[®]AM dye mixture was prepared with PBS containing 0.24 % Pluronic[®]F-127 and 6 mM Probenecid. Cells were introduced with dye mixture for 90 min at 37 °C and 30 min at RT. Ten thousand events of the cell were collected by flow cytometry for each measurement.

3.8.4 Mitochondrial calcium

Mitochondrial calcium was stained by Rhod-2, an acetoxymethyl ester fluorescent calcium indicator. Rhod-2 dye selectively aggregates in mitochondria and binds with mitochondrial calcium. Briefly, cells were seeded at a density of 1*10⁵ cells per well in a 24-well plate and incubated for 24 h prior to stimulation. 1 μ M of Rhod-2 was introduced and incubated for 1h. Cells were rinsed with PBS and incubated in a complete medium for 30 min to exclude the residue indicator. Ten thousand events of the cells were collected by flow cytometry.

3.8.5 Mitochondrial ROS

Detection of mitochondrial ROS was conducted by a fluorogenic dye MitoSox, which can be easily oxidised by superoxide in mitochondria. Briefly, cells were seeded at a density of 1*10⁵ cells per well in a 24 well plate and incubated for 24 h prior to indicated stimulation. Mitosox dye was used at a final concentration of 1 μ M for 1h. Residue indicators were washed by using centrifugation (400 xg, 5 min, RT) before resuspending in PBS, and 10,000 events of cells were eventually collected using flow cytometry.

3.9 Immunofluorescence Analysis

3.9.1 Mitochondrial morphology

Cells were seeded on 8-well μ -Slide at a density of 5*10³ for 24 h prior to the indicated stimulation. The cells were rinsed with PBS twice and incubated with 100 nM of MitoTracker[™] Red for 30 min, followed by nuclei staining with Hoechst 33342 (2.5 μ g/ml) for 30 min. All images were observed and obtained by fluorescence microscopy. The mitochondria length was measured using a straight line tool in Fiji [68].

3.9.2 Lysosomal morphology

To determine lysosomal morphology, cells were seeded on 8-well μ -Slide at a density of 3*10⁴ and allowed to adhere for 24 h before the indicated stimulation. After the stimulation, cells were incubated with 500 nM LysoTracker[™] Red DND-99 for 30 min and then nuclei staining

with Hoechst 33342 for 30 min. All images were observed by fluorescence microscopy, followed by diameter measurement using a straight line tool in Fiji [68].

3.9.3 Actin morphology

Cells were seeded on 8-well μ -Slide for 24 h prior and rinsed with PBS twice, followed by fixation with 4% formaldehyde solution for 20 min on ice. Next, cells were permeabilized using 0.5% TritonX-100 for 10 min at RT on the shaker. After three times rinsing with PBS for 5 min each, cells were incubated with 1% BSA for at least 1 h in RT, followed by Rhodamine Phalloidin staining and together with Hoechst 33342 (2.5 μ g/ml) for 1 h at RT on the shaker. Cells were rinsed 3 times with 1X PBS for 5 min each, mounted with Fluorsave reagent, and sealed with a coverslip. All images were observed and obtained by fluorescence microscopy.

3.9.4 E-cadherin morphology

Cells were seeded on 8-well μ -Slide for 24 h prior and rinsed with PBS twice, followed by fixation and permeabilization with methanol for 10 min at -20°C . Next, excessive methanol was removed and subsequently incubated with acetone for 1 min at -20°C . After being rinsed three times with PBS for 5 min each, cells were incubated with 1% BSA for at least 1 h in RT, followed by incubation with E-cadherin primary antibody (3195S, Cell signaling, Massachusetts, USA; 1:200 in 1% BSA) overnight. Cells were rinsed 3 times with 1X PBS for 5 min each and co-stained with Alexa Fluor 488, goat anti-rabbit IgG (A-11008, Invitrogen, Massachusetts, USA; 1:400 in 1% BSA) and Hoechst 33342 (2.5 μ g/ml) for 1 h at RT on the shaker. Cells were mounted with Fluorsave reagent and sealed with a coverslip. All images were observed and obtained by fluorescence microscopy.

3.10 Transmission electron microscopy (TEM)

Observation of mitochondria and lysosomes via TEM was conducted by Yaschar Kaibiri (Prof.Zischka, Technical University of Munich, Germany). Samples were subjected to electron microscopy with minor variations from previous study [69]. Briefly, 3×10^5 cells were immediately pelleted, fixed in 2.5% glutaraldehyde, fixed with 1% osmium tetroxide, dehydrated with acetone, and embedded in EPON resin. Ultra-thin sections were stained with lead citrate and UranylLess and imaged on a 1200EX electron microscope at 60 kV. Electron micrographs were recorded with a KeenView II digital camera with iTEM Ver. 5.0 (analySIS FIVE, Olympus, Germany).

3.11 Western blot

3.11.1 Cell lysis and total protein isolation

Cell samples were harvested and washed by ice-cold PBS twice. After centrifugation (400 xg, 5 min, RT), RIPA lysis buffer was added into cell lysates and stored at -80°C for at least 1 h. The cells were scraped repeatedly and transferred into 0.5 mL microtubes, followed by centrifugation (20,000 xg, 10 min, 4°C). The supernatant was collected and transferred to new 0.5 mL microtubes. To determine the protein concentration, all samples were diluted 1:5 and were assessed by Bradford Assay to detect absorbance at 592 nm using SpectraFluor Plus™. The final protein concentration was calculated from a linear regression formula established from BSA diluted standard curve. Each cell lysate was further synchronised by adding a 1X SDS sample buffer. The samples were then kept at -20 °C until Western Blot analysis.

3.11.2 Sodium Dodecyl Sulfate Polyacrylamide Gel Electrophoresis (SDS-PAGE) and Immunoblotting

An equal amount of protein was separated by SDS-PAGE in electrophoresis buffer (100 V, 21 min then 200 V, 43 min) and then transferred to nitrocellulose membranes in 1X tank buffer (100 V, 90 min, 4 °C). The membranes were incubated with blocking buffer (5% BSA in PBS with 0.1% Tween 20) for 1 h, followed by incubating with primary antibody overnight at 4°C. The primary antibody was removed, and the membrane was washed 3 times by 1X TBS-T for 5 min each. The membrane was then exposed to secondary antibodies for 1 h, followed by 3 washing steps with TBS-T for 5 min each. Membranes were conjugated with ECL solution with 2.5 mM luminol afterwards, and conjugated proteins were detected by the ChemiDoc™ Touch Imaging System (Bio-Rad). The bands were identified by comparison with Page Ruler™ Plus Prestained Protein Ladder. The protein level was normalised with total protein level and quantified by Image Lab™ Software (Bio-Rad).

Materials and Methods

RIPA Lysis buffer		Separation Gel	6-12 %
Tris/HCL	50 mM	Rotiophorese™ Gel 30	40-80%
NaCl	150 mM	Tris (pH 8.8)	375 mM
Nonidet NP-40	1%	SDS	0.1 %
Sodium deoxycholate	0.25%	TEMED	0.1 %
SDS	0.10%	APS	0.05%
H2O			
Added before use:			
Complete® EDTAfree	4 mM		
PMSF	0.5 mM		
Activated Na ₃ VO ₄	2 mM		
5X SDS sample buffer		Electrophoresis buffer	
Tris/HCL pH6.8	3.125 M	Tris	4.9 mM
Glycerol	50 %	Glycine	38 mM
SDS	5%	SDS	0.1 %
DTT	2 %	H2O	
Pryonin Y	0.025 %		
H2O			
TBS-T (pH 7.6)		Tank buffer	
Tris/HCL	50 mM	Tris base	48 mM
NaCl	150 mM	Glycine	39 mM
Tween 20	0.05%	Methanol	20 %
		H2O	

Table 12. Buffers and solutions for western blot analysis

Antigen	Product Number	Providers	Dilution
PARP	9542	Cell Signaling	1:1000
Caspase 3	sc-7148	Santa Cruz	1:1000
Caspase 3, active	C8487	Sigma Aldrich	1:1000
OPA-1	80471	Cell Signaling	1:1000
eIF2 α	sc-133132	Santa Cruz	1:1000
phospho-eIF2 α	9721	Cell Signaling	1:1000
Lamp2	51-200	Invitrogen	1:2000
E-cadherin	3195	Cell Signaling	1:1000
N-cadherin	4061	Cell Signaling	1:1000
Podoplanin	Sc-134483	Santa Cruz	1:1000
Rac1	05-389	Upstate	1:1000
LC-3	4108	Cell Signaling	1:1000
SQSTM1/p62	8025	Cell Signaling	1:1000

Table 13. Primary antibodies for western blot analysis

Antigen	Product Number	Providers	Dilution
goat anti-mouse IgG1, HRP	BZL07046	Biozol	1:1000
goat anti-rabbit IgG (H+L)-HRP conjugate	172-1019	Bio-Rad	1:1000

Table 14. Secondary antibodies for western blot analysis

3.12 Seahorse measurement

The cellular mitostress was performed using an Agilent Seahorse 96XF device according to the manufacturer's protocol (#103020-400, #103015-100). In brief, cells were seeded and pre-treated for 24 h. The medium was replaced by Seahorse medium one hour before measuring. For the mitostress test, 1,5 μ M oligomycin, 0,5 μ M FCCP, and 0.5 μ M Rotenone/Antimycin A were automatically injected into the Seahorse cartridge. Hoechst 33342 was simultaneously injected at the end of the test, and cell density was subsequently measured by BioTek Cytation Cell Imaging Reader. The data were normalised with cell intensity and analysed by Seahorse Wave Software (Agilent Technologies).

3.13 High-resolution respirometry

High-resolution respirometry experiments were conducted by Yaschar Kaibiri (Prof. Zischka, Technical University of Munich, Germany). Mitochondrial respiration was measured using an Oxygraph-2k and described previously [70]. Briefly, cells were centrifuged, resuspended in the culture medium, and injected into the chamber of the oxygraph for stimulation and measurement of cellular oxygen consumption. Data were analysed using Datlab 6.1.

3.13.1 Mitochondria isolation

Mitochondria from the cell culture were isolated as previously described [71] with minor variations. Briefly, cell suspensions were pumped through cell homogeniser three times at a flow rate of 1000 $\mu\text{L}/\text{min}$ and a clearance of 6 μm . The homogenate was centrifuged at 1000 $\times g$ (10 min, 4 $^{\circ}\text{C}$), and the resulting supernatant was centrifuged at 10000 $\times g$ (10 min, 4 $^{\circ}\text{C}$) to obtain a pelleted mitochondrial fraction.

3.14 Migration assays

3.14.1 Boyden chamber

One hundred thousand cells were seeded on an 8 μm pore size Boyden chamber insert with starvation medium (without FCS). Next, the insert was placed in a 24-well plate, which was filled with a complete medium. The chamber was incubated at 37 $^{\circ}\text{C}$ for 24 h for MDA-MB-231 and SKMEL5 or 6 h for RIL175. The inserts were then stained with crystal violet for 2 minutes and rinsed by ddH₂O twice. The immobile cell was removed using a cotton swab. Migrated cells were observed under a light microscope and counted by ImageJ.

3.14.2 Microcontact printing live-cell imaging

The circular micropatterning was performed as previously described [72]. In brief, uncoated $\mu\text{-Slide 8 Well}$ was conducted plasma treatment using plasma cleaner at 0.3 bar for reactivation, followed by incubation with 0.05 mg/mL of fibronectin for 2 h. After washing with Milli-Q H₂O, a highly activated surface was stamped with a PDMS circular pattern. The PDMS pattern was created with 11.25 mg of PDMS and 1.25 mg of polymerizer. The PDMS was homogenously mixed for 2 – 3 min and poured into a template dish, followed by 2 times vacuum and incubated overnight at 60 $^{\circ}\text{C}$. Next, $\mu\text{-Slide}$ was treated with plasma cleaner to eliminate the fibronectin coating in the surrounding area. The 7 μL of 1 mg/mL PLL(20)-g[3.5]-

PEG-N3(3) (APP) was added for 30 min in RT. The APP was rinsed with Milli-Q H₂O, and 80,000 cells were seeded, followed by 24 h incubation. The medium was removed, and the cell population was stained with Hoechst 33342 for 20 min. After that, the circular cell population was rinsed twice using a stain-free medium and replaced with 250 μ L fresh complete medium. The suitable circular cell population was observed using Eclipse Ti inverted microscope with a 10x phase contrast objective. Finally, 10 μ L of 100 μ M BCN-cRGDfk was added to initiate cell migration.

3.15 Statistical analysis

All figures are indicated as mean \pm SD (standard deviation) of at least 3 independent experiments unless stated otherwise. The significant symbol indicated as following: *, p-value<0.05, **, p-value <0.01, ***, p-value<0.005, and ****, p-value<0.0001. Statistical differences for the two groups were calculated using either a two-tailed Student's t-test or a one-tailed Student's t-test. For comparison, for more than 2 groups, one- or two-way Analysis of Variance (ANOVA) was applied and followed by a stated posthoc test. Sketch and calculation were performed with Prism 8.

RESULTS



4 Results

4.1 Part 1: Lysosomal ion channel TRPML1, a novel regulator of mitochondrial function in hepatocellular carcinoma cells

4.1.1 Generation of a cellular model with CRISPR/Cas9 system to study TRPML1 function

In order to study TRPML1 function in HCC cells, we established a model system for activating or inhibiting the TRPML1 channel function. Several TRPML1 activators are available and extensively utilised, such as ML-SA1, MLSA-5 and MK6-83. However, these activators lack specificity for TRPML1 since they activate TRPML2 and TRPML3 as well [65, 73, 74]. Recently, our collaborator (Dr. Eva Plesch, Prof. Bracher, Department of Pharmacy, LMU Munich) developed an isoform-selective activator for TRPML1, which is modified from MLSA-1 by substituting 4 additional chlorine groups in the phthalimide subunit (**Figure 10A**). The selectivity of the ML1-SA1 has been reported in previous literature [75]. Hence, we have utilised this selective TRPML1 activator to study biological consequences after the channel's activation, and we generated a TRPML1 knockout cell line using the CRISPR/Cas9 system. We deleted exon 2 of the MCOLN1 gene, which is encoded for channel pore (**Figure 28**), as described previously [62]. Next, an endolysosomal patch-clamp was performed by Dr. Yu-Kai, Chao and Rachel Tang (Prof. Grimm, Walther Straub Institute of Pharmacology and Toxicology, LMU Munich) to validate knockout clone, and data were obtained as described previously [64]. Aside from TRPML1 wildtype (WT, **Figure 10B**), knockout (KO, **Figure 10C**) cells showed an absence of TRPML1 currents after ML1-SA-1 activation (**Figure 10D**), which confirmed a successful loss-of-function of TRPML1. The successful deletion of exon 2 was further confirmed by Sanger-Sequencing PCR methods (**Figure 28**). It is noticeable that sgRNA can bind to an undesired target, creating off-target cleavage [76]. Therefore, we next detected putative off-target sequences with top 10 cutting frequency determination (CFD) score by PCR. We confirmed that none of the off-target sequences were eliminated from the TRPML1 KO clone (**Table 16, Table 17**). In summary, we have generated a cellular model in which we can activate TRPML1 specifically and in which we have successfully depleted the TRPML1 channel in Ril175 cells (TRPML1KO) to study the consequences of both over-activation and depletion.

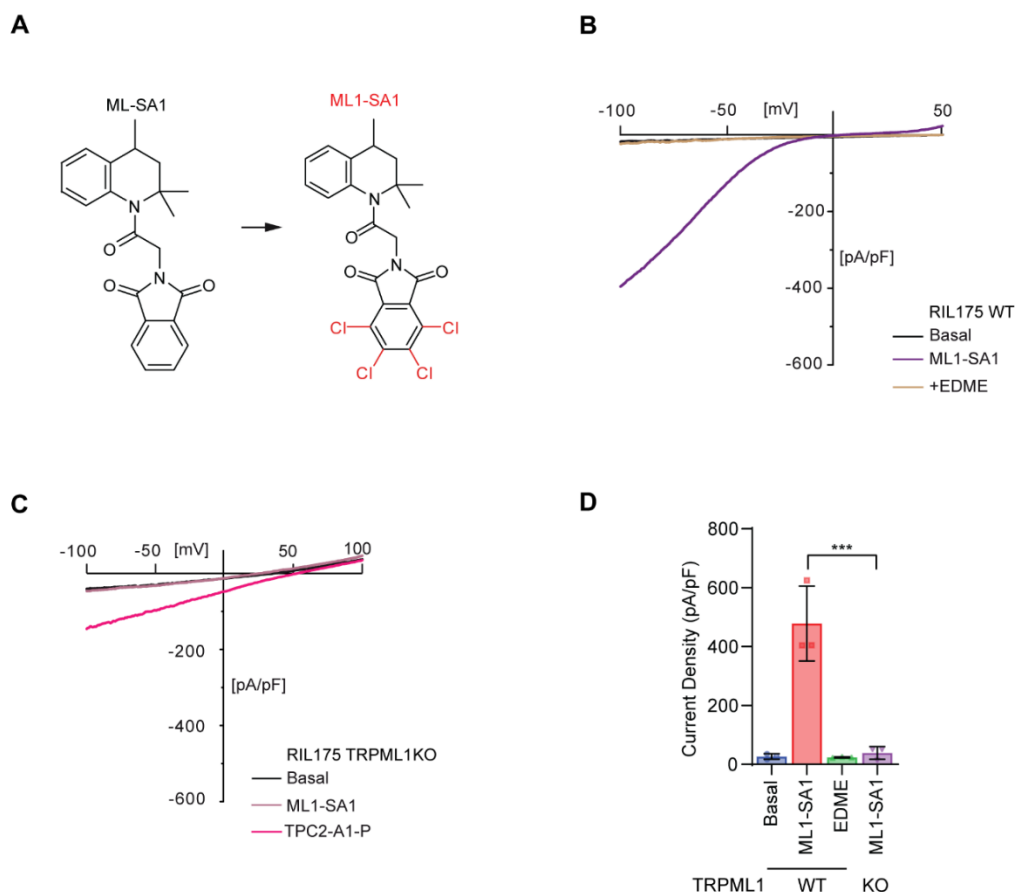


Figure 10. Generation of a cellular model to study TRPML1 function.

(A) Chemical structures of ML-SA1 and ML1-SA1. (B, C) Representative I/V-plots of whole-endolysosome recordings from RIL175 WT (B) and TRPML1 KO (C) cells after treatment with ML1-SA1, TPC2-A1-P or EDME. TRPML1 inhibitor EDME [36] and TPC2 activator TPC2-A1-P [77] served as experimental controls. (D) Statistical analysis of current densities evoked by treatment. Results represent mean \pm SEM; $n = 3$; One-way ANOVA, followed by Tukey's posthoc test ***, p -value < 0.005 .

4.1.2 Functional characterisation of cellular activation and knockout models

To investigate the role of TRPML1 in anti-cancer therapy for HCC, we performed cell viability tests on various HCC cell lines and on the non-malignant endothelial cell line HUVEC (**Figure 11A**), which express TRPML1 (**Figure 11B**). We determined IC_{50} values for ML1-SA1 are in the low micromolar range and are significantly higher than HUVEC and TRPML1 KO cells (**Figure 11A**, **Table 15**), suggesting that the compound is TRPML1 specific and underlying a certain degree of cancer specificity.

Cell lines	IC ₅₀ [μM]	p-value ¹
RIL175 WT	16.44	<0.0001
RIL175 TRPML1KO	36.45	<0.0001
HUH-7	6.31	<0.0001
HepG2	9.97	<0.0001
Hep3B	5.24	<0.0001
HUVEC	24.09	<0.0001

Table 15. Cytotoxicity of ML1-SA1 in different cells.

HCC and non-malignant (HUVEC) cell lines were assessed by CellTiter® Blue cell viability assay. Data were analysed by a non-linear curve fit log(inhibitor) vs response -- variable slope (four parameters) IC₅₀ values have been compared by extra sum-of-squares F-test.

To analyse whether ML1-SA1 enhanced cell death contributed to TRPML1 activation, an Annexin V/PI apoptosis assay was performed (**Figure 11C**). Channel activation by ML1-SA1 increased early and late apoptosis in concentrations starting from 30 μM. TRPML1 KO was shown to have no influence on basal apoptosis levels. Notably, cytotoxicity of ML1-SA1 did not induce apoptosis in TRPML1 KO cells up to 50 μM. Therefore, these results indicate that apoptosis and cytotoxicity in wild type cells were caused by TRPML1 activation, not by off-target cytotoxicity (**Figure 11C**). To further validate apoptosis induction of ML1-SA1, detection of PARP cleavage and caspase 3 activation were performed (**Figure 11D-F**). The cleavage of PARP and activation of Caspase 3 are considered as cells undergoing apoptosis. Both protein levels are significantly increased at concentrations of 30-50 μM. Similarly, TRPML1 KO showed no effect on apoptosis marker expression levels as well as ML1-SA1 treatment of TRPML1 KO cells. These results suggested that TRPML1 activation is relevant for apoptosis induction. Furthermore, our tools and models are appropriate to study the role of TRPML1 function in HCC cells.

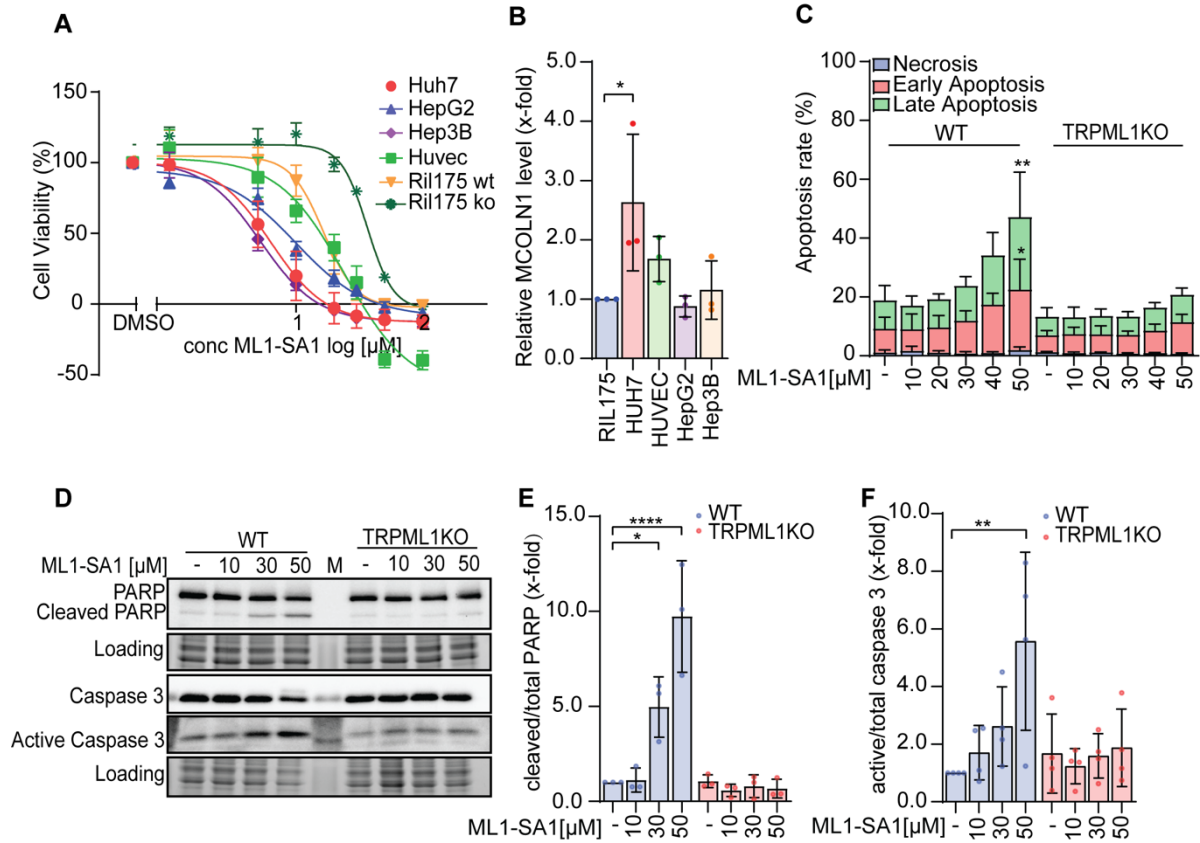


Figure 11. Functional characterisation of TRPML1 function in HCC cells.

(A) Proliferation of different cell lines after ML1-SA1 treatment was assessed by CellTiter Blue™ assay. (B) Relative mRNA levels of MCOLN1 were determined by qPCR in different cell lines. (C) Quantification of apoptotic cells was determined by Annexin V-PI staining and followed by flow cytometry after 48 h treatment. (D) Western Blot of PARP, Caspase 3 and Active Caspase 3 protein level after 24 h treatment of indicated concentration of ML1-SA1. One representative image is shown. Quantification of (E) cleaved PARP/total PARP level and (F) active Caspase 3/total Caspase 3. Results represent mean \pm SD, n=3; two-way ANOVA for C-F and One-way ANOVA for B, followed by Tukey's posthoc test *, p-value <0.05, **, p-value <0.01, and ****, p-value <0.0001.

4.1.3 TRPML1 plays a critical role in the regulation of mitochondrial morphology

Following previous experiments, we established a suitable cellular model to determine cellular outcomes triggered by modulating the TRPML1 function. Next, we analysed the proteome in untreated RIL175 cells and compared it with TRPML1 activated or TRPML1 KO cells. Protein mass spectrometry was conducted by Dr. Flenkenthaler (Dr. Fröhlich, Gene Center Munich, Laboratory for Functional Genome Analysis, LMU Munich). Over 3,000 proteins were identified and several proteins were changed in abundance by ML1-SA1 treatment (**Figure 12A**) and TRPML1 KO (**Figure 12B**). A functional gene-set enrichment analysis between ML1-SA1 treated and untreated cells demonstrated that several proteins related to mitochondrial structure and mitochondrial function were downregulated (**Figure**

12C). Functional analysis of TRPML1 KO cells depicted trend deregulation in mitochondrial regulatory circuits and an apparent upregulation of glutathione metabolism (**Figure 12D**).

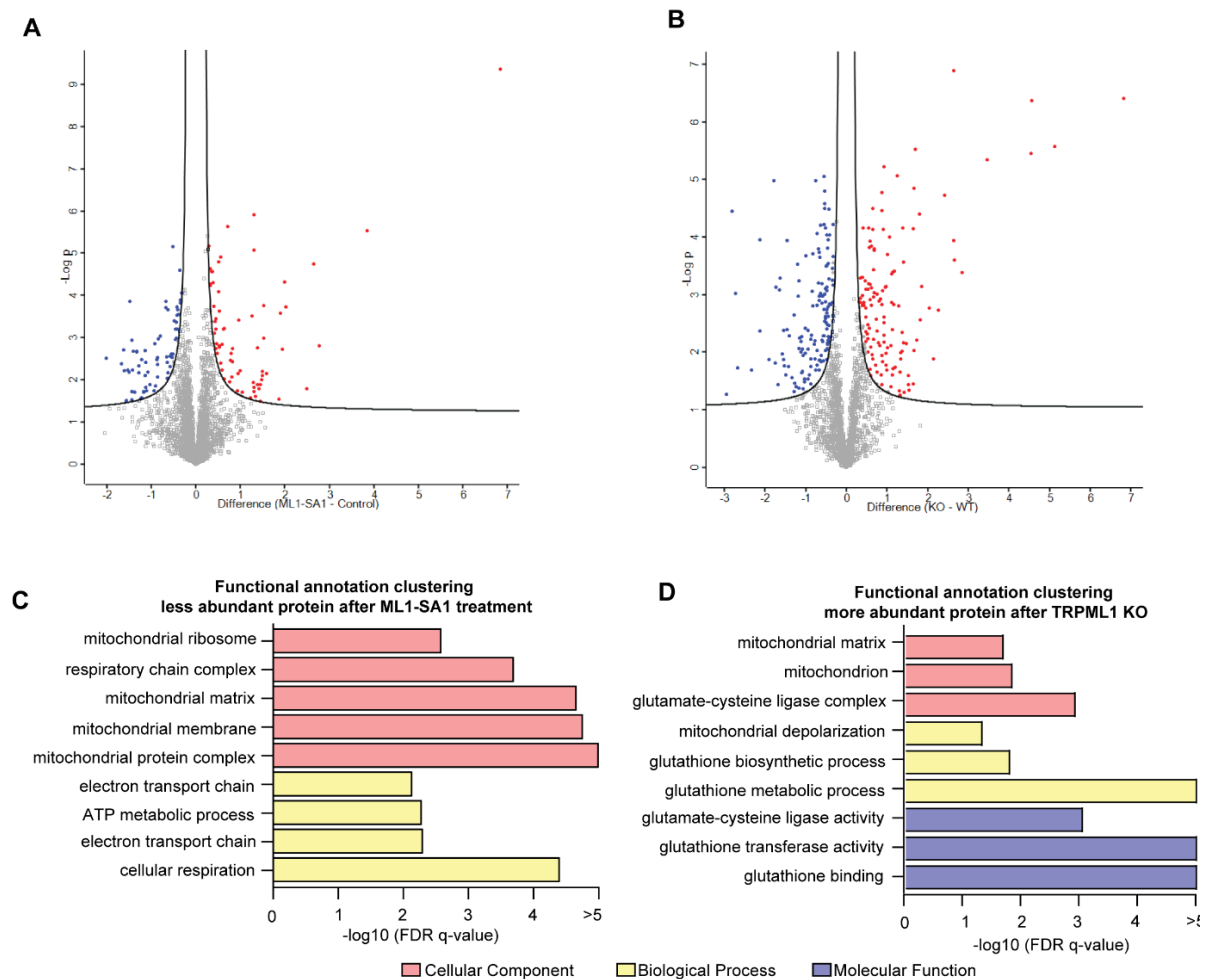


Figure 12. Proteome analysis of ML1-SA1 treated and TRPML1 KO cells.

(A) Aberration of the ML1-SA1 treated vs untreated RIL175 WT cell and (B) WT vs TRPML1 KO cell proteome. Proteins differentially more abundant in ML1-SA1 treated or TRPML1 KO are highlighted in red. Proteins less abundant in ML1-SA1 treated or TRPML1 KO are highlighted in blue (p -value < 0.05 ; \log_2 -fold change $> |0.6|$). (C) Proteomic analysis was performed by LC-MS/MS. Gene set enrichment analysis (GSEA) showed significantly enriched gene sets of 30 μ M ML1-SA1 treated vs untreated cells with FDR q -value ≤ 0.05 . The STRING data analysis indicates downregulated protein clusters after ML1-SA1 treatment. The protein-protein interaction map of protein hits after ML1-SA1 treatment is created with string-db.org, proteins with values/ranks-functional enrichment analysis (permanent link: shorturl.at/kHNOR). (D) The STRING data analysis indicates up-regulated protein clusters in TRPML1 KO cells. The protein interaction map of protein hits more abundant and less abundant in TRPML1 KO cells was analysed by multiple protein analysis in string-db.org. (more abundant - permanent link: shorturl.at/jEL68 and less abundant - permanent link: shorturl.at/hwCJ5). The gene ontologies of the cellular component, the biological process, and the molecular function are coded in pink, yellow, and purple, respectively. The x-axis shows the enrichment significance in $-\log_{10}$ (FDR q -value).

Along with these findings, we decided to further investigate the morphology and function of mitochondria after modulating the TRPML1 function. In order to observe mitochondria morphology, cells were stained with MitoTracker™ Red and followed by confocal microscopy. The confocal images revealed that TRPML1 activation by ML1-SA1 led to a morphological alteration (**Figure 13A**). The mitochondrial length upon ML1-SA1 treated and TRPML1 KO cells were measured and revealed that the shape of mitochondria was shifted from elongated mitochondria to short, round-shaped structures in RIL175 as well as HUH7 cells (**Figure 13B**). Interestingly, an identical phenotype was observed in TRPML1 KO cells (**Figure 13A, B**). Since we observed an altered phenotype upon TRPML1 KO cells, we introduced a potent TRPML1 inhibitor, 17 β -estradiol methyl ether (EDME), to mimic the knockout effect. Similar results were observed up to 50 μ M EDME treated RIL175 WT (**Figure 13A, B**). Next, a more detailed analysis of mitochondrial morphology using transmission electron microscopy was performed by Yaschar Kaibiri (Prof. Zischka, Institute of Toxicology and Environmental Hygiene, TUM Munich). Further, the analysis validated the switch of an elongated morphology in wildtype cells to short, round-shaped mitochondria in both ML1-SA1 treatment or TRPML1 (**Figure 13C**). In particular, TRPML1 activation by ML1-SA1 leads to a reduction in mitochondrial roundness and cristae density (**Figure 13D**), which is associated with aggravated mitochondrial function. These results demonstrated that mitochondrial morphology is strongly altered by modulating TRPML1 function either by activation or knockout.

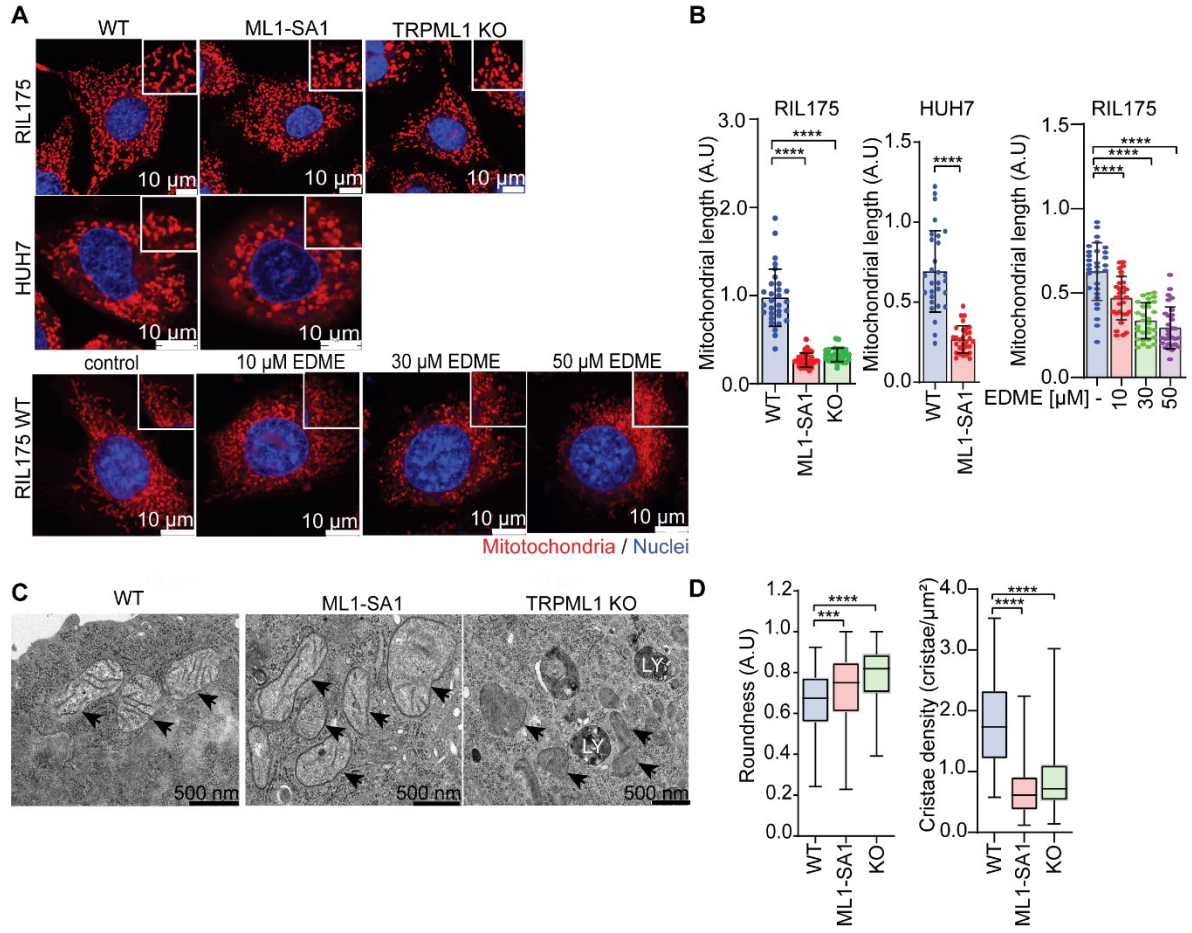


Figure 13. TRPML1 regulates mitochondrial morphology.

(A) The mitochondrial morphology of ML1-SA1 treated RIL175 WT or TRPML1 KO (30 μ M) or HUH7 (5 μ M) and EDME treated RIL175 WT were observed by Mitotracker red (mitochondria) and Hoechst 33342 (nuclei) using confocal live-cell imaging. Scale bar: 10 μ M. One representative image is shown. (B) Mitochondrial length of 30 cells per replicate was quantitatively measured by Image J. (C) Representative TEM images of WT, 30 μ M ML1-SA1 treated, and TRPML1 KO cells; scale bar: 500 nm. (D) The roundness and (E) cristae density (number of cristae/ area of mitochondria) of WT, TRPML1 KO and ML1-SA1 treated RIL175 cells were quantified by Image J. A total of 150 mitochondria per replicate were measured in D, and 100 mitochondria in E. Results represent mean \pm SD; n=3 for A-E; One-way ANOVA, for B and E, followed by Dunnett's posthoc test; Kruskal-Wallis test for D, followed by Dunn's posthoc test. ***, p-value <0.005, and ****, p-value <0.0001.

4.1.4 Modulation of TRPML1 activity interferes with mitochondrial function

Since modulation of TRPML1 showed an apparent alteration of mitochondrial structure, we further investigated mitochondrial integrity and respiratory capacity. To assess the damage of mitochondria, we used lipophilic cationic molecular probe JC1 to measure membrane potential. Shifting from red to green fluorescence of JC1 indicates a loss of membrane potential ($\Delta\psi$ m) and illustrates mitochondrial damage. Activation of TRPML1 by ML1-SA1 strikingly reduced mitochondrial membrane potential, as well as in TRPML1 KO cell (**Figure**

14A). Notably, a similar effect could be observed with other commercialised TRPML1 agonists, for instance, MLSA1 (**Figure 14B**), MK6-83 (**Figure 14C**) and MLSA5 (**Figure 14D**). Depolarisation of mitochondrial $\Delta\psi_m$ is often related to mitochondrial membrane permeability transition (mPT), which is regulated by a specific protein, namely, mitochondrial permeability transition pore (mPTP) in the inner membrane of mitochondria. Opening of mPTP can be inhibited by cyclosporin A (CsA). The combination of ML1-SA1 with CsA showed a rescue effect upon mitochondrial depolarisation, thereby suggesting a loss of membrane potential mediated by mPTP activation (**Figure 14E**).

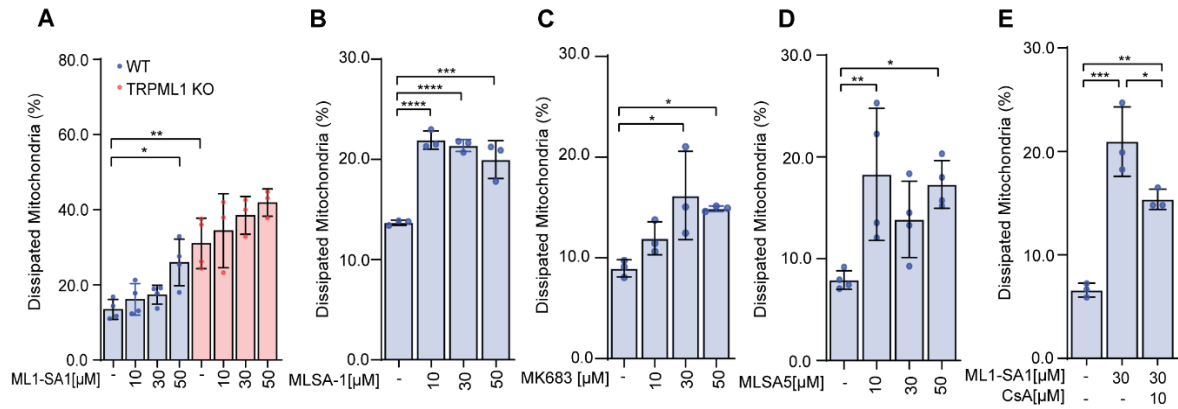


Figure 14. TRPML1 activity alters mitochondrial membrane potential by regulating mPTP.

The mitochondrial membrane potential of (A) RIL175 WT and RIL175 TRPML1 KO cells after 24 h stimulation with indicated concentrations of ML1-SA1 were measured by flow cytometry after JC1 staining. TRPML1 activators (B) ML-SA1, (C) MK6-83, and (D) MLSA5 were measured by flow cytometry after JC-1 staining. (E) JC-1 staining of RIL175 cells with or without pretreatment with the mPTP inhibitor cyclosporin A (CsA) for 2 h prior to the 24 h incubation with ML1-SA1. Results represent mean \pm SD, n=3, n=4 for A, n=4 for D; One-way ANOVA, followed by Dunnett's posthoc test; Sidak's posthoc for A; Tukey's posthoc for E; *, p-value <0.05, **, p-value <0.01, ***, p-value <0.005, and ****, p-value <0.0001.

To further validate the effect of TRPML1 upon mitochondrial function, we monitored cellular oxygen consumption rates (OCR) as a measure of mitochondrial respiration using a Seahorse Extracellular Flux analyser with mitostress test. In the mitostress test, different inhibitors were added stepwise to determine mitochondrial function. First, oligomycin, an inhibitor of ATP synthase, is added, which strongly reduces mitochondrial oxygen consumption and allows the calculation of basal respiration. Secondly, uncoupling agent FCCP is added, collapsing the proton gradient and causing maximal oxygen consumption. Lastly, rotenone (Rot) and antimycin A (AA) are added consecutively to inhibit mitochondrial function and determine non-mitochondrial oxygen consumption. The results of ML1-SA1 pre-treated RIL175 cells shows a reduction of basal respiration, ATP production and maximal respiratory

capacity of mitochondria in a dose-dependent manner (**Figure 15A**), indicating that activation of TRPML1 leads to mitochondrial dysfunction. Although TRPML1 KO was prominently altered upon mitochondrial structure (**Figure 13A**), we could only observe a slight decrease in basal respiration and ATP production and no changes in maximal respiratory capacity (**Figure 15B**). To further validate these findings, we analysed cellular ATP levels using a luminescence-based ATP detection assay. The ATP detection assay confirmed a significant reduction in cellular ATP upon ML1-SA1 treatment and no significant change upon TRPML1 KO, consistent with the mitostress test (**Figure 15C**). These data demonstrated that even if mitochondria are structurally altered by ML1-SA1 activation and loss of function, functional consequences could vary in quantity and quality.

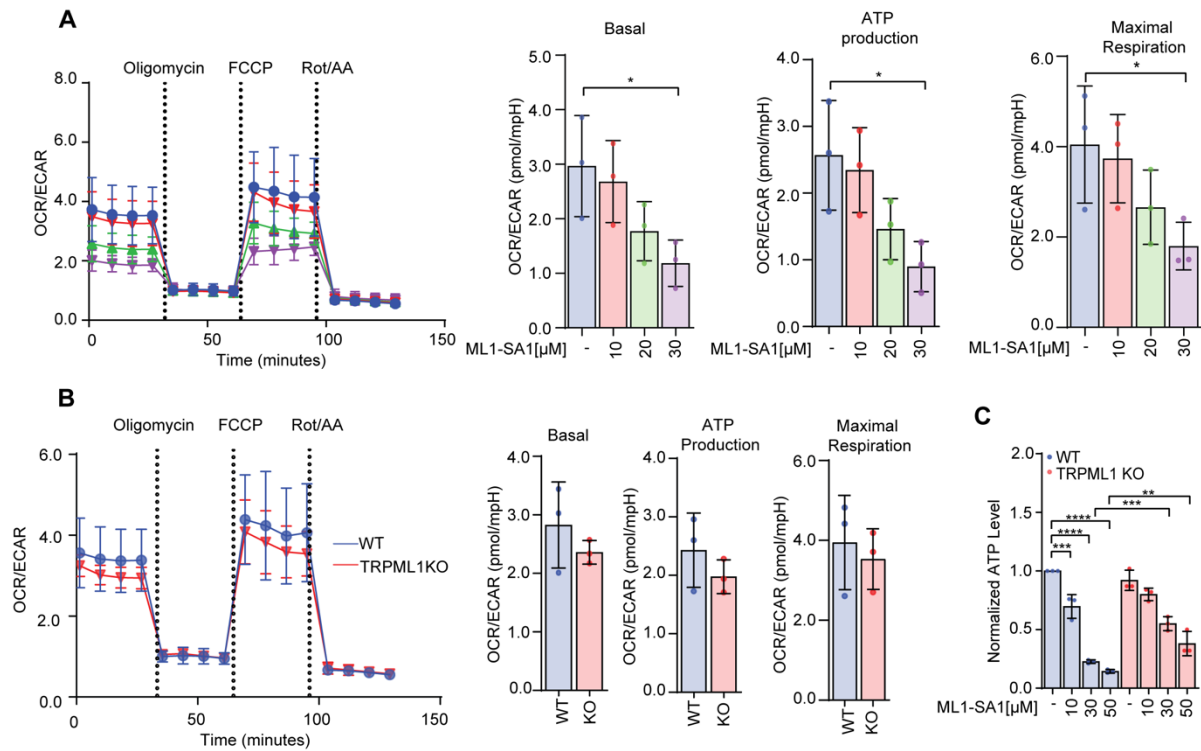


Figure 15. TRPML1 activity regulates mitochondrial function.

Extracellular acidification rate (ECAR) and oxygen consumption rate (OCR) were measured in RIL175 cells in the mitostress test using a Seahorse 96XF analyser. The ratio of OCR/ECAR was calculated to indicate the measure of metabolic phenotype. (A) RIL175 WT cells were pre-treated with 10, 30 and 50 μ M of ML1-SA1 for 24 h and followed by ATP production and maximal respiration of ML1-SA1 treated cells. (B) RIL175 WT and TRPML1 KO cells were compared. The SeahorseTM measurement was normalised to cell number prior to calculation of OCR/ECAR ratio. (C) ATP levels of RIL175 WT and TRPML1 KO with or without ML1-SA1 treated cells were determined by CellTiter GloTM assay. Results represent mean \pm SD, n=3; One-way ANOVA, followed by Dunnett's posthoc test ; Sidak's posthoc test for A; Tukey's posthoc test for C; *, p-value <0.05, **, p-value <0.01, ***, p-value <0.005, and ****, p-value <0.0001.

4.1.5 TRPML1 activation induces mitochondrial stress via calcium overloading

How TRPML1 channel activation or loss of function leads to functional changes in mitochondria remains unclear. In order to discover the mechanistic regulation behind it, we next assessed the effects of TRPML1 activation on mitochondria in more detail. Since TRPML1 is a calcium permeable ion channel, we assessed intracellular calcium levels using a calcium-sensitive fluorescent dye, followed by flow cytometry. The results indicated that ML1-SA1 leads to a dose-dependent increase of intracellular calcium levels, but not in TRPML1 KO cells (**Figure 16A**). Additionally, using Rhod2/AM, a mitochondrial calcium-sensitive fluorescent dye, we showed mitochondrial calcium levels are increased after ML1-SA1 activation (**Figure 16B**), as well as in commercialised activators MLSA1 (**Figure 16C**), MK6-83 (**Figure 16D**), and MLSA5 (**Figure 16E**) but not after KO (**Figure 16A**). A more potent enhancement of mitochondrial calcium levels could be observed in HUH7 cells (**Figure 16F**).

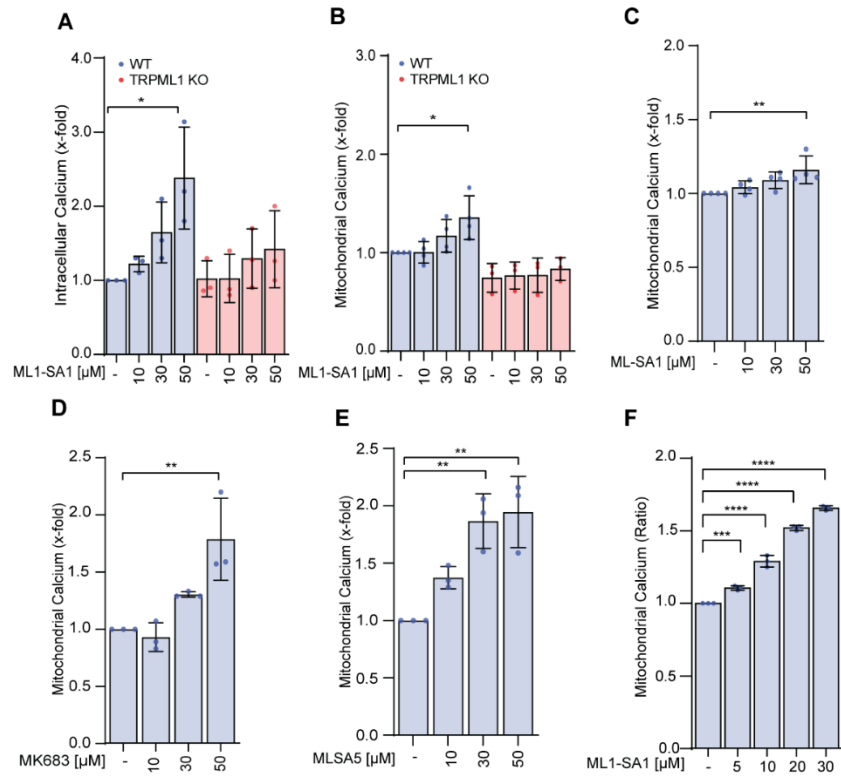


Figure 16. TRPML1 activation induces lysosomal calcium efflux and mitochondrial influx.

(A) Intracellular and (B) mitochondrial calcium levels after stimulation with ML1-SA1 in RIL175 WT cells for 24 h were measured by Cal520 and Rhod-2 staining and flow cytometry, respectively. Commercialised TRPML1 activators (C) ML-SA1, (D) MK6-83, and (E) MLSA5 were used for mitochondrial calcium measurements by Rhod-2 and flow cytometry. (F) Mitochondrial calcium was measured by Rhod-2 in the HUH7 cell line. Results represent mean \pm SD, n=3; n=4 for B,C; One-way ANOVA, followed by Dunnett's posthoc test; Tukey's posthoc test for A; Sidak's posthoc test for B; *, p-value <0.05, **, p-value <0.01, ***, p-value <0.005, ****, p-value <0.001.

Overloading calcium in mitochondria can lead to tremendous mitochondrial stress [78]. Therefore, we assessed mitochondrial reactive oxygen species (ROS), and we observed that treatment with ML1-SA1 led to an increase in mitochondrial ROS. Intriguingly, TRPML1 KO cells did not increase the ROS level, and the level was even slightly decreased (**Figure 17A**). An upregulation of glutathione metabolism might explain this somewhat puzzling effect in TRPML1 KO cells, indicated in proteome analysis (**Figure 12D**). Further, we assessed mitochondrial membrane protein marker, OPA-1, an inner mitochondrial membrane protein regulating mitochondrial fusion and cristae structure, contributing to ATP synthesis and apoptosis. The OPA1 is typically cleaved during mitochondrial stress [79, 80]. OPA-1 (L-OPA-1) analysis showed a clear induction of protein cleavage (S-OPA-1) (**Figure 17B, D**). We also assessed eIF2 α , a protein undergoing phosphorylation at early stress response in mitochondria, stabilising the mitochondrial function [81]. Our results indicated that eIF2 α phosphorylation is decreased upon TRPML1 activation and increased upon loss of channel function (**Figure 17B, C**). This finding supports the observed mitochondrial dysfunction is increased upon TRPML1 activation and increased upon loss of channel function (**Figure 17A-D**). Taken together, our data demonstrated that activating TRPML1 by ML1-SA1 abrogated mitochondrial morphology and function, which was caused by calcium overloading. Subsequently, the excessive amount of calcium could induce mitochondrial stress and mPTP opening, which can be impeded by adding CsA (**Figure 14E**).

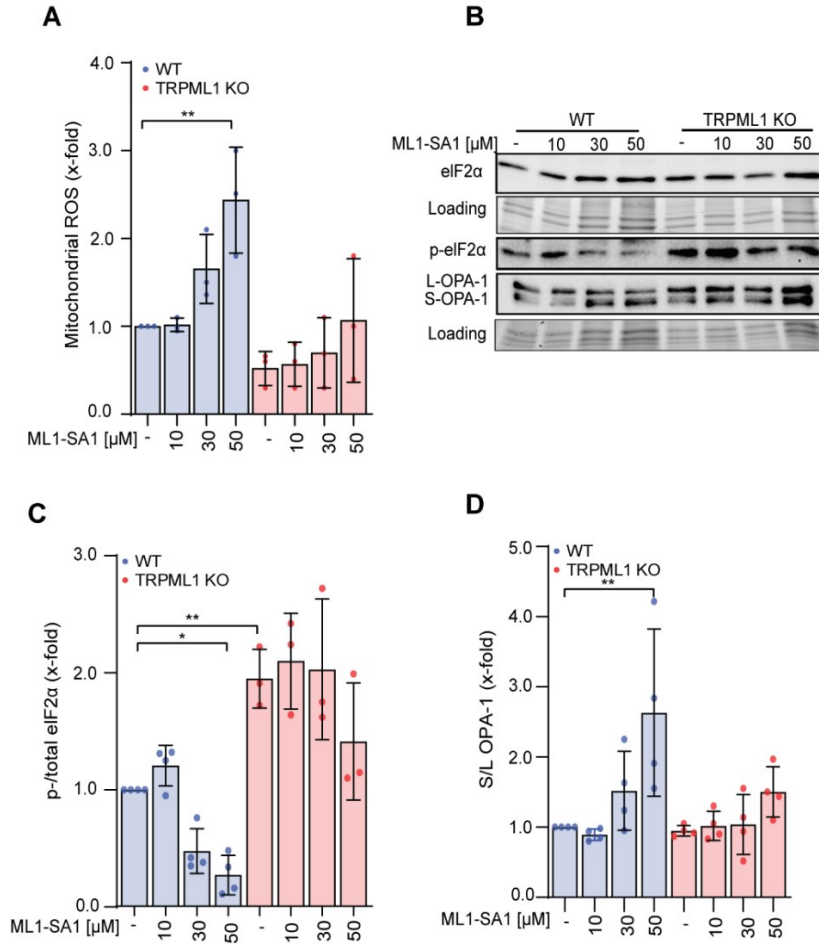


Figure 17. TRPML1 activation induces mitochondrial stress via calcium overloading.

(A) Oxidative stress in mitochondria after 24 h stimulation of ML1-SA1 was measured by MitoSox staining, followed by flow cytometry. (B) Representative Western Blots of mitochondrial functional proteins after 24 h stimulation with ML1-SA1. Quantification of (C) S/L -OPA1 and (D) p-/total eIF2α. Results represent mean \pm SD, n=3; n=4 for C,D. One-way ANOVA, followed by Tukey's posthoc test; Sidak's posthoc test for A and C; *, p-value <0.05 and **, p-value <0.01.

4.2 Loss of TRPML1 function disturbs mitochondrial function by deregulation of mitophagy

Since we observed activation or loss of function of TRPML1, resulting in a similar effect upon mitochondrial structure and function. However, effects on mitochondrial function upon TRPML1 KO have remained unclear (**Figure 11**, **Figure 13**). Although cells do not die from knockout (**Figure 11**), the proliferation of cells was significantly decreased after knockout or inhibition of TRPML1 activity (**Figure 18A, B**). As previously shown, mitochondrial function is likely to be impaired in KO mitochondria, as evidenced by a significantly elevated proton leak, which might explain that KO cells' proliferation is slower than WT cells.

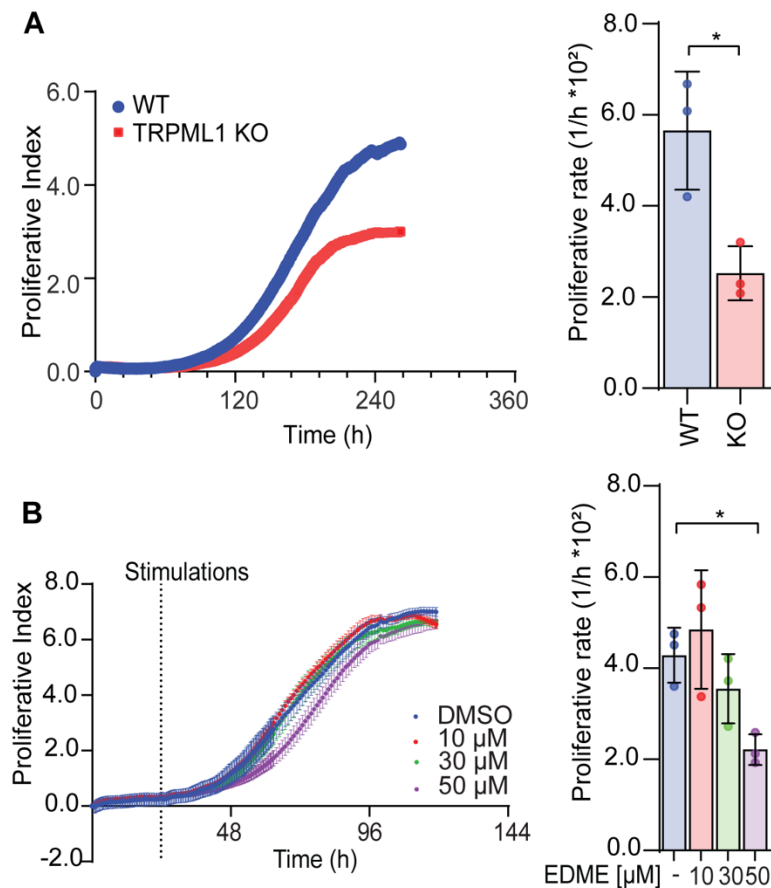


Figure 18. Loss of TRPML1 reduces cell proliferation.

(A) The proliferation of RIL175 WT and TRPML1 KO cells was determined by impedance measurements. (B) The proliferation of EDME treated RIL175 WT cells was determined by impedance measurements. Indicated concentrations of EDME was added at 23.4 h. Results represent mean \pm SD, $n=3$; unpair t-test for A, One-way ANOVA, followed by Dunnett's posthoc test for B; *, p -value <0.05 .

Next, our collaborator (Yaschar Kaibiri, Prof. Zischka, Institute of Toxicology and Environmental Hygiene, TUM Munich) used a high-resolution respirometry, Oroboros® O2k-fluorespirometer, to investigate how mitochondrial respiratory parameters are affected in TRPML1 KO cells. The detailed analysis of the contribution of different mitochondrial complexes was detected by the sequential addition of specific substrates or inhibitors (**Figure 19A**). We found a significant proton leak in KO cells (**Figure 19B**), which is consistent with the previously altered mitochondrial structure and membrane potential (**Figure 14A**). Furthermore, the respiratory control ratio (RCR) showed that NADH-linked respiration (complex 1, C1) and succinate-linked respiration (complex 2, C2) were decreased in KO cells. This decrease in RCR is highly related to an increased proton leak (LEAK) in TRPML1 KO cells since physiological respiration did not change (**Figure 19B**). In addition to RCR, we found that

non-mitochondrial respiration (residual oxygen consumption, ROX) increased after C1 inhibition with rotenone (**Figure 19C**). Intriguingly, the level of mitochondrial ROS was unchanged (**Figure 17A**), and surprisingly glutathione (GSH) metabolism was up-regulated upon TRPML1 KO (**Figure 12D**). Hence, GSH level was measured by Yaschar Kaibiri (Prof. Zischka, Institute of Toxicology and Environmental Hygiene, TUM Munich) in RIL175 WT and KO cells. In principle, GSH is oxidized to glutathione disulfide (GSSG) as the presence of ROS, thereby detoxifying cells from excessive ROS [82]. The result showed that the ratio between GSH and GSSG was decreased (**Figure 19D**), suggesting that KO cells detoxified ROS by facilitating GSH conversion. Together with mitostress data (**Figure 15B**), these results suggest that TRPML1 KO endowed impairment of mitochondrial phenotype and function. However, cells can somehow compensate for the loss in order to maintain respiration.

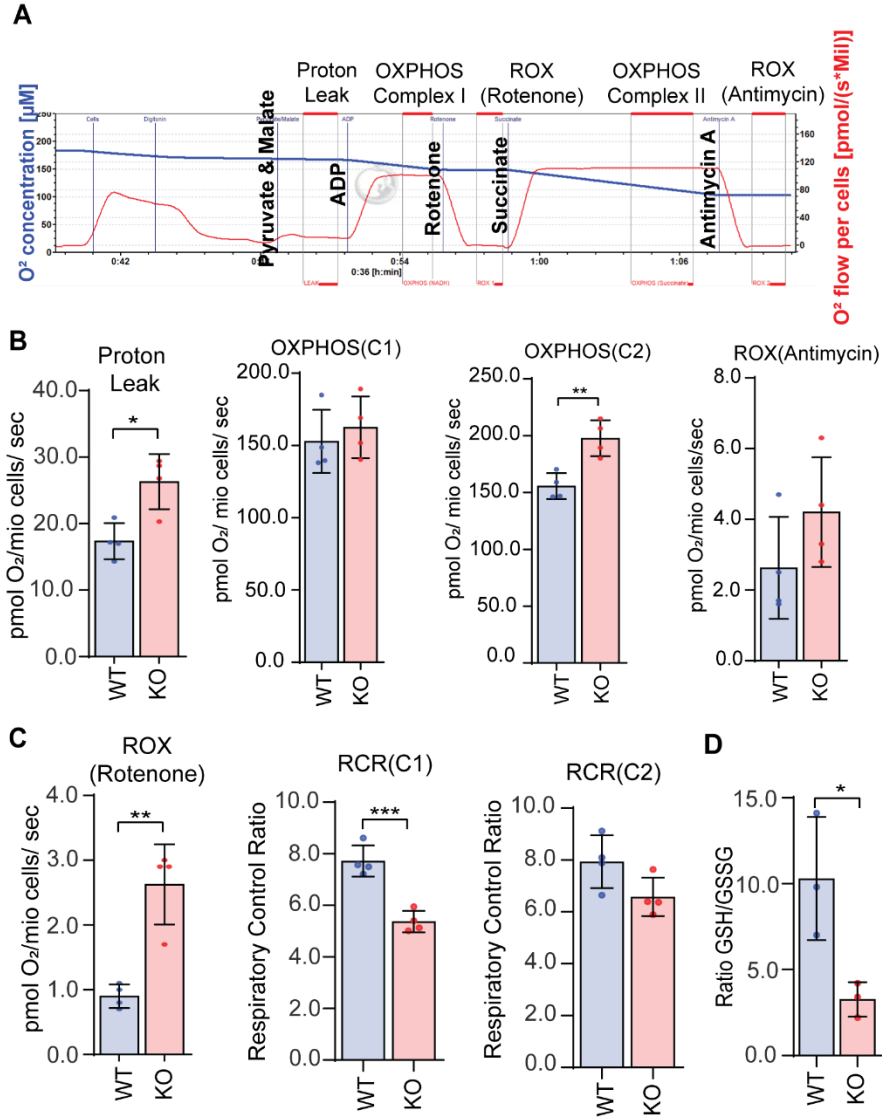


Figure 19. Loss of TRPML1 disturbs the mitochondrial respiratory function.

(A) Schematic figure for mitochondrial respiration measurements with Oroboros® O2k. (B) Impairment of mitochondria in RIL175 KO cells was revealed by Oroboros® O2K measurement. (C) Respiratory Control Ratio (RCR) was calculated to indicate mitochondrial efficiency (OXPHOS/LEAK). The values were corrected for residual oxygen consumption (ROX of antimycin). (D) The ratio of GSH and GSSG between WT and TRPML1 KO cells (n=4). Results represent mean ± SD, n=4; n=3 for D; unpair t-test; *, p-value <0.05.

Furthermore, we wanted to investigate how the loss of TRPML1 function leads to mitochondrial alterations. Since the loss of TRPML1 impairs autophagy and could subsequently disrupt mitochondrial turnover [83], we subsequently assessed the lysosome of RIL175 WT and KO cells. We observed lysosomal swelling in KO cells in confocal microscopy (**Figure 20A**) and transmission electron microscopy (**Figure 13C**) but did not affect lysosomal mass (**Figure 20B**). Moreover, the lysosome size in KO cells presents larger lysosomal structures with membranous inclusions (**Figure 20C**).

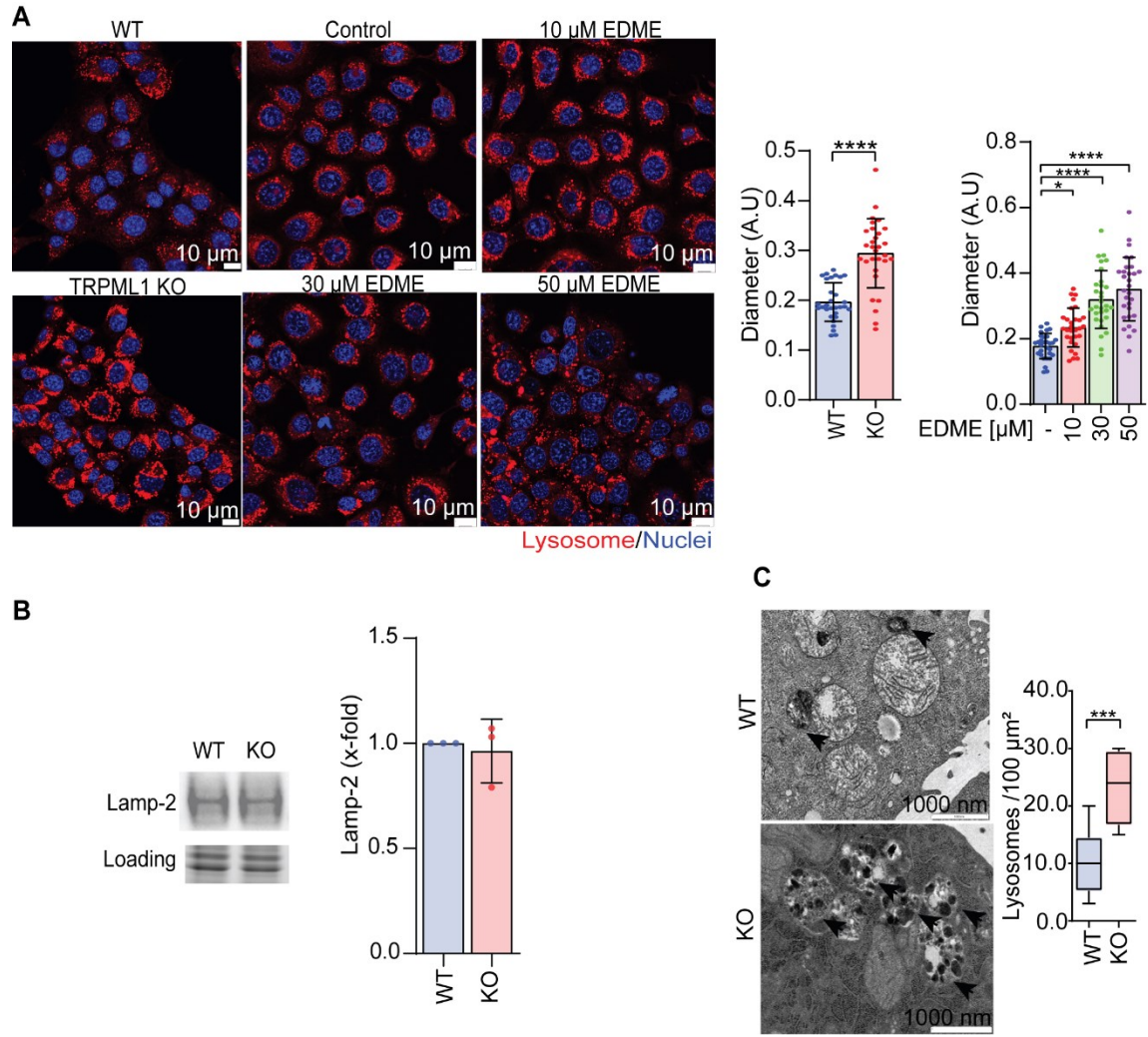


Figure 20. Loss of TRPML1 alters lysosome morphology.

(A) Morphology of lysosomes in RIL175 WT and TRPML1 KO was observed by lysotracker red staining, and the diameter of lysosomes was measured by Image J (n=30); scale bar = 10 μ m. (F) Representative TEM images of lysosome in WT and TRPML1 KO cells; scale bar: 1000 nm. Results represent mean \pm SD, n=3; unpair t-test; One-way ANOVA, followed by Tukey's posthoc test; *, p-value <0.05, ***, p-value <0.005, ****, p-value <0.001.

Since the lysosomal morphology was altered, we further investigated the mitophagy process. We detected autophagic flux by LC3-II turnover and degradation of autophagic substrate p62. An apparent decrease of autophagic flux and degradation of p62 (**Figure 21**) were observed in TRPML1 KO cells as well as EDME treated WT cells. These results suggest that loss of TRPML1 function might disturb the renewal of mitochondria and lead to a decrease in cancer cell proliferation.

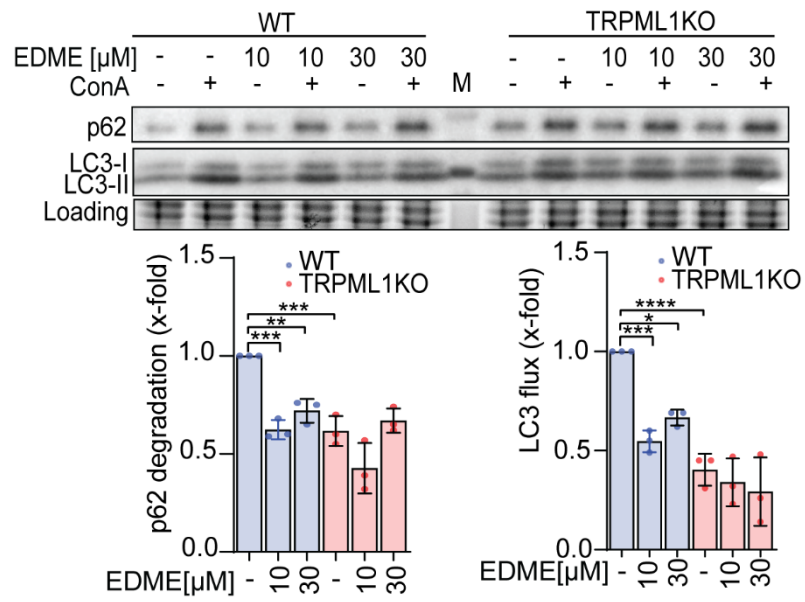


Figure 21. Loss of TRPML1 disrupts mitophagy.

(A) Representative western blot of mitophagy markers in RIL175 WT and TRPML1 KO. Quantification of LC3-II flux and p62 degradation were shown in H and I, respectively. Results represent mean \pm SD, n=3; One-way ANOVA, followed by Tukey's posthoc; *, p-value <0.05, **, p-value <0.01, ***, p-value <0.005, and ****, p-value <0.0001

4.3 Part 1: Summary

Here, we established a genetic TRPML1 knockout using the CRISPR-Cas9 model for investigating the function of TRPML1 in hepatocarcinoma cell lines. Mechanistically, we used a specific TRPML1 compound to over-activate the TRPML1 channel, which inhibits cancer cell proliferation and induces cancer cell apoptosis. Besides, ML1-SA1 impaired mitochondrial morphology and mitochondrial membrane potential, altering mitochondrial function and respiratory parameters. Along with this line, we demonstrated that ML1-SA1 successfully triggered the lysosomal calcium efflux and subsequently increased intracellular calcium. The calcium further accumulated in mitochondria, inducing mitochondrial stress, which deregulated mitochondrial function.

In addition to over-activation of the channel, loss of TRPML1 could also impair mitochondrial morphology and depolarized mitochondrial membrane. Although the loss of TRPML1 increased the mitochondrial proton leak, physiological respiration remained unchanged. Along with this line, we could show that TRPML1 KO builds a defence mechanism by up-regulating glutathione metabolism to maintain mitochondrial respiration. Importantly, we demonstrated that genetic or pharmacological inhibition of TRPML1 leads to lysosomal swelling and dysfunction. The deregulation of lysosomes prevents mitochondrial turnover, thus hindering the proliferation of cancer cells.

Taken together, we successfully discovered a promising candidate to treat liver cancer cells by over-activating TRPML1. Furthermore, we further hindered the proliferation of cancer cells by genetic knockout or pharmacological inhibition, suggesting a rheostat effect of TRPML1 in hepatocellular carcinoma cell lines. These results provide a basis for studying the underlying mechanism of TRPML1 in HCC.

5 Part 2: TRPML1 as a novel modulator of cancer cell movement

5.1 Functional characterization of TRPML1 in cancer cell migration

Cancer metastasis is very problematic and tricky since metastasis is hard to monitor. The migration movement or epithelial-mesenchymal transition commonly is a primary clue for metastasis diagnosis. Therefore, understanding cancer migration is beneficial for strategically postulating a therapy option. To investigate whether TRPML1 is crucial for cancer migration, a transwell migration assay of different cancer cell lines was performed. Our results indicate that hepatocarcinoma (RIL175), melanoma (SKMEL5), and breast cancer (MDA-MB-231) cell lines significantly decrease cell migration in KO cells (**Figure 22**), suggesting that loss of TRPML1 impair cancer cell migration.

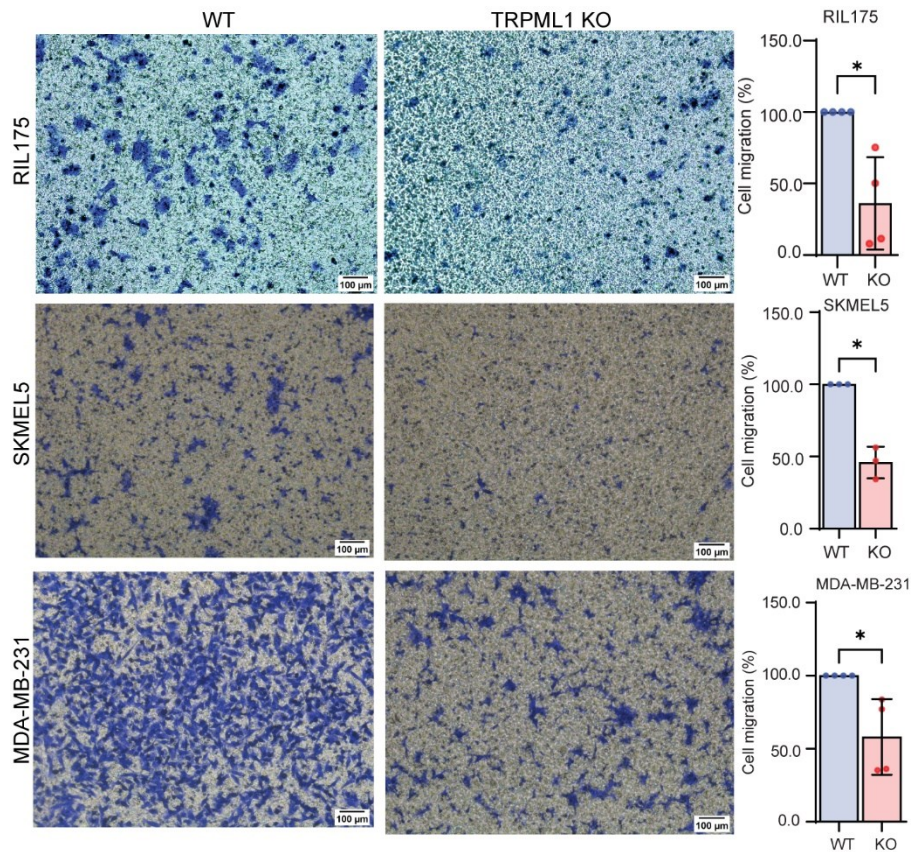


Figure 22. Loss of TRPML1 impairs cancer cell migration.

Migration assay of RIL175, SKMEL5 and MDA-MB-231 using transwell system. Scale bar = 100 μ m. Data represents mean \pm SD n=3, MDA-MB-231, n=4; unpaired t-test; *, p<0.05.

5.2 TRPML1 plays a critical role in cancer cell movement and cell-cell contact

Since cancer cells predominantly proceed with collective migration during metastasis [47], we next investigate migration movement after the knockout of TRPML1. Intriguingly, RIL175 and SKMEL5 cells migrate more individually after knockout, but not in MDA-MB-231 cells (**Figure 23A**). In order to monitor the phenotype in more detail, live time micropatterning imaging was performed. Although RIL175 WT migrated further than TRPML1 KO in micro-contact modelling, WT and KO cells' speeds remained unchanged (**Figure 23B**). Moreover, we also observed that TRPML1 KO cells disrupted the cell-cell tension, leading to cell disintegration. These results show that loss of TRPML1 altered migration movement, leading to lower migration displacement.

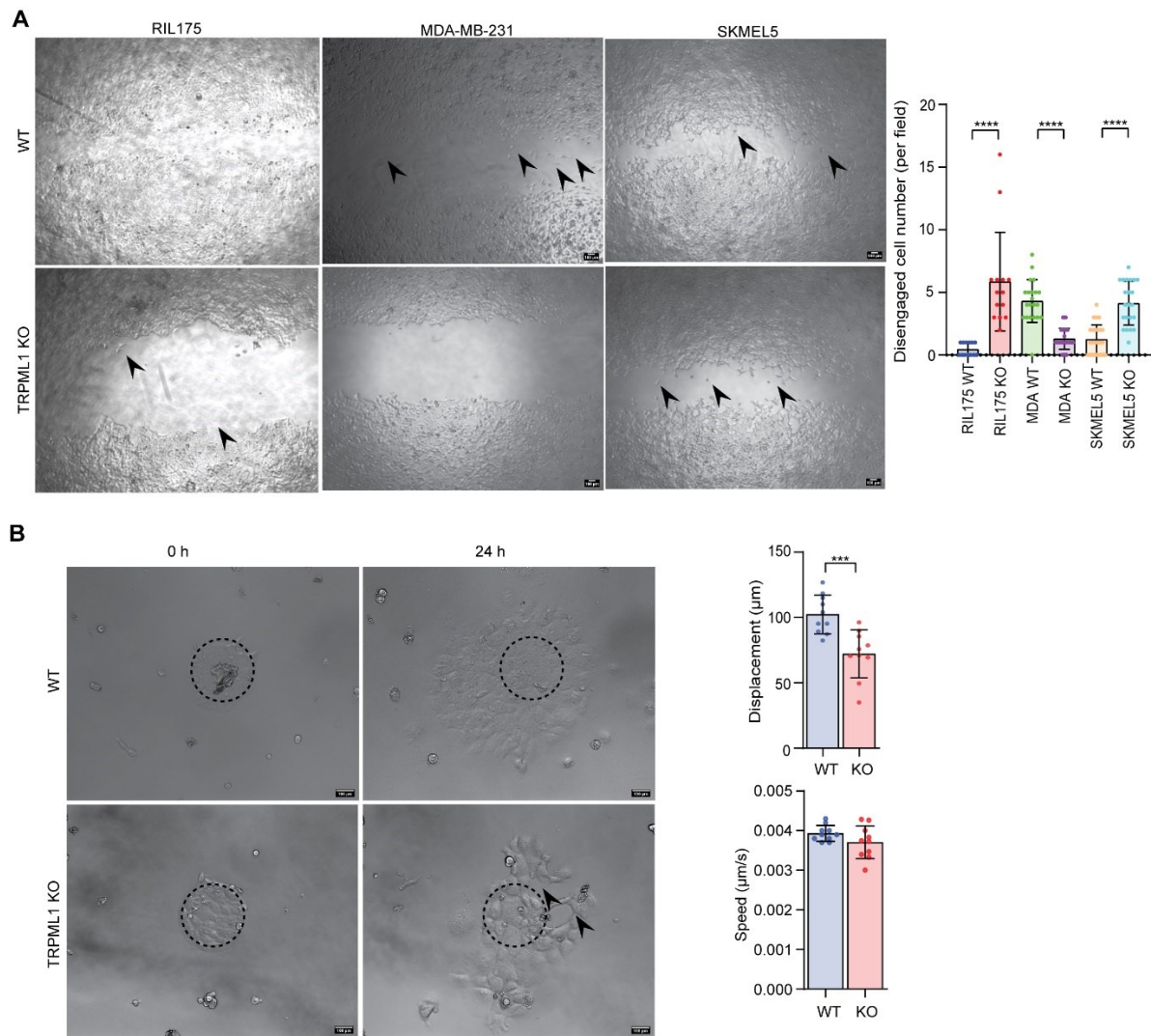


Figure 23. Loss of TRPML1 changes the migrating movement and cell-cell adhesion of cancer cells.

(A) Scratch assay of RIL175 for 12 h, MDA-MB-231 for 4.6 h, and SKMEL5 for 21.5 h (video). The black arrow indicates the disengaged cell from the cluster and calculated by Image J. Data represents mean \pm SD, $n=3$. (B) Micropatterning migration of RIL175 WT and KO were recorded, followed by speed and displacement analysis by Image J. Black arrow indicates the disintegration of the cell-cell contact. Scale bar = 100 μm . Data represent mean \pm SD, $n=3$; unpaired t-test; ***, $p<0,005$; ****, $p<0,001$.

5.3 Loss of TRPML1 alters cytoskeleton morphology and adjunctive cellular protein

As we observed alteration of cell-cell tension in KO cells, we hypothesized that loss of TRPML1 disrupts cytoskeleton and adjunctive cellular protein. Next, we investigated cytoskeleton and E-cadherin using confocal microscopy. Interestingly, cell morphology changed tremendously, which became shrank, and the cytoskeleton organization was distorted in KO cells (**Figure 24A**). Moreover, the expression of the cell-cell adjunctive protein, E-cadherin, was

significantly downregulated in RIL175 and SKMEL5 KO cells (**Figure 24B**). Intriguingly, we also observed that expression of E-cadherin was somehow rescued from TRPML1 KO cells (**Figure 24B**), leading to more compact cell morphology.

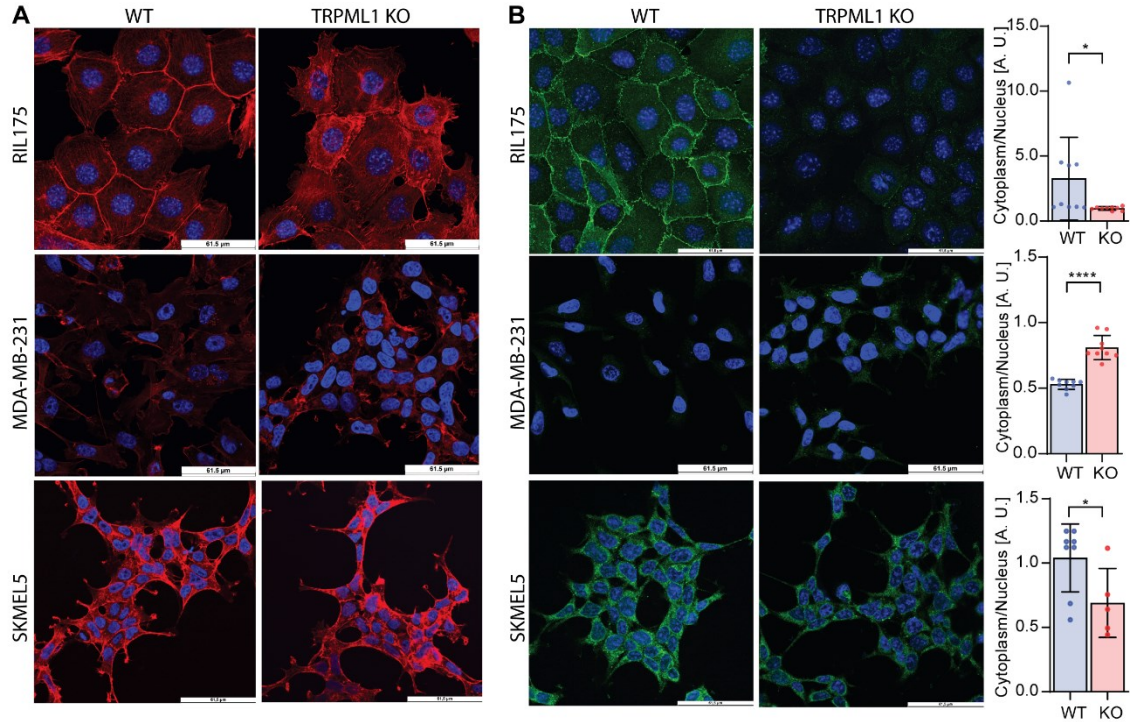


Figure 24. Alteration of the cytoskeleton and cell junction after the loss of TRPML1 in cancer cells.

(A) The cytoskeleton of RIL175, MDA-MB-231 and SKMEL5 in WT or TRPML1 KO were observed by Rhodamine (actin) and Hoechst 33342 (nuclei) using confocal imaging. Scale bar: 61.5 μ m. One representative image is shown. (B) Morphology of cell junction was observed using confocal microscopy and quantitatively measured by Image J. Scale bar: 61.5 μ m, One representative figure from three independent experiments. Data represents as mean \pm SD, n=3; unpaired t-test; *, p<0,05; ****, p<0,001.

In order to confirm the expression of E-cadherin among all cell lines, western blot analysis was performed. In accordance with results from western blot, the protein level of E-cadherin was significantly decreased in RIL175 and SKMEL5 KO cells but greatly increased in MDA-MB-231 KO cells (**Figure 25**). These results summarized that loss of the TRPML1 channel altered E-cadherin expression, leading to the reformation of the actin cytoskeleton and changes in cellular morphology.

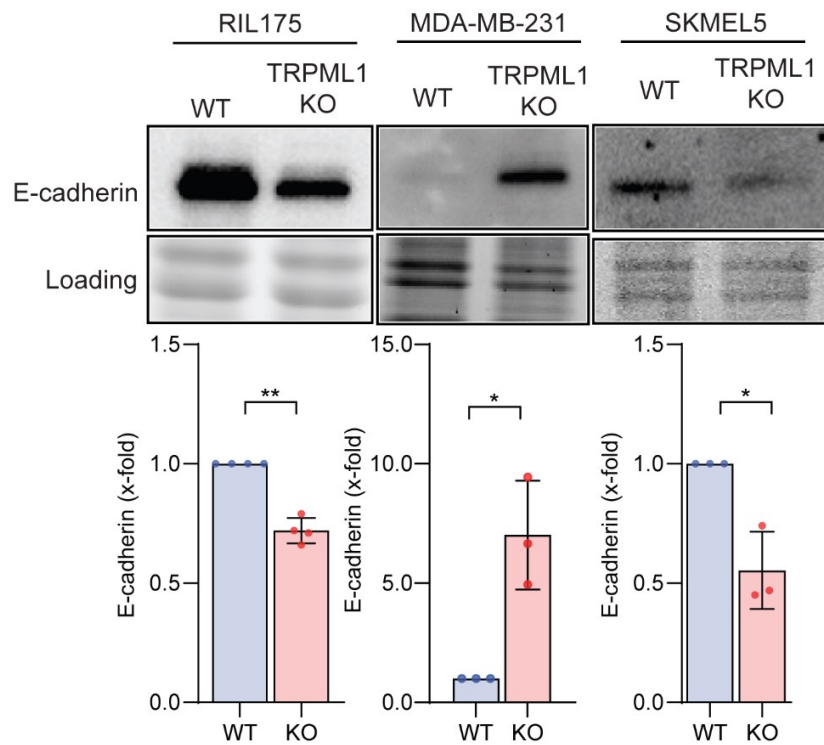


Figure 25. TRPML1 KO alters the expression of E-cadherin.

E-cadherin expression of RIL175, MDA-MB-231 and SKMEL5 in WT or TRPML1 KO were detected by western blot. Data represents as mean \pm SD, n=3; unpaired t-test; *, p-value <0.05, and **, p-value <0.01

E-cadherin plays a vital role in maintaining cell-cell tension during collective migration based on previous findings. Since E-cadherin was strongly decreased in KO cells, we postulated that KO of TRPML1 could disrupt the connection of cells, leading to individual migration. Further, we detected N-cadherin, Rac1 and podoplanin; these are markers generally upregulated while the cells start to transit into individual migration. The western blot analysis indicates that all markers were increased after TRPML1 KO (**Figure 26**), suggesting that KO cells might execute the transition from collective to individual migration.

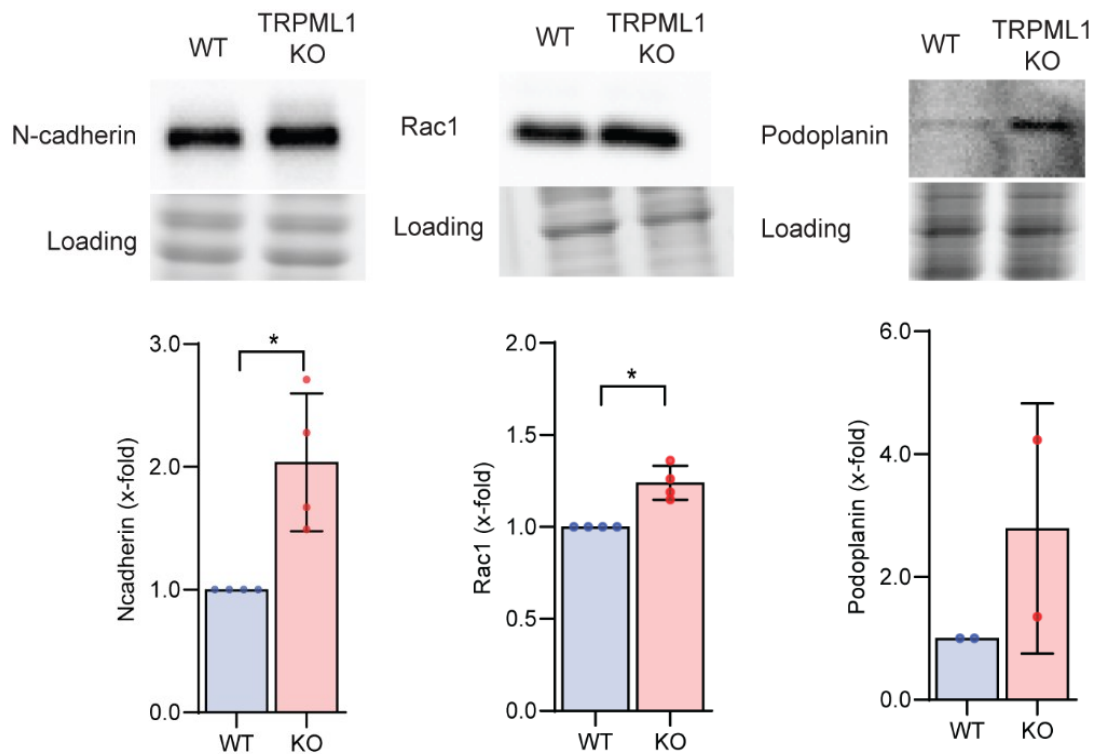


Figure 26. TRPML1 KO induces the transition of collective to individual migration.

Protein expression of collective to individual migration markers in RIL175 TRPML1 WT and KO cell. Data represents as mean \pm SD, n=3; n=2 for podoplanin; unpaired t-test; *, p-value <0.05 and **, p-value <0.01

5.4 TRPML1 regulates the cell-cell contact via Notch1

Along with this line, we demonstrated that loss of TRPML1 leads to severe alteration of cellular movement, morphology and cell-cell contact, which possibly caused down-regulation of cancer migration. However, the underlying mechanism of how TRPML1 regulates cell migration has remained unknown. As cell-cell contact is highly connected to Notch1 signalling, we investigated if we could observe a difference of Notch1 between TRPML1 WT and KO cells in our model. The dual-luciferase assay indicated that Notch1 activity was significantly reduced in KO cells (**Figure 27**), suggesting the connection of TRPML1 and Noctch1 might be a causative mediator for TRPML1-related dysregulation of migration.

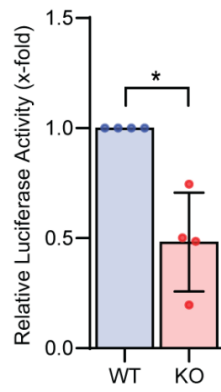


Figure 27. TRPML1 KO reduces the regulation of Notch1 activity.

Dual-luciferase assay was performed transiently transfected with TP1-Luciferase plasmid vectors containing a constitutive Renilla reporter and a Firefly reporter as a control of a gene-specific promoter. Data represents as mean \pm SD, n=4; unpaired t-test; *, p-value <0.05.

5.5 Part 2: Summary

The second part of the project described the consequences of losing TRPML1 in cancer cell migration using genetic knockout hepatocarcinoma cell line, breast cancer cell line, and melanoma cell line. We revealed that loss of TRPML1 reduces migration capacity in different cancer cells. Further, the movement of cells was different after TRPML1 knockout, which tends to migrate individually instead of collectively. Disruption of the adjunctive protein, E-cadherin, and cytoskeleton alteration indicates that KO cells have a loose connection and less tension between cells, followed by escaping from the migrating cluster. The upregulation of individual migration markers strengthened the evidence that KO cells are likely to migrate individually. Although we were able to show that TRPML1 is somehow connected to Notch1 signalling, the underlying mechanism of how TRPML1 plays a role in alternative migration still needs to be defined, leaving an open question for further investigation in order to draft a new strategy for inhibiting cancer metastasis.

DISCUSSION



6 Discussion

6.1 Part 1: Lysosomal ion channel TRPML1, a novel regulator of mitochondrial function in hepatocellular carcinoma cells

6.1.1 Modulating mitochondria by transient receptor potential mucolipin 1 channel as a therapeutical target for hepatocarcinoma cancer

The treatment of HCC patients is often challenging due to the lack of a specific target. Therefore, identifying a novel and druggable target denotes a critical step for improving cancer therapy. MCOLN1 was shown to be a balancer in different gene expression analyses, which delicately adjusts expression in different cancer cells to optimise cell growth [20, 84]. High expression of TRPML1 acts as a negative prognosis factor in HRAS-positive pancreatic patients [17] but inversely in glioblastoma patients [18]. Along with this line, our study demonstrated that loss or over-activation of TRPML1 influences cancer cell proliferation by different extent and mechanisms. This, in turn, highlights multiple roles of TRPML1 in cancer, providing multiple strategies to design suitable inhibitors and activators.

6.1.2 Multiple functions of TRPML1 – Overloading mitochondria calcium

The lysosomal TRPML1 channel has been extensively discussed as an essential regulator of calcium and autophagy homeostasis, making it crucial for mitochondria [85, 86]. Calcium has a vital function in maintaining mitochondrial fitness by modulating mitochondrial structure, membrane potential and generation of ROS. Nevertheless, calcium's role in mitophagy remains unclear [87]. Given the importance of calcium in mitochondrial regulation, it is plausible that modulating calcium-permeable TRPML1 could influence the mitochondrial function. Our results illustrate that activating TRPML1 by ML1-SA1 subsequently elevated cytosolic calcium levels as well as mitochondrial calcium levels (**Figure 16**). The phenotype is consistent with the previous finding, indicating mitochondria to increase uptake of excessive calcium from the cytosol [88] in order to augment ATP production [28, 89, 90]. Nonetheless, the overloading of calcium is harmful to mitochondria. Excessive mitochondrial calcium enhances ROS generation, triggers the opening of the permeability transition pore (mPTP), and releases cytochrome c, leading to cell apoptosis eventually [91-93]. In line with our findings, we unravelled that TRPML1 activation disrupted the mitochondrial membrane

potential (**Figure 14A-D**), which most likely resulted from the opening of mPTP, as loss of the membrane potential could be rescued by adding cyclosporin A (**Figure 14E**), a known blocker of transition pore formation [91].

Moreover, an imbalance of mitochondrial ROS can lead to oxidative damage, impairing the ability of ATP production [94], which further supports our findings that activation of TRPML1 increases mitochondrial ROS (**Figure 15A**) and thus decreases mitochondrial ATP production capacity (**Figure 13C**). Since we observed an increase of cytosolic calcium after the over-activation of TRPML1, we hypothesized that calcium levels could be further amplified by calcium-induced calcium release (CICR). It has been reported that calcium efflux of TRPML1 could further induce calcium release from the endoplasmic reticulum (ER) or production of calcium-releasing messengers such as inositol trisphosphate (IP₃) to initiate ER calcium efflux, which is mediated by IP₃ receptor and ryanodine receptors (RyR) [95]. The CICR further enhances cytosolic calcium and mitochondrial calcium influx via voltage-dependent anion-selective channel proteins (VDACs) and mitochondrial calcium uniporter (MCU) complex [32]. Excessive calcium influx of mitochondria, leads to aberrant structural integrity, membrane potential and ROS level, followed by cell death. A recently published study further supports our data, demonstrating that the lysosomal TRPML1 channel contributes to calcium dynamics at lysosome-mitochondria contact sites, suggesting calcium influx is highly dependent on TRPML1 [96]. Additionally, TRPML1 is a non-selective cation channel residing on the lysosome. It is also worth mentioning that activation of TRPML1 could also increase mitochondrial Zn²⁺ level, which has been reported to induce cancer cell death in melanoma cell lines [97].

Taken together, we could show that ML1-SA1, as a potent activator, stimulates lysosomal calcium efflux by TRPML1 and readily increases mitochondrial calcium influx. Moreover, we found that a substantial amount of mitochondrial calcium could lead to hazardous ROS production and mPTP opening, eventually reducing cancer cell proliferation and inducing death.

6.1.3 Multiple functions of TRPML1 – Deficit mitochondrial renewal

Mitochondria play a critical role in ATP production by oxidative phosphorylation (OXPHOS). However, many cancer cells preferentially rely on glycolysis more than OXPHOS, even in the presence of oxygen. This phenomenon is termed the Warburg effect [98]. Although glycolysis produces less ATP than mitochondrial OXPHOS, it has been reported that cancer cells constantly upregulate glycolysis, which provides rapid ATP production [99] and sufficient glycolytic intermediates for biosynthesis need of rapid proliferation [100]. As over-activation of TRPML1, we observed that a knock-out of the TRPML1 in HCC cells leads to similar alterations in mitochondrial morphology (**Figure 13**). However, these changes do not alter ATP production (**Figure 15**) and do not induce cell death (**Figure 11**). Considering the Warburg effect, we hypothesized that TRPML1 KO cells somehow compensate for ATP supply by glycolysis since the OCR/ECAR ratio is slightly decreased, deciphering that TRPML1 KO can switch metabolic activity more on glycolytic metabolism. This is in line with a previous study, reporting that cancer cells switch between OXPHOS and glycolysis to maintain a hybrid metabolic phenotype, and to maximize cell proliferation [101].

Moreover, our results illustrate a puzzling impairment in mitochondrial membrane potential (**Figure 14**) and an increase of proton leak (**Figure 19**), indicating that mitochondria of TRPML1 knockout cells are indeed damaged to some extent. As mentioned above, lysosomal function plays an essential role in mitochondrial renewal, such as mitophagy, which assists mitochondria to maintain physiological fitness. TRPML1 plays an important role in maintaining lysosomal function [102-104], and loss-of-function of the TRPML1 channel could lead to well-known lysosomal storage diseases, like mucopolipidosis type IV (ML IV) [105]. The lysosome often appears enlarged and swollen in mucopolipidosis type IV patients [105, 106]. Our work is consistent with previous findings [106], showing the loss of TRPML1 enlarged lysosomal structures in confocal and transmission electron microscopy (**Figure 20**), which suggests lysosomal impairment. The lysosome function determines autophagy function, which is essential for maintaining cellular homeostasis. Cellular organelles usually undergo a biological cycle of degradation and renewal, optimizing their proper function. Organelles or fragments are engulfed in autophagosomes and subsequently fused with lysosomes for further degradation; afterwards, organelles are renewed [107, 108]. In mitophagy, cellular

stress conditions initiate ubiquitination of mitochondrial outer membrane proteins, which are identified by p62 adaptor protein. The autophagosome formation is furthered occurred by binding with LC3 [109]. Our data show that loss of function of TRPML1 leads to impairment of autophagy flux and p62 degradation (**Figure 21**). This is in line with previous results, reporting a regulatory role for TRPML1 in autophagy [85, 86]. In ML IV patients, it has been reported that autophagic markers LC3 and p62 were accumulated during macroautophagy [110-112]. Additionally, TRPML1-mediated calcium release leads to activation of TFEB translocation and subsequently activates transcription of lysosomal and autophagic genes [113, 114]. Recently, TRPML1 has been described as a multistep regulator during autophagy. TRPML1 plays a role in generating phosphatidylinositol 3-phosphate (PI3P) and recruitment of PI3P-binding proteins, which is required for the calcium-dependent kinase CaMKK β and AMPK to initiate ULK1 and VPS34 autophagic protein complexes [85].

Furthermore, our results illustrate that loss or inhibition of TRPML1 impair mitophagy. We observed that KO cells or EDME treated cells show lower autophagy flux and p62 degradation in comparison to WT cells (**Figure 21**). Additionally, loss of TRPML1 leads to apparent enlargement of lysosomes. By observing TEM results, we found that an enlarged lysosome consists of membranous incisions, which probably resembles mitochondrial fragments (**Figure 20C**), suggesting the impairment of mitochondrial recycling. Our findings illustrate that KO cells or EDME treated cells exhibit lower mitophagy (**Figure 21**) and a slower proliferative rate (**Figure 18**), which is further supported by a recent study, showing that defective mitophagy leads to dysfunction of mitochondria and hinders cancer cell growth [115]. Moreover, mitophagy impairment was connected with increased ROS levels and changes in cellular calcium, leading to inflammation and apoptosis [109]. Intriguingly, our data revealed no alteration in mitochondrial ROS levels (**Figure 17A**); thus, we hypothesized that this is a consequence of an adapted glutathione (GSH) metabolism. We found an upregulation of GSH metabolism and an increased GSSG: GSH ratio in the TRPML1 KO cells (**Figure 19D**). It has been revealed that ROS could be neutralized during GSH to GSSG oxidation, whereby the cell can be detoxified from excessive ROS and maintain mitochondrial function [116]. As for cancer cells, a greater ROS level was needed for enhanced metabolism and rapid proliferation [117]. The GSH antioxidant system was activated to cope with higher ROS levels, facilitating redox balance [118]. Many cancer cells reprogram the GSH antioxidant system to

increase antioxidant capacity and resistance to excessive ROS levels [119]. Thus, it is plausible that TRPML1 KO cells reprogram GSH metabolism, and thus the increase of ROS might be rapidly eliminated by GSH oxidation.

In summary, we pioneered discovering a novel and potential cancer therapeutical strategy by modulating calcium levels in mitochondria with a promising agonist, ML1-SA1, in hepatocellular carcinoma cells. In addition to novel drug discovery, we propose that the loss of function of TRPML1 interferes the mitophagy, which impairs mitochondrial function and reduces cell proliferation rates. Taken together, we propose that activating or inhibiting TRPML1 could be a promising approach to target HCC by modulating the mitochondrial function.

6.2 Part 2: TRPML1 as a novel modulator of cancer cell movement

Metastasis of cancer increases the challenge of cancer therapy and worsens cancer patients' survival rates. Cancer patients often die from metastatic tumours instead of the primary tumour. In the context of this thesis, we present that loss of TRPML1 inhibits cancer cell migration. The anti-migratory effect of TRPML1 was discovered by CRISPR-Cas9 knockout studies (**Figure 22**). This result is in line with previous studies, reporting that genetically knock-down or pharmacologically inhibition of TRPML1 reduces migration in triple-negative cancer cell lines [19, 36]. Next, we unravelled that loss of TRPML1 decreases migration displacement, suggesting that cells lose polarity and undergo non-directional migration. It has been reported that TRPML1 controls the directional migration of dendritic cells and macrophages [34, 35]. Upon bacterial sensing, dendritic cells modulate lysosomal calcium release by TRPML1, further reprogramming the actin-based motor protein myosin II at the cell rear, accelerating directional migration [34, 120]. A direct modulator, Rab7b, a small GTPase that mediates late endosome or lysosomal activity, is hypothesised to play a critical role in regulating directional migration [120]. Moreover, myosin II has been associated with F-actin contractility in neurons [121] and cancer cells [122], emphasising its role in cell protrusion. Since actin filaments are crucial for initiating cell protrusion, we observed a rearrangement of the actin cytoskeleton in TRPML1 KO cells (**Figure 24**), which aligns with the previous study indicating that loss of TRPML1 reorganises actin filaments and further disrupts directional migration [35]. This, in turn, highlights a promising approach to target TRPML1 to fight against cancer cell migration as well as metastasis.

Cancer cell migration is a highly complex and dynamic process. Cell migration is initiated by triggering a process called epithelial-mesenchymal transition (EMT). During EMT, cancer cells invade the bloodstream, followed by residing to an alternative destination as a secondary tumour [38]. Cancer cells migrate collectively instead of individually during the cellular invasion to maximize migration efficiency [47]. In order to migrate collectively, the tight junction protein E-cadherin plays an essential role to maintain cell-cell interactions [52, 72]. On the one hand, E-cadherin strengthens cell-cell tension by connecting with tension sensitive proteins such as p120, α -, and β -catenin, facilitating actomyosin contractility and collective migration [49]. Along with this line, we found that loss of TRPML1 altered migratory

movement and E-cadherin levels in different cancer cell lines (**Figure 23**, **Figure 24** and **Figure 25**) and alteration of the actin cytoskeleton (**Figure 24**). Of note, we observed that HCC and melanoma TRPML1KO cell lines shift collective migration into individual migration, whereas breast cancer cells showed an opposite phenotype (**Figure 23**). Hence, we surprisingly found that loss of TRPML1 somehow rescued E-cadherin levels (**Figure 25**) since MDA-MB-231 breast cancer cell lines do not express E-cadherin [123, 124], deciphering opposite cell movement of MDA-MB-231 cell lines. Notably, various markers, for instance, N-cadherin, Rac1 and podoplanin, have been reported to facilitate the transition of collective to individual migration [53]. Depending on the direction of collective migration, cells can be distinguished into leader cells, which generally localize at the front edges of the migrating group, and follower cells, which follow leader cell clusters [125]. During the transition of collective to individual migration, on the one hand, Rac1 and podoplanin control actin-driven protrusions at the front edge of leader cells [126, 127]. On the other hand, E- and N-cadherin switch disassemble at border cells [40]. Taken together, these changes lead to cells moving away from each other, facilitating individual migration. As expected, our results illustrate that loss of TRPML1 increased protein expression of N-cadherin, Rac1 and podoplanin (**Figure 26**) and decreased the E-cadherin level (**Figure 25**), further strengthening our hypothesis that TRPML1 might regulate the migratory movement of cancer cells, which is E-cadherin dependent.

While consequences of a defective TRPML1 channel in collective migration was discovered, the molecular machinery behind it is rather challenging. As mentioned above, collective migration was mediated by cell-cell contact. It has been reported that the Notch1 signalling pathway is essential for cell-cell communication pathways since the Notch1 receptor is generally triggered by direct cell-cell contact and activates the following cascade [54]. Activation of Notch1 signalling requires binding of any ligands such as Dll4 with an EGF-like repeat on the Notch receptor and triggers endocytosis of the Notch1-ligand complex [59]. During endocytosis, the acidic endolysosomal compartment activates γ -secretase, resulting in the release of the Notch1 intracellular domain (NICD), which translocates to the nucleus to activate Notch1 target genes [128]. Since impairment of endolysosomal function dysregulates the Notch1 signalling pathway [129, 130], we further observed that loss of TRPML1 disrupted lysosomal function (**Figure 20**) and expression of Notch1 in TRPML1 KO cells (**Figure 27**); this possibly leads to inadequate cell support between cells, followed by disruption of cell-cell

contacts. Since TRPML1 is calcium permeable, it is also plausible that the alteration of calcium homeostasis dysregulates Notch1 expression directly or indirectly. However, further investigation is needed to validate the cell adhesion network.

In summary, we identified TRPML1 as a novel regulator in cancer cell migration, possibly impacting metastasis by altering the movement behaviour. Moreover, we discovered that cancer cells require TRPML1 to maintain cell-cell contact in the regulation of collective migration. Additionally, TRPML1 was an unknown player in regulating cell-cell contact, supposedly associated with Notch1 signalling, which alters the E-cadherin levels and changes the cell movement. Hence, our findings established a better understanding of the role of TRPML1 upon cancer cell migration, allowing further analysis to decipher its mechanistic function and exploring antimetastatic strategies soon.

REFERENCES



7 References

1. Villanueva, A., *Hepatocellular Carcinoma*. New England Journal of Medicine, 2019. **380**(15): p. 1450-1462.
2. Kim, E. and P. Viatour, *Hepatocellular carcinoma: old friends and new tricks*. Experimental & Molecular Medicine, 2020. **52**(12): p. 1898-1907.
3. Dimri, M. and A. Satyanarayana, *Molecular Signaling Pathways and Therapeutic Targets in Hepatocellular Carcinoma*. Cancers, 2020. **12**(2): p. 491.
4. Liu, P.H., et al., *Prognosis of hepatocellular carcinoma: Assessment of eleven staging systems*. J Hepatol, 2016. **64**(3): p. 601-8.
5. Chen, Z., et al., *Recent progress in treatment of hepatocellular carcinoma*. American journal of cancer research, 2020. **10**(9): p. 2993-3036.
6. Grimm, C., et al., *Endolysosomal Cation Channels and Cancer-A Link with Great Potential*. Pharmaceuticals (Basel), 2018. **11**(1).
7. Chavez-Dominguez, R., et al., *The Double-Edge Sword of Autophagy in Cancer: From Tumor Suppression to Pro-tumor Activity*. Frontiers in Oncology, 2020. **10**(2064).
8. Cheng, X., et al., *Mucolipins: Intracellular TRPML1-3 Channels*. FEBS letters, 2010. **584**(10): p. 2013-2021.
9. Samanta, A., T.E.T. Hughes, and V.Y. Moiseenkova-Bell, *Transient Receptor Potential (TRP) Channels*. Sub-cellular biochemistry, 2018. **87**: p. 141-165.
10. Chen, Q., et al., *Structure of mammalian endolysosomal TRPML1 channel in nanodiscs*. Nature, 2017. **550**(7676): p. 415-418.
11. Schmiede, P., et al., *Human TRPML1 channel structures in open and closed conformations*. Nature, 2017. **550**: p. 366.
12. Hirschi, M., et al., *Cryo-electron microscopy structure of the lysosomal calcium-permeable channel TRPML3*. Nature, 2017. **550**(7676): p. 411-414.
13. Fine, M., P. Schmiede, and X. Li, *Structural basis for PtdInsP2-mediated human TRPML1 regulation*. Nature Communications, 2018. **9**(1): p. 4192.
14. Bargal, R., et al., *Identification of the gene causing mucopolipidosis type IV*. Nat Genet, 2000. **26**(1): p. 118-23.
15. Sun, M., et al., *Mucopolipidosis type IV is caused by mutations in a gene encoding a novel transient receptor potential channel*. Hum Mol Genet, 2000. **9**(17): p. 2471-8.
16. Altarescu, G., et al., *The neurogenetics of mucopolipidosis type IV*. Neurology, 2002. **59**(3): p. 306-13.

References

17. Jung, J., et al., *HRAS-driven cancer cells are vulnerable to TRPML1 inhibition*. EMBO reports, 2019: p. e46685.
18. Morelli, M.B., et al., *Transient Receptor Potential Mucolipin-1 Channels in Glioblastoma: Role in Patient's Survival*. Cancers (Basel), 2019. **11**(4).
19. Xu, M., et al., *The lysosomal TRPML1 channel regulates triple negative breast cancer development by promoting mTORC1 and purinergic signaling pathways*. Cell Calcium, 2019. **79**: p. 80-88.
20. Kasitinon, S.Y., et al., *TRPML1 Promotes Protein Homeostasis in Melanoma Cells by Negatively Regulating MAPK and mTORC1 Signaling*. Cell Reports, 2019. **28**(9): p. 2293-2305.e9.
21. Hu, Z.-D., et al., *MCOLN1 Promotes Proliferation and Predicts Poor Survival of Patients with Pancreatic Ductal Adenocarcinoma*. Disease markers, 2019. **2019**: p. 9436047-9436047.
22. Li, R.-J., et al., *Regulation of mTORC1 by lysosomal calcium and calmodulin*. eLife, 2016. **5**: p. e19360.
23. Qi, J., et al., *MCOLN1/TRPML1 finely controls oncogenic autophagy in cancer by mediating zinc influx*. Autophagy, 2021: p. 1-22.
24. Du, W., et al., *Lysosomal Zn²⁺ release triggers rapid, mitochondria-mediated, non-apoptotic cell death in metastatic melanoma*. Cell Reports, 2021. **37**(3): p. 109848.
25. Peng, W., Y.C. Wong, and D. Krainc, *Mitochondria-lysosome contacts regulate mitochondrial Ca²⁺ dynamics via lysosomal TRPML1*. Proceedings of the National Academy of Sciences, 2020: p. 202003236.
26. Humeau, J., et al., *Calcium signaling and cell cycle: Progression or death*. Cell Calcium, 2018. **70**: p. 3-15.
27. Bagur, R. and G. Hajnóczky, *Intracellular Ca(2+) Sensing: Its Role in Calcium Homeostasis and Signaling*. Molecular cell, 2017. **66**(6): p. 780-788.
28. Finkel, T., et al., *The Ins and Outs of Mitochondrial Calcium*. Circulation Research, 2015. **116**(11): p. 1810-1819.
29. Hamilton, J., et al., *Deletion of mitochondrial calcium uniporter incompletely inhibits calcium uptake and induction of the permeability transition pore in brain mitochondria*. J Biol Chem, 2018. **293**(40): p. 15652-15663.
30. Griffiths, E.J. and G.A. Rutter, *Mitochondrial calcium as a key regulator of mitochondrial ATP production in mammalian cells*. Biochimica et Biophysica Acta (BBA) - Bioenergetics, 2009. **1787**(11): p. 1324-1333.

References

31. Jouaville, L.S., et al., *Regulation of mitochondrial ATP synthesis by calcium: Evidence for a long-term metabolic priming*. Proceedings of the National Academy of Sciences, 1999. **96**(24): p. 13807.
32. Giorgi, C., S. Marchi, and P. Pinton, *The machineries, regulation and cellular functions of mitochondrial calcium*. Nature Reviews Molecular Cell Biology, 2018. **19**(11): p. 713-730.
33. Fares, J., et al., *Molecular principles of metastasis: a hallmark of cancer revisited*. Signal Transduction and Targeted Therapy, 2020. **5**(1): p. 28.
34. Bretou, M., et al., *Lysosome signaling controls the migration of dendritic cells*. Sci Immunol, 2017. **2**(16).
35. Edwards-Jorquera, S.S., et al., *Trpml controls actomyosin contractility and couples migration to phagocytosis in fly macrophages*. Journal of Cell Biology, 2020. **219**(3).
36. Rühl, P., et al., *Estradiol analogs attenuate autophagy, cell migration and invasion by direct and selective inhibition of TRPML1, independent of estrogen receptors*. Scientific Reports, 2021. **11**(1): p. 8313.
37. Xing, Y., et al., *Autophagy inhibition mediated by MCOLN1/TRPML1 suppresses cancer metastasis via regulating a ROS-driven TP53/p53 pathway*. Autophagy, 2021: p. 1-23.
38. Kalita, B. and M.S. Coumar, *Deciphering molecular mechanisms of metastasis: novel insights into targets and therapeutics*. Cell Oncol (Dordr), 2021. **44**(4): p. 751-775.
39. Son, H. and A. Moon, *Epithelial-mesenchymal Transition and Cell Invasion*. Toxicological research, 2010. **26**(4): p. 245-252.
40. Scarpa, E., et al., *Cadherin Switch during EMT in Neural Crest Cells Leads to Contact Inhibition of Locomotion via Repolarization of Forces*. Developmental Cell, 2015. **34**(4): p. 421-434.
41. Loh, C.-Y., et al., *The E-Cadherin and N-Cadherin Switch in Epithelial-to-Mesenchymal Transition: Signaling, Therapeutic Implications, and Challenges*. Cells, 2019. **8**(10): p. 1118.
42. Araki, K., et al., *E/N-cadherin switch mediates cancer progression via TGF- β -induced epithelial-to-mesenchymal transition in extrahepatic cholangiocarcinoma*. Br J Cancer, 2011. **105**(12): p. 1885-93.
43. Aleskandarany, M.A., et al., *Epithelial mesenchymal transition in early invasive breast cancer: an immunohistochemical and reverse phase protein array study*. Breast Cancer Res Treat, 2014. **145**(2): p. 339-48.
44. Qi, J., et al., *Transendothelial migration of melanoma cells involves N-cadherin-mediated adhesion and activation of the beta-catenin signaling pathway*. Mol Biol Cell, 2005. **16**(9): p. 4386-97.

References

45. Datta, A., et al., *Cytoskeletal Dynamics in Epithelial-Mesenchymal Transition: Insights into Therapeutic Targets for Cancer Metastasis*. *Cancers*, 2021. **13**(8): p. 1882.
46. Kallergi, G., et al., *Activation of FAK/PI3K/Rac1 signaling controls actin reorganization and inhibits cell motility in human cancer cells*. *Cell Physiol Biochem*, 2007. **20**(6): p. 977-86.
47. Yang, Y., et al., *An emerging tumor invasion mechanism about the collective cell migration*. *Am J Transl Res*, 2019. **11**(9): p. 5301-5312.
48. George, M., F. Bullo, and O. Campàs, *Connecting individual to collective cell migration*. *Sci Rep*, 2017. **7**(1): p. 9720.
49. De Pascalis, C. and S. Etienne-Manneville, *Single and collective cell migration: the mechanics of adhesions*. *Mol Biol Cell*, 2017. **28**(14): p. 1833-1846.
50. Li, L., et al., *E-cadherin plays an essential role in collective directional migration of large epithelial sheets*. *Cell Mol Life Sci*, 2012. **69**(16): p. 2779-89.
51. Park, S.-Y., et al., *Expression of E-Cadherin in Epithelial Cancer Cells Increases Cell Motility and Directionality through the Localization of ZO-1 during Collective Cell Migration*. *Bioengineering*, 2021. **8**(5): p. 65.
52. Friedl, P. and R. Mayor, *Tuning Collective Cell Migration by Cell-Cell Junction Regulation*. *Cold Spring Harbor perspectives in biology*, 2017. **9** 4.
53. Friedl, P. and S. Alexander, *Cancer Invasion and the Microenvironment: Plasticity and Reciprocity*. *Cell*, 2011. **147**(5): p. 992-1009.
54. Shaya, O., et al., *Cell-Cell Contact Area Affects Notch Signaling and Notch-Dependent Patterning*. *Developmental Cell*, 2017. **40**(5): p. 505-511.e6.
55. Wang, X.Q., et al., *Notch1-Snail1-E-cadherin pathway in metastatic hepatocellular carcinoma*. *International Journal of Cancer*, 2012. **131**(3): p. E163-E172.
56. Kim, A., et al., *Notch1 destabilizes the adherens junction complex through upregulation of the Snail family of E-cadherin repressors in non-small cell lung cancer*. *Oncol Rep*, 2013. **30**(3): p. 1423-1429.
57. Gharaibeh, L., et al., *Notch1 in Cancer Therapy: Possible Clinical Implications and Challenges*. *Molecular Pharmacology*, 2020. **98**(5): p. 559.
58. Wang, Z., et al., *The role of Notch signaling pathway in epithelial-mesenchymal transition (EMT) during development and tumor aggressiveness*. *Current drug targets*, 2010. **11**(6): p. 745-751.
59. Murata, A. and S.-I. Hayashi, *Notch-Mediated Cell Adhesion*. *Biology*, 2016. **5**(1): p. 5.
60. Wang, K., et al., *Dll4/Notch1 signalling pathway is required in collective invasion of salivary adenoid cystic carcinoma*. *Oncol Rep*, 2021. **45**(3): p. 1011-1022.

References

61. Torab, P., et al., *Intratumoral Heterogeneity Promotes Collective Cancer Invasion through NOTCH1 Variation*. Cells, 2021. **10**(11).
62. Bauer, D.E., M.C. Canver, and S.H. Orkin, *Generation of genomic deletions in mammalian cell lines via CRISPR/Cas9*. J Vis Exp, 2015(95): p. e52118.
63. Fleige, S., et al., *Comparison of relative mRNA quantification models and the impact of RNA integrity in quantitative real-time RT-PCR*. Biotechnol Lett, 2006. **28**(19): p. 1601-13.
64. Chen, C.C., et al., *Patch-clamp technique to characterize ion channels in enlarged individual endolysosomes*. Nat Protoc, 2017. **12**(8): p. 1639-1658.
65. Plesch, E., et al., *Selective agonist of TRPML2 reveals direct role in chemokine release from innate immune cells*. eLife, 2018. **7**: p. e39720.
66. Chen, C.-C., et al., *Small Molecules for Early Endosome-Specific Patch Clamping*. Cell Chemical Biology, 2017. **24**(7): p. 907-916.e4.
67. Cox, J. and M. Mann, *MaxQuant enables high peptide identification rates, individualized p.p.b.-range mass accuracies and proteome-wide protein quantification*. Nature Biotechnology, 2008. **26**(12): p. 1367-1372.
68. Schindelin, J., et al., *Fiji: an open-source platform for biological-image analysis*. Nature Methods, 2012. **9**(7): p. 676-682.
69. Zischka, H., et al., *Electrophoretic analysis of the mitochondrial outer membrane rupture induced by permeability transition*. Anal Chem, 2008. **80**(13): p. 5051-8.
70. Einer, C., et al., *A High-Calorie Diet Aggravates Mitochondrial Dysfunction and Triggers Severe Liver Damage in Wilson Disease Rats*. Cellular and Molecular Gastroenterology and Hepatology, 2019. **7**(3): p. 571-596.
71. Schmitt, S., et al., *A semi-automated method for isolating functionally intact mitochondria from cultured cells and tissue biopsies*. Anal Biochem, 2013. **443**(1): p. 66-74.
72. Zisis, T., et al., *Disentangling cadherin-mediated cell-cell interactions in collective cancer cell migration*. Biophysical Journal, 2022. **121**(1): p. 44-60.
73. Grimm, C., *Endolysosomal Cation Channels as Therapeutic Targets; Pharmacology of TRPML Channels*. Messenger, 2016. **5**(1-2): p. 30-36.
74. Shen, D., et al., *Lipid storage disorders block lysosomal trafficking by inhibiting a TRP channel and lysosomal calcium release*. Nature Communications, 2012. **3**: p. 731.
75. Spix, B., et al., *Lung emphysema and impaired macrophage elastase clearance in mucolipin 3 deficient mice*. Nature Communications, 2022. **13**(1): p. 318.

References

76. Liu, G., Y. Zhang, and T. Zhang, *Computational approaches for effective CRISPR guide RNA design and evaluation*. Computational and Structural Biotechnology Journal, 2020. **18**: p. 35-44.
77. Gerndt, S., et al., *Agonist-mediated switching of ion selectivity in TPC2 differentially promotes lysosomal function*. Elife, 2020. **9**.
78. Brookes, P.S., et al., *Calcium, ATP, and ROS: a mitochondrial love-hate triangle*. Am J Physiol Cell Physiol, 2004. **287**(4): p. C817-33.
79. Baker, M.J., et al., *Stress-induced OMA1 activation and autocatalytic turnover regulate OPA1-dependent mitochondrial dynamics*. Embo j, 2014. **33**(6): p. 578-93.
80. MacVicar, T. and T. Langer, *OPA1 processing in cell death and disease – the long and short of it*. Journal of Cell Science, 2016. **129**(12): p. 2297-2306.
81. Rajesh, K., et al., *eIF2 α phosphorylation bypasses premature senescence caused by oxidative stress and pro-oxidant antitumor therapies*. Aging (Albany NY), 2013. **5**(12): p. 884-901.
82. Zitka, O., et al., *Redox status expressed as GSH:GSSG ratio as a marker for oxidative stress in paediatric tumour patients*. Oncol Lett, 2012. **4**(6): p. 1247-1253.
83. Ma, K., et al., *Mitophagy, Mitochondrial Homeostasis, and Cell Fate*. Frontiers in Cell and Developmental Biology, 2020. **8**(467).
84. Jung, J. and K. Venkatachalam, *TRPing the homeostatic alarm — Melanoma cells are selectively vulnerable to TRPML1 deletion*. Cell Calcium, 2019. **84**: p. 102082.
85. Scotto Rosato, A., et al., *TRPML1 links lysosomal calcium to autophagosome biogenesis through the activation of the CaMKK β /VPS34 pathway*. Nature Communications, 2019. **10**(1): p. 5630.
86. Huang, P., et al., *Multiple facets of TRPML1 in autophagy*. Cell Calcium, 2020. **88**: p. 102196.
87. Rimessi, A., et al., *Perturbed mitochondrial Ca $^{2+}$ signals as causes or consequences of mitophagy induction*. Autophagy, 2013. **9**(11): p. 1677-86.
88. Duchen, M.R., *Mitochondria and calcium: from cell signalling to cell death*. The Journal of physiology, 2000. **529 Pt 1**(Pt 1): p. 57-68.
89. Hansford, R.G. and D. Zorov, *Role of mitochondrial calcium transport in the control of substrate oxidation*. Mol Cell Biochem, 1998. **184**(1-2): p. 359-69.
90. McCormack, J.G. and R.M. Denton, *Mitochondrial Ca $^{2+}$ transport and the role of intramitochondrial Ca $^{2+}$ in the regulation of energy metabolism*. Dev Neurosci, 1993. **15**(3-5): p. 165-73.
91. Brookes, P.S., et al., *Calcium, ATP, and ROS: a mitochondrial love-hate triangle*. American Journal of Physiology-Cell Physiology, 2004. **287**(4): p. C817-C833.

References

92. Grijalba, M.T., A.E. Vercesi, and S. Schreier, *Ca²⁺-induced increased lipid packing and domain formation in submitochondrial particles. A possible early step in the mechanism of Ca²⁺-stimulated generation of reactive oxygen species by the respiratory chain*. *Biochemistry*, 1999. **38**(40): p. 13279-87.
93. Ott, M., et al., *Cytochrome c release from mitochondria proceeds by a two-step process*. *Proc Natl Acad Sci U S A*, 2002. **99**(3): p. 1259-63.
94. Murphy, M.P., *How mitochondria produce reactive oxygen species*. *The Biochemical journal*, 2009. **417**(1): p. 1-13.
95. Wu, Y., P. Huang, and X.-P. Dong, *Lysosomal Calcium Channels in Autophagy and Cancer*. *Cancers*, 2021. **13**(6): p. 1299.
96. Peng, W., Y.C. Wong, and D. Krainc, *Mitochondria-lysosome contacts regulate mitochondrial Ca(2+) dynamics via lysosomal TRPML1*. *Proc Natl Acad Sci U S A*, 2020. **117**(32): p. 19266-19275.
97. Du, W., et al., *Lysosomal Zn²⁺ release triggers rapid, mitochondria-mediated, non-apoptotic cell death in metastatic melanoma*. *Cell Reports*, 2021. **37**(3).
98. Hanahan, D. and R.A. Weinberg, *Hallmarks of cancer: the next generation*. *Cell*, 2011. **144**(5): p. 646-74.
99. Locasale, J.W. and L.C. Cantley, *Altered metabolism in cancer*. *BMC Biology*, 2010. **8**(1): p. 88.
100. Hamanaka, R.B. and N.S. Chandel, *Targeting glucose metabolism for cancer therapy*. *J Exp Med*, 2012. **209**(2): p. 211-5.
101. Jia, D., et al., *Elucidating cancer metabolic plasticity by coupling gene regulation with metabolic pathways*. *Proceedings of the National Academy of Sciences*, 2019. **116**(9): p. 3909.
102. Medina, D.L., et al., *Lysosomal calcium signalling regulates autophagy through calcineurin and TFEB*. *Nat Cell Biol*, 2015. **17**(3): p. 288-99.
103. Settembre, C., et al., *A lysosome-to-nucleus signalling mechanism senses and regulates the lysosome via mTOR and TFEB*. *Embo j*, 2012. **31**(5): p. 1095-108.
104. Venkatachalam, K., C.O. Wong, and M.X. Zhu, *The role of TRPMLs in endolysosomal trafficking and function*. *Cell Calcium*, 2015. **58**(1): p. 48-56.
105. Schmiede, P., M. Fine, and X. Li, *The regulatory mechanism of mammalian TRPMLs revealed by cryo-EM*. *The FEBS Journal*, 2018. **285**(14): p. 2579-2585.
106. Marques, A.R.A. and P. Saftig, *Lysosomal storage disorders – challenges, concepts and avenues for therapy: beyond rare diseases*. *Journal of Cell Science*, 2019. **132**(2): p. jcs221739.
107. Høyer-Hansen, M. and M. Jäättelä, *Autophagy: An emerging target for cancer therapy*. *Autophagy*, 2008. **4**(5): p. 574-580.

References

108. Mulcahy Levy, J.M. and A. Thorburn, *Autophagy in cancer: moving from understanding mechanism to improving therapy responses in patients*. Cell Death & Differentiation, 2020. **27**(3): p. 843-857.
109. Palikaras, K., E. Lionaki, and N. Tavernarakis, *Mechanisms of mitophagy in cellular homeostasis, physiology and pathology*. Nature Cell Biology, 2018. **20**(9): p. 1013-1022.
110. Curcio-Morelli, C., et al., *Macroautophagy is defective in mucopolipin-1-deficient mouse neurons*. Neurobiology of Disease, 2010. **40**(2): p. 370-377.
111. Vergarajauregui, S., et al., *Autophagic dysfunction in mucopolipidosis type IV patients*. Human Molecular Genetics, 2008. **17**(17): p. 2723-2737.
112. Di Paola, S., A. Scotto-Rosato, and D.L. Medina, *TRPML1: The Ca²⁺retaker of the lysosome*. Cell Calcium, 2018. **69**: p. 112-121.
113. Lieberman, A.P., et al., *Autophagy in lysosomal storage disorders*. Autophagy, 2012. **8**(5): p. 719-730.
114. Medina, D.L. and A. Ballabio, *Lysosomal calcium regulates autophagy*. Autophagy, 2015. **11**(6): p. 970-971.
115. Devenport, S.N., et al., *Colorectal cancer cells utilize autophagy to maintain mitochondrial metabolism for cell proliferation under nutrient stress*. JCI Insight, 2021. **6**(14).
116. Zitka, O., et al., *Redox status expressed as GSH:GSSG ratio as a marker for oxidative stress in paediatric tumour patients*. Oncology letters, 2012. **4**(6): p. 1247-1253.
117. Galadari, S., et al., *Reactive oxygen species and cancer paradox: To promote or to suppress?* Free Radical Biology and Medicine, 2017. **104**: p. 144-164.
118. Circu, M.L. and T.Y. Aw, *Reactive oxygen species, cellular redox systems, and apoptosis*. Free Radic Biol Med, 2010. **48**(6): p. 749-62.
119. Traverso, N., et al., *Role of glutathione in cancer progression and chemoresistance*. Oxid Med Cell Longev, 2013. **2013**: p. 972913.
120. Vestre, K., et al., *Rab7b regulates dendritic cell migration by linking lysosomes to the actomyosin cytoskeleton*. Journal of Cell Science, 2021. **134**(18).
121. Medeiros, N.A., D.T. Burnette, and P. Forscher, *Myosin II functions in actin-bundle turnover in neuronal growth cones*. Nat Cell Biol, 2006. **8**(3): p. 215-26.
122. Olson, M.F. and E. Sahai, *The actin cytoskeleton in cancer cell motility*. Clinical & Experimental Metastasis, 2008. **26**(4): p. 273.
123. Kong, X., et al., *MicroRNA-7 Inhibits Epithelial-to-Mesenchymal Transition and Metastasis of Breast Cancer Cells via Targeting FAK Expression*. PloS one, 2012. **7**: p. e41523.

References

124. Benton, G., E. Crooke, and J. George, *Laminin-1 induces E-cadherin expression in 3-dimensional cultured breast cancer cells by inhibiting DNA methyltransferase 1 and reversing promoter methylation status*. FASEB journal : official publication of the Federation of American Societies for Experimental Biology, 2009. **23**: p. 3884-95.
125. Mayor, R. and S. Etienne-Manneville, *The front and rear of collective cell migration*. Nature Reviews Molecular Cell Biology, 2016. **17**(2): p. 97-109.
126. Yang, Hee W., et al., *Cooperative Activation of PI3K by Ras and Rho Family Small GTPases*. Molecular Cell, 2012. **47**(2): p. 281-290.
127. Li, Y.Y., C.X. Zhou, and Y. Gao, *Podoplanin promotes the invasion of oral squamous cell carcinoma in coordination with MT1-MMP and Rho GTPases*. Am J Cancer Res, 2015. **5**(2): p. 514-29.
128. Sorkin, A. and M. von Zastrow, *Endocytosis and signalling: intertwining molecular networks*. Nature reviews. Molecular cell biology, 2009. **10**(9): p. 609-622.
129. Valapala, M., et al., *Impaired endolysosomal function disrupts Notch signalling in optic nerve astrocytes*. Nature communications, 2013. **4**: p. 1629-1629.
130. Hounjet, J. and M. Vooijs, *The Role of Intracellular Trafficking of Notch Receptors in Ligand-Independent Notch Activation*. Biomolecules, 2021. **11**(9).

APPENDIX



8 Appendix

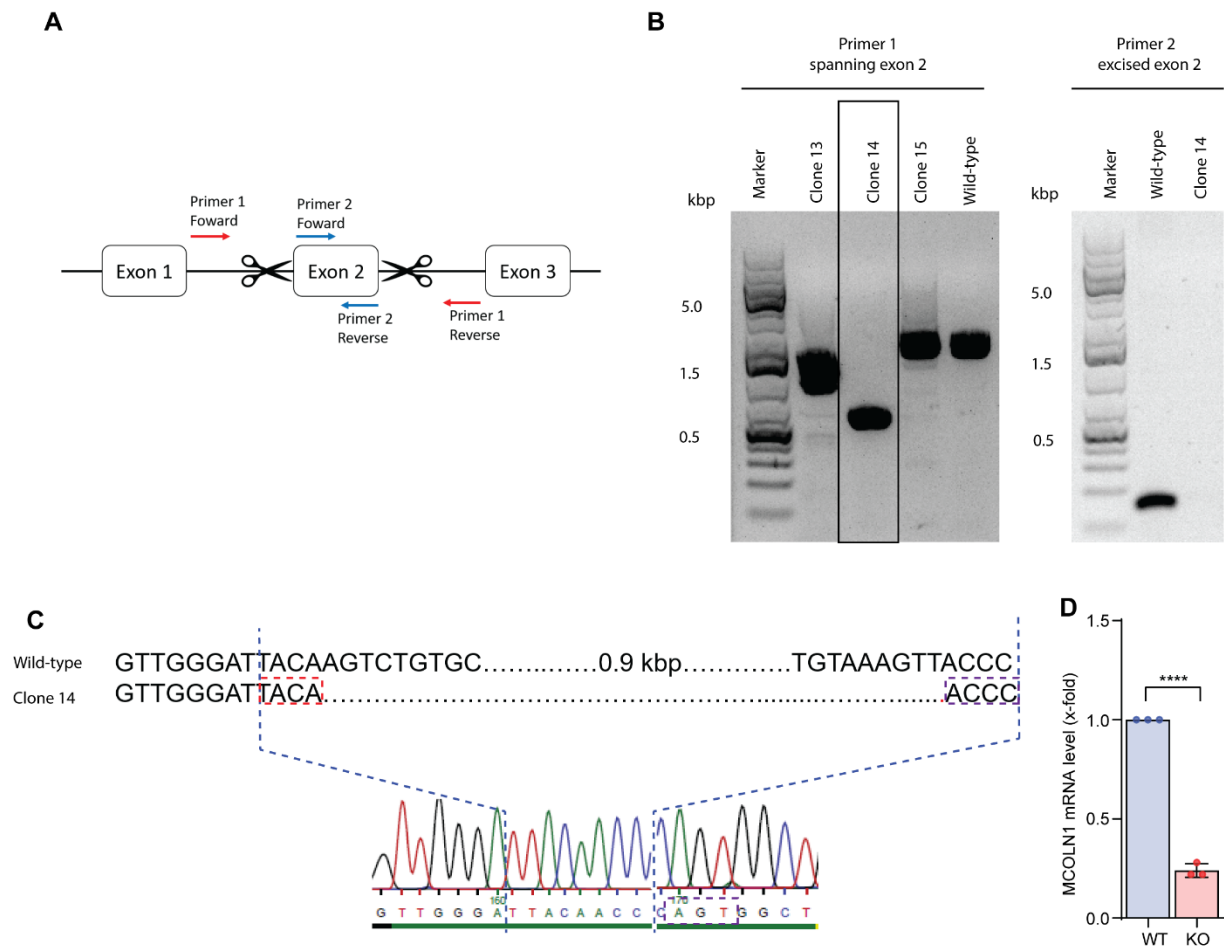

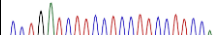




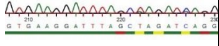
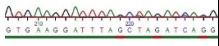
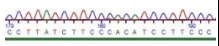
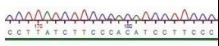
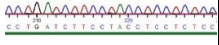


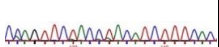
Figure 28. Generation of TRPML1 KO Clone.

(A) Strategy of creating TRPML1 KO clone. In brief, exon 2 (ex2) was the target for the designated sgRNA (scissors). 2 pairs of primers were designed for validation. Primer 1 was designed to detect the spanning ex 2, and primer 2 was designed to detect the excised ex 2. (B) Agarose gel analysis indicated that clone 14 was the potential TRPML1 KO clone and subsequently validated by excised ex2 primer, which binds within the ex2. (C) The clone 14's band on agarose gel was incised for Sanger sequencing. The deleted region was detected in clone 14, and the residues base pair was ligated precisely. (D) The mRNA was extracted to perform qPCR. mRNA level of MCOLN1 was strongly reduced in clone 14, which indicates that nonsense-mediated decay occurred due to the deletion ex2. Results represent mean \pm SD; n=3; unpaired t-test; ****, p-value<0.0001.

Appendix

CFD score	Gene potential	TRPML1	PCR forward primer (5'-3')	PCR reverse primer (5'-3')	sequencing primer (5'-3')	Potential off target: sanger sequencing (5'-3')	Sanger sequencing
0.39	4930595D18Rik	WT	AAACCCCTA	TGTCGTGTCT	TGTCGTGTCT	CCTGATCTAT	
		KO	CTCATGCTG GC	GGGGATTGT G	GGGGATTGT G	CTACTTCCCTC TC	
0.32	Slc1a2	WT	ACGGTTGAT	TTCTCGTGA	ACGGTTGATG	GGGAACGAA	
		KO	GACTTCTGG GG	GCCACTGAA GC	ACTTCTGGGG	GTGGATAGAT CTGG	
0.30	Epha4	WT	TGTGGTTCA	GGATAGCTG	GAGGATGAA	GAGGATGAA	
		KO	TGCAGACTG AGA	GTTCACCCA CC	GTAGGTAGAT CAGG	GTAGGTAGAT CAGG	
0.20	Slc37a3	WT	CTTGGGAGA	ATATCCTACA	ATATCCTACA	TGGAAGGAA	
		KO	CAGAGGCAA AT	CAGCCCAGA GA	CAGCCCAGA GA	GGAGGAAGA TCAGG	

Appendix

0.20	Efemp1	WT	CCTCCCATTG TTGCCAGTC	AGCTGATTG TGTGTGGAG	AGCTGATTGT GTGTGGAGG	GAAAAGGAG GTAGGTAGAT	
		KO	T	GA	A	AGGG	
0.19	Syt1	WT	TGCTCTTGCT CAGCTTGCT	ACCATGCCT GTGTGTCTA	ACCATGCCTG TGTGTCTACA	GTGAAGGATT TAGCTAGATC	
		KO	T	CA		AGG	
0.18	Gm14281/	WT	ACTTGTTGG AAGCAACAC	TGTTTTCTGC ATTGGCCAG	ACTTGTTGGA AGCAACACGC	CCTTATCTTCC CACATCCTTCC	
		KO	GC	C		C	
0.17	Shc4	WT	CGCTCTGTC CAAGTGTC	CATCTGTGC GGTTGTTTG	CATCTGTGCG GTTGTTTGCA	CCTGATCTTCC TACCTCCTCTC	
		KO	CA	CA		C	
0.16	Ano2	WT	AAGAGCGGC TTCAGCTTA	GGACTGACT CTGTGCCCA	AAGAGCGGC TTCAGCTTAG	CCAGTTCTAC CTACATCTTTC	
		KO	GG	TC	G	A	

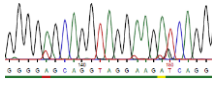
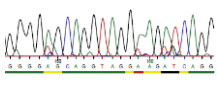
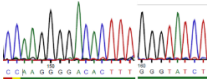
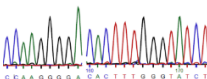
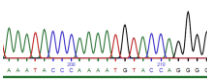
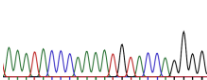
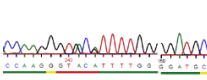
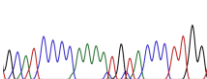
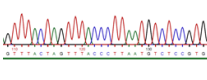
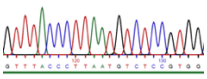
0.15	Aasdh	WT	GCAAAGGTC	ACTCAGATC	GCAAAGGTCC	GGGGAGCAG	
			CGAGGTTAG	CACAGAGAG	GAGGTTAGTA	GTAGGAAGAT	
		KO	TAAT	AGAG	AT	CAGG	

Table 16. Off-target screening 5'sgRNA

CFD score	Gene potential	TRPML1	PCR forward primer (5'-3')	PCR reverse primer (5'-3')	sequencing primer (5'-3')	Potential off-target: sanger sequencing (5'-3')	Sanger sequencing
0.38	Rbfox1	WT	TGTGCCTCTG	TACACACCG ATGCTCTTGC	TACACACCGA TGCTCTTGCC	AGATACCCAA AGTGTCCCCTT GG	
		KO	TGTCCAAGTC	C			
0.33	Bmp7	WT	TTGCTGCCTT	GTTCCGCAA TGTCCTGAA	GTTCCGCAAT GTCCCGAAAC	AAATACCCAAA ATGTACCAGG GG	
		KO	GCACAATTCC	AC			
0.30	Gbp4	WT	TTGGTCAAG	TCCCAACATC	TTGGTCAAGG ATGCTGGGTC	GCATCCCCAAA ATGTACCCTTG	
		KO	GATGCTGGG TC	CACATCAGG C	TCCCAACATC CACATCAGGC	G	
0.17	Scn8a	WT	CCTTTACTGT	CAGAGGACC	CAGAGGACC	GTTTACCCTTA	
		KO	GAGGGCTGG G	ACAACCGGA AA	ACAACCGGAA A	ATGTCTCCGTG G	

Appendix

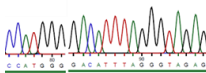
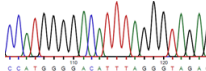
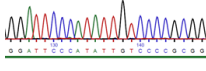
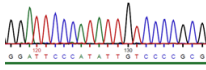
0.17	Samd4	WT	GCTGGCCTTT	TTTGCCAAG	TTTGCCAAGG	CTCTACCCTAA	
		KO	CTCACAGACT	GTAGCTGGA GG	TAGCTGGAG G	ATGTCCCCATG G	
0.09	Pou4f2	WT	TGTGTTTCGCT	TGCACCTAA	TGTGTTTCGCT	GGATTCCCATA	
		KO	TTGGCCTAGT	GGCTGGGAA AG	TTGGCCTAGT	TTGTCCCCGCG G	

Table 17. Off-target screening 3'sgRNA

8.1 Abbreviations

Abbrev.	Name
°C	Degree celsius
AA	Antimycin A
ANOVA	Analysis of variance analysis
ATCC	American Type Culture Collection
ATP	Adenosine triphosphate
BCLC	Barcelona clinic liver cancer
BSA	Bovine serum albumin
c	Centi
C1	complex 1
C2	complex 2
Ca ²⁺	Calcium
CFD	Cutting frequency determination
CICR	Calcium-induced calcium release
CsA	Cyclosporin A
DMEM	Dulbecco's modified eagle medium
DMSO	Dimethylsulfoxide
DNA	Deoxyribonucleic acid
DTT	Dithiothreitol
EDME	17 β -estradiol methyl ether
EDTA	Ethylenediaminetetraacetic acid
EGF	Epidermal growth factor
EMEM	Eagle's minimum essential medium
EMT	Epithelial-mesenchymal transition
ES	Endolysosomal system
FCS	Fetal calf serum
g	Gram
GSH	Glutathione
GSSG	Glutathione disulfide
h	Hour

HBV	Hepatitis virus B
HBV	Hepatitis virus C
HCC	Hepatocellular carcinoma
Hz	Hertz
IP ₃	Inositol trisphosphate
IP ₃ R	Inositol trisphosphate receptor
JCRB	Japanese collection of research bioresources
k	Kilo
KO	knockout
L	Litre
LSD	Lysosomal disorder
m	Milli
M	Molar
MCU	Mitochondrial uniporter
min	Minute
ML IV	Mucopolysaccharidosis type IV
mPTP	Mitochondrial permeability transition pore
mTORC1	Mammalian target of rapamycin complex 1
n	Nano
Na ₃ VO ₄	Sodium orthovanadate
NICD	Notch1 intracellular domain
OXPHOS	Oxidative phosphorylation
PBS	Phosphate-buffered saline
PI	Propidium iodide
PVDF	Polyvinylidene difluoride
qPCR	Quantitative real-time PCR
RCR	Respiratory control ratio
RNA	Ribonucleic acid
ROS	Reactive oxidative species
Rot	Rotenone
ROX	Residual oxygen consumption

RT	Room temperature
RyR	Ryanodine receptors
SD	Standard deviation
SDS	Sodiumdodecylsulfate
SDS-PAGE	Sodium dodecyl sulfate polyacrylamide gel electrophoresis
TBS-T	Tris-buffered Saline with Tween 20
TEM	Transmission electron microscopy
TFEB	Transcription factor EB
TRP	Transient receptor potential
TRPML1	Transient receptor potential mucolipin-1
TRPML2	Transient receptor potential mucolipin-2
TRPML3	Transient receptor potential mucolipin-3
VDAC	Voltage-dependent anion-selective channel proteins
WT	wildtype
Zn ²⁺	Zinc
μ	Micro

Table 18. Abbreviations

8.2 Index of figures

Figure 1. Model of TRPML1 as a mitochondrial balancer function in HCC – the project at a glance.....	8
Figure 2. Characterization of TRPML1 in cancer collective migration – the project at a glance.	9
Figure 3. Classification of HCC patients and treatment options.....	12
Figure 4. Structure of human TRPML1.....	13
Figure 5. Regulation of cadherin switch and Rac1 in epithelial-mesenchymal transition.	16
Figure 6. Modes of collective and individual migration	17
Figure 7. Notch1 signalling pathway.....	18
Figure 8. Gating strategy for Annexin V-FITC Apoptosis assay.....	34
Figure 9. Gating strategy for identifying dissipated mitochondria.....	35
Figure 10. Generation of a cellular model to study TRPML1 function.	45
Figure 11. Functional characterisation of TRPML1 function in HCC cells.....	47
Figure 12. Proteome analysis of ML1-SA1 treated and TRPML1 KO cells.	48
Figure 13. TRPML1 regulates mitochondrial morphology.....	50
Figure 14. TRPML1 activity alters mitochondrial membrane potential by regulating mPTP. .	51
Figure 15. TRPML1 activity regulates mitochondrial function.	52
Figure 16. TRPML1 activation induces lysosomal calcium efflux and mitochondrial influx...	53
Figure 17. TRPML1 activation induces mitochondrial stress via calcium overloading.....	55
Figure 18. Loss of TRPML1 reduces cell proliferation.....	56
Figure 19. Loss of TRPML1 disturbs the mitochondrial respiratory function.....	58
Figure 20. Loss of TRPML1 alters lysosome morphology.	59
Figure 21. Loss of TRPML1 disrupts mitophagy.	60
Figure 22. Loss of TRPML1 impairs cancer cell migration.	62
Figure 23. Loss of TRPML1 changes the migrating movement and cell-cell adhesion of cancer cells.	64
Figure 24. Alteration of the cytoskeleton and cell junction after the loss of TRPML1 in cancer cells.	65
Figure 25. TRPML1 KO alters the expression of E-cadherin.	66
Figure 26. TRPML1 KO induces the transition of collective to individual migration.....	67

Figure 27. TRPML1 KO reduces the regulation of Notch1 activity.	68
Figure 28. Generation of TRPML1 KO Clone.	90

8.3 Index of tables

Table 1. Compounds	21
Table 2. Reagents.....	24
Table 3. Cell culture buffers and solutions	26
Table 4. Sequencing primers for exon 2	28
Table 5. sgRNA sequences	28
Table 6. Oligo-annealing master mix	28
Table 7. Digestion of Cas9 plasmid	29
Table 8. Ligation of annealed oligos and Cas9 plasmid	29
Table 9. Digestion of non-ligated plasmid	29
Table 10. Primers used for PCR analysis of exon 2 deletion.....	31
Table 11. Primers used for PCR analysis	31
Table 12. Buffers and solutions for western blot analysis.....	39
Table 13. Primary antibodies for western blot analysis	40
Table 14. Secondary antibodies for western blot analysis	40
Table 15. Cytotoxicity of ML1-SA1 in different cells.....	46
Table 16. Off-target screening 5'sgRNA.....	93
Table 17. Off-target screening 3'sgRNA.....	95
Table 18. Abbreviations	98

8.4 List of Publications

Lysosomal TRPML1 regulates mitochondrial function in hepatocellular carcinoma cells

Wei Xiong Siow, Yaschar Kabiri, Rachel Tang, Yu-Kai Chao, Eva Plesch, Carola Eberhagen, Florian Flenkenthaler, Thomas Fröhlich, Franz Bracher, Christian Grimm, Martin Biel, Hans Zischka, Angelika M. Vollmar, Karin Bartel. Journal of Cell Science (2022).
<https://doi.org/10.1242/jcs.259455>.

Disentangling cadherin-mediated cell-cell interactions in collective cancer cell migration

Zisis, Themistoklis, Brückner, David B., Brandstätter, Tom, Siow, Wei Xiong, d'Alessandro, Jose, Vollmar, Angelika M., Broedersz, Chase P., Zahler, Stefan. Biophysical Journal (2022).
<https://doi.org/10.1016/j.bpj.2021.12.006>

Thioholgamide A, a new anti-proliferative anti-tumor agent, modulates macrophage polarization and metabolism

Charlotte Dahlem, Wei Xiong Siow, Maria Lopatniuk, William K. F. Tse, Sonja M. Kessler, Susanne H. Kirsch, Jessica Hopstädter, Angelika M. Vollmar, Rolf Müller, Andriy Luzhetskyy, Karin Bartel and Alexandra K. Kiemer. Cancers (2020).
<https://doi.org/10.3390/cancers12051288>

Antioxidant polymer-modified maghemite nanoparticles

Vitalii Patsula, Maksym Moskvyn, Wei Xiong Siow, Rafal Konefal, Yunn-Hwa Ma, Daniel Horák. Journal of Magnetism and Magnetic Materials (2018).
<https://doi.org/10.1016/j.jmmm.2018.10.081>

Interaction of poly-L-lysine coating and heparan sulfate proteoglycan on magnetic nanoparticle uptake by tumor cells

Wei Xiong Siow, Yi-Ting Chang, Michal Babič, Yi-Ching Lu, Daniel Horák, Yunn-Hwa Ma. International Journal of Nanomedicine (2018).
<https://doi.org/10.2147/IJN.S156029>

9 Acknowledgements

First and foremost, I must thank my Doktormutter, Prof. Dr. Angelika Vollmar. I would like to express my gratitude for supporting me financially and mentally. Without your assistance and involvement in my works, this thesis would not have been completed. Thank you so much for making me helpful comments and for guiding me when I made mistakes. I have learned a lot from you concerning developing a professional attitude towards research. I appreciate that you always encouraged me when I felt depressed, especially at the beginning of my PhD study.

I would also like to thank Dr. Karin Bartel for kindly supervision during my PhD study. Thank you for giving advice and comments on my work and giving me guidance regarding paper writing and rebuttal. I hope you will have great success in your career. Thank you to Dr. Martin Müller, for giving me advice, teaching me CRISPR/Cas9, and being a funny and professional instructor during my internship. Thanks to Prof. Stefan Zahler for the comment and advice on confocal techniques.

I would also like to show gratitude to my committee, including Prof. Dr. Angelika Vollmar, Prof. Dr. Stefan Zahler, Prof. Dr. Franz Bracher, Prof. Dr. Dr. Christian Grimm, Prof. Dr. Oliver Merkel, and PD Dr. Stefanie Fenske. Thank you for your time and efforts.

Thanks to Prof. Dr. Dr. Christian Grimm and his colleagues Rachel Tang and Dr. Yu-Kai Chao for the patch clamp experiments. Thanks to Prof. Dr. Franz Bracher and colleagues for providing excellent molecules. Thanks to our collaborators, Dr. Thomas Fröhlich and his colleague Dr. Florian Flenkenthaler in Gene Center, Ludwig Maximilians Universität München, for the proteomic results and teaching me how to analyse the results. Thanks to Prof. Dr. Hans Zischka and the PhD student, Yaschar Kaibiri in Technische Universität München, for mitochondrial experiments.

I want to thank our technicians, Frau Bernadette Grohs, Frau Silvia Schnegg, Frau Jana Peliskova, Frau Rita Socher and Julia Blenninger, for helping me with all experimental problems, giving me technical advice when I made enquiries regarding materials for experiment. I enjoyed the environment in AK Vollmar due to the relationship I enjoyed with

my colleague and friends who I would like to take this opportunity to thank Flo L and Conny for teaching me about German culture. Thanks to Ling, YuDong, Peng and Crystal for the hotpot party. Thanks to Themis for the volleyball game. Thanks to the team members in LMU Shakers for the fun moments, Flo G, Maibritt, Katrin, etc. Besides, I would also like to thank my previous intern student, Laura, Moritz, and Nadine, for assisting with experiments.

At last, I would love to thank my family for all the support and encouragement, especially my mother, Ng Chong Lowi and my father, Siow Xin Fook, for all the encouragement they have given me since my childhood. Thanks to my sister, Siow Pei Kwan, who takes care of me all the time. It has been a long journey and thanks to my family for always giving me the best and accompanying me. I would also like to praise God and thank him for offering me strength and wisdom to finish my study and the courage to overcome negative influences and depression. Without any one of you, it would not have been possible to complete. Thank you all, and I love you all!